

Impact ditch on dike stability during uplift

Factual report centrifuge tests



Impact ditch on dike stability during uplift
Factual report centrifuge tests

Author(s)

Benthe Noijons

Impact ditch on dike stability during uplift

Factual report centrifuge tests

Client	SITO Moonshot 2
Contact	Ap van Dongeren
Reference	-
Keywords	Dike stability, uplift, centrifuge testing

Document control

Version	1.1
Date	23-01-2025
Project nr.	11210298-020
Document ID	11210298-020-GEO-0002
Pages	82
Classification	Public
Status	Final

Author(s)

	Benthe Noijons	

Summary

Recent studies on dike stability under uplift conditions showed that the present guidelines on dike stability assessment are too conservative. Optimization in the design rules, regarding dike improvement has considerable impact both financially as well as in terms of societal impact.

Uplift conditions at the toe of a dike emerge during high water conditions in combination to a hydraulic connection between river water and sandy subsoil layers. The hydraulic head in the subsoil might rise at the landward side of the dike such that low permeable top layers are lifted. Such conditions reduce dike stability and might be the start of backward erosion piping.

The recent studies mentioned above do not include the influence of a ditch at the toe the dike, which is typically present in Dutch conditions. In terms of stability, the ditch might have both a positive and a negative effect. The positive effect could be the formation of a release well reducing the hydraulic head in the sand layer. The negative effect could be the reduction in lateral resistance, compared to the situation without a ditch, leading to a reduction in dike stability.

A test series of 6 tests has been conducted, with the aim of:

- Establishing the reproducibility of the tests.
- Establishing the impact of the presence of a ditch on uplift.

The results of test 1 and 2 illustrate the good reproducibility of the tests. Although within the test series a good reproducibility is found, the reproducibility with previous test series is less. This is mainly due to the preparation of the sand body which models the dike. Different approaches for densification leads to different results.

Remarkably, the presence of the ditch does not influence the failure load. However, the presence of a ditch has a strong impact on the shape of the failure mechanism.

This factual report collects all relevant information about the execution of the tests and forms the basis for scientific publications. Moreover, the test results provide a wealth of information for validation of geotechnical software tools.

Contents

	Summary	4
1	Introduction	8
1.1	Context	8
1.2	Aim of the study	8
1.3	Previous test series	9
2	Test set-up	10
2.1	Reproduction	10
2.2	Ditch configurations	10
2.3	Changes in model set-up	11
2.4	Consolidation and remoulding	11
3	Calibration	13
4	Overview test characteristics	16
5	Test 1: reproduction	19
5.1	General observations	19
5.2	Consolidation	19
5.3	Centrifuge test	21
5.3.1	Preliminary analysis and commentary on the data	21
5.3.2	Observations, notes and remarks	22
5.3.3	Uplift	22
5.3.4	Failure	23
5.4	Post-test observations	24
5.4.1	Sliding planes, sand-boils, piping	24
5.4.2	Laser scan	25
6	Test 2: reproduction	26
6.1	General observations	26
6.2	Consolidation	26
6.3	Centrifuge test	26
6.3.1	Preliminary analysis and commentary on the data	26
6.3.2	Observations, notes and remarks	27
6.3.3	Uplift	28
6.3.4	Failure	28
6.4	Post-test observations	29
6.4.1	Sliding planes, sand-boils, piping	29
6.4.2	Laser scan	31
7	Test 3: without uplift	32

7.1	General observations	32
7.2	Centrifuge test	32
7.2.1	Preliminary analysis and commentary on the data	32
7.2.2	Observations, notes and remarks	33
7.2.3	Uplift	33
7.2.4	Failure	34
7.3	Post-test observations	35
7.3.1	Sliding planes, sand-boils, piping	35
7.3.2	Laser scan	36
8	Test 4: ditch close – narrow	37
8.1	General observations	37
8.2	Centrifuge test	37
8.2.1	Preliminary analysis and commentary on the data	37
8.2.2	Observations, notes and remarks	38
8.2.3	Uplift	38
8.2.4	Failure	39
8.3	Post-test observations	39
8.3.1	Sliding planes, sand-boils, piping	39
8.3.2	Laser scan	42
9	Test 5: ditch far – wide	44
9.1	General observations	44
9.2	Centrifuge test	44
9.2.1	Preliminary analysis and commentary on the data	44
10	Test 6: ditch close – wide	50
10.1	General observations	50
10.2	Centrifuge test	50
10.2.1	Preliminary analysis and commentary on the data	50
A	Design and prediction	56
A.1	Introduction	56
A.2	Model Geometry	56
A.3	Soil parameters	57
A.4	Phreatic line – hydraulic heads	58
A.5	Test procedure	58
A.6	Modelling ditch	59
A.7	Results	61
A.8	Case of the weaker dike	69
A.9	New permeability properties	70
B	Additional laboratory testing	75
B.1	Introduction	75

B.2	Comparison	75
B.3	Test results	79
B.3.1	K0-CRS 4A	79
B.3.2	DSS 4B	80
B.3.3	DSS 4C	81

1 Introduction

1.1 Context

Hydraulic loading of water retaining structures not only includes the elevated sea or river level, but also an increase in hydraulic head in sub-soil layers. Figure 1.1 sketches a typical situation for deltaic regions. The subsoil contains multiple layers, including a shallow permeable sand layer and a low permeable cover layer on top. The shallow sand layer is in hydraulic contact with the free water at the front of the dike. A rise in the free water level causes a corresponding rise in hydraulic head in the sand layer. At the toe of the dike the increased hydraulic head can result in uplift of the cover layer, which might crack or break. This uplift has consequences for the stability of the dike. It could initiate slope failure or backward erosion piping.

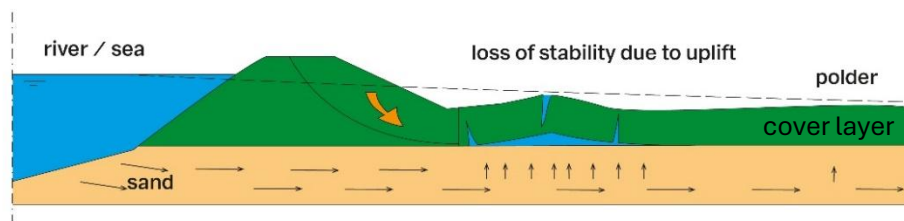


Figure 1.1 Sketch uplift mechanism, the cover layer is lifted and breaks.

Recent study, see Section 1.3, shows that uplift induced failure planes are dominated by active part of the failure plane and the failure plane at the passive part is not clearly developed. Instead the cover layer is lifted further or compressed horizontally, while slope failure occurs.

Ditches are used to either facilitate drainage of the dike core and / or dewatering of the land at the polder side of the dike. The presence of such a ditch might create a weakening in the cover layer which would facilitate the deformation of the cover layer and as such enhance failure at uplift. Typical dike cross sections have a ditch near the toe of the dike.

To study the impact of a ditch on failure load and shape of the failure mechanism a series of centrifuge tests has been conducted. The test series are additional to the test series conducted in the research Programme Opbarsten bij Dijken, POD.

To be able to conclude on the significance of the differences in test results for tests with and without a ditch, the reproducibility of the test results should be established first. Therefore, the tests series, reported in this report, contain two parts:

- Tests to establish the repeatability of the test results.
- Tests to determine the impact of the presence of a ditch.

Besides conclusions on the impact of the presence of a ditch, the tests provide valuable data for validation of software tools and design procedures.

1.2 Aim of the study

The study aims to establish the impact of a ditch on dike failure due to uplift. To reach a conclusion on the impact, two additional goals are formulated:

- Establishing the repeatability of the tests.
- Collecting a dataset for validation of software tools and design procedures.

This factual report aims to lay down:

- Details of the test set-up.
- Details of the test procedure.
- All the relevant measurement data.

1.3 Previous test series

The test series is additional to the series conducted as part of the research Programme Opbarsten bij Dijken, POD. The POD-test series includes a variation in cover layer thickness and pre-consolidation of the clay. The test with the cover layer thickness of 30 mm and a pre-consolidation stress of 40 kN/m² is selected as reference case for the present study.

The POD test series is reported in several documents:

- 11207357-028-GEO-0001_v1.0-Ontwerp centrifugeproeven. This report discusses the initial design and corresponding design choices, which are also adopted in the tests reported in this document.
- 11207357-031-GEO-0001_v1.0-Factual Report Centrifuge Tests conducted at Deltares. This report contains relevant information on the conduction of the tests and the test results.
- 11203757-033-GEO-0001_v1.0-Analyse centrifugeproeven opdrijven en opbarsten bij dijken. This report describes the analysis of the test data and a comparison of the test results to numerical simulations.

2 Test set-up

2.1 Reproduction

The first goal of this test series is to reproduce a test from the previous centrifuge test series. Test 10 was selected as the benchmark test. Test 10 was conducted on 16 February 2023 and used the slurry consolidation method to form the cover layer. An overview of the model set-up and the locations of the various sensors is given in Figure 2.1 below.

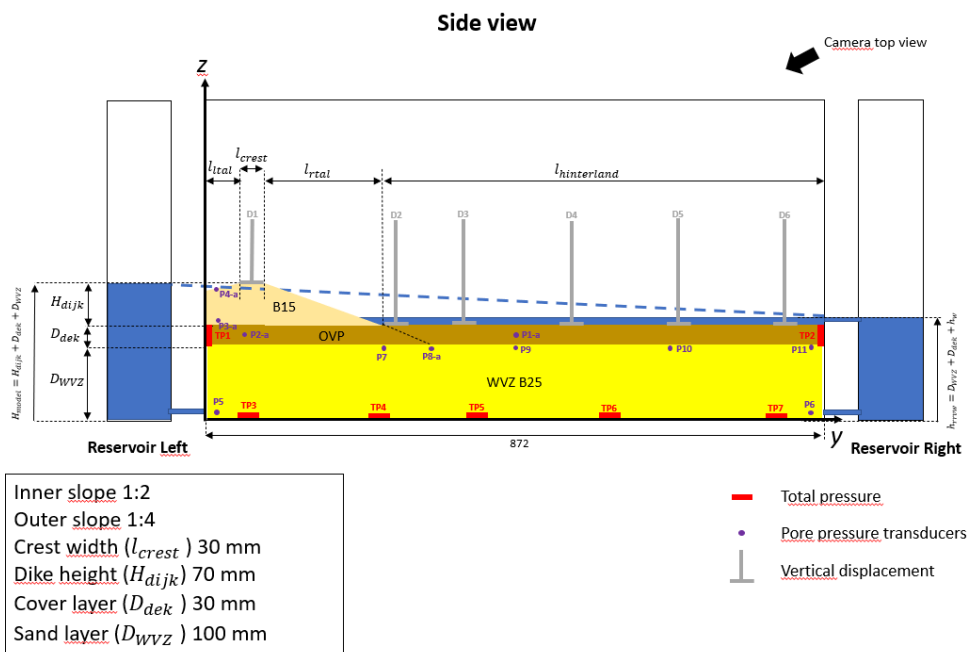


Figure 2.1 Model set-up and sensor locations, not shown here are two cameras at the front.

2.2 Ditch configurations

The second part of the test series is meant to demonstrate the effect of a ditch in the hinterland on the stability of the levee. The same base model is used, and the ditch is scraped out of the clay layer. Several sizes of the ditch were considered, at various distances from the toe of the levee. Based on the results of numerical calculations in Plaxis (see elaborate analysis in Appendix A), the four configurations in Figure 2.2 below were selected to be tested in the centrifuge. Along the course of this part of the test series, it was decided to skip the Far-Narrow configuration, since the Close-Narrow and Far-Wide configurations already gave valuable insights and the Far-Narrow option is not expected to add new information.

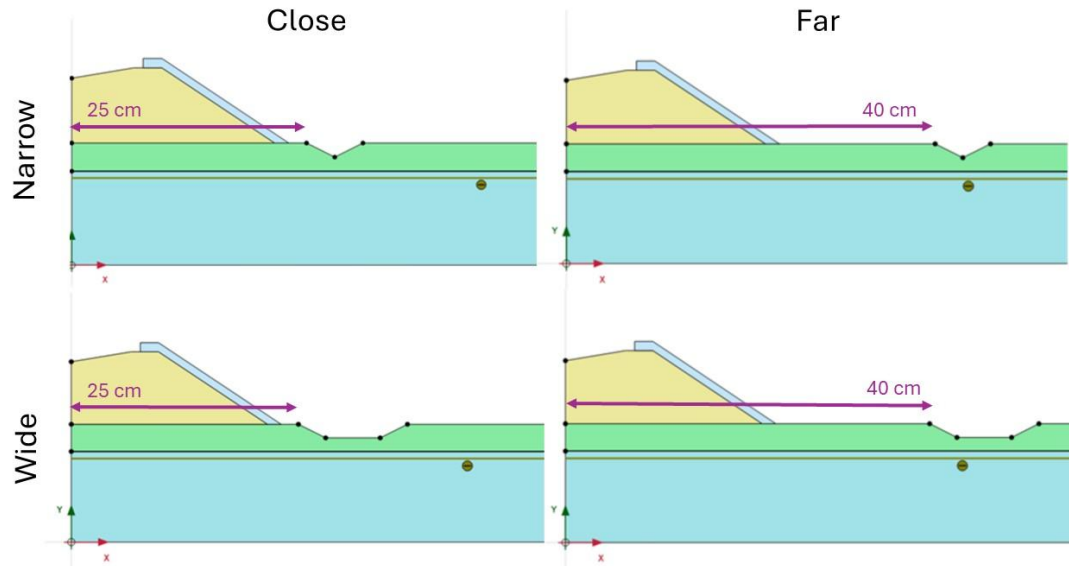


Figure 2.2 Configurations of the dike model with the ditch in the hinterland at two different distances and two different sizes.

For the configurations where the ditch is close to the dike, changes had to be made in the sensor set-up. These changes are elaborated upon in the respective test chapters.

2.3 Changes in model set-up

Compared to the POD-test series a new pump was installed in the centrifuge basket. Adjustments to the water inlet of the model containers resulted in a more direct response of the hydraulic head when lifting the hydraulic plunger. In test 10 of the POD series, the sand layer thickness was increased by 15 mm compared to other tests, making the permeable B15 sand layer 115 mm instead of 100 mm. However, in the tests in this series, the original thickness of 100 mm was applied.

2.4 Consolidation and remoulding

Since the goal is to have minimal changes compared to the previous series of centrifuge tests, the same clay was used, being Oostvaardersplassen (OVP) clay from 2023. To achieve the same characteristics of the clay in the model, the clay is remoulded, made into a slurry and consolidated again for every test. The thickness of the clay layer before consolidation, after consolidation and before the start of the test are documented and shown in Table 2.1 **Error! Reference source not found.** below. The water content of the slurry and after the test measured at two locations is shown in Table 2.2.

Table 2.1 Thickness of the cover layer per test.

Test	Thickness cover layer OVP clay [mm]			Time between consolidation and start test [hours]
	Before consolidation	After consolidation	At start test	
10 ^a	52.55	28.33	~28.8	24
1	53.43	31.67	31.67	6
2	53	32	33.33	19

3	52.66	33.66	33.16	23
4	52	32	33	24
5	52	35 (31.56 after levelling)	32.75	22
6	50.78	31	32.0	23

^a previous test series, added for comparison

Table 2.2 Water content OVP clay [%].

Test	Slurry	After test	
		Right side	Under levee
10^a	200	121,79	108,53
1	210,90	122,29	112,07
2	197,89	120,55	105,92
3	209,38	121,25	101,78
4	207,94	128,53	104,83
5	172,63	114,71	94,07
6	175,44	118,90	96,43

^a previous test series added for comparison

3 Calibration

A calibration test was conducted to test the cameras and the pore water pressure transducers. The test ran with an empty strongbox except for water and a checkerboard for the cameras. The applied g-level went stepwise up to 130 g and down again. The centrifugal acceleration plan is shown in Figure 3.1 below. The target pressure for the PPTs can be calculated from the water level, which was at 170 mm throughout most of the test based on camera footage, taking into account the position of the sensor within the strongbox. These positions are shown in Figure 2.1 and the vertical distances are presented in Table 3.1. For PPT 7-11, the measured pore water pressures and calculated value per g-level is shown in **Error! Reference source not found.** below. To calibrate the sensors, a fitting factor is calculated for each sensor. This is based on the ratio between the calculated value at a certain g-level and the measured value at that g-level for each sensor. The fitting factors (shown in Table 3.2) are then applied to the sensor measurements, as shown in **Error! Reference source not found.** As the data from PPT 11 deviates much from the other sensors and is not stable at g-levels, it is advised to be careful in the interpretation of PPT 11. The same was done for PPT 5 and 6, standpipes and for the total pressure transducers. These are found in **Error! Reference source not found.** to **Error! Reference source not found.**

Table 3.1 Sensor locations and distance from water level during calibration test (170 mm).

Sensor	Vertical distance from strongbox bottom [mm]	Vertical distance from water level [mm]
PPT 1 and 2	140	30
PPT 3	165	5
PPT 5 and 6	35	135
PPT 7 – 11	120	50
TP 3 - 7	25	145

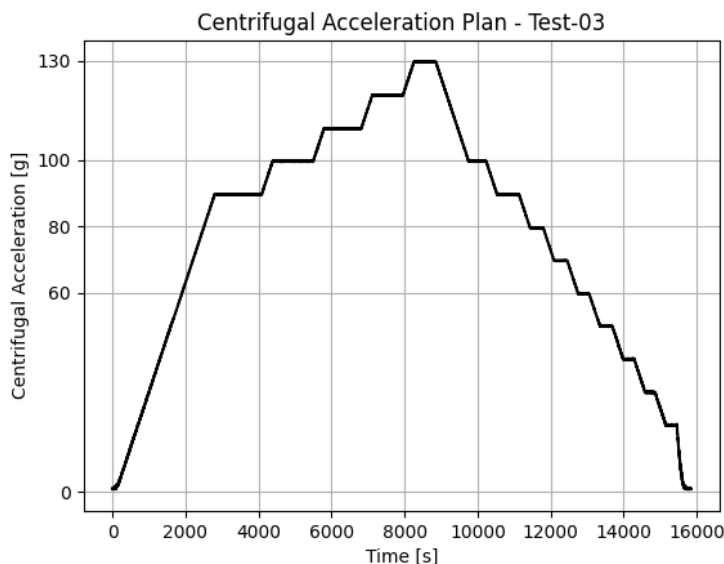


Figure 3.1 Centrifugal acceleration plan of calibration Test 03.

Table 3.2 Fitting factors at each g-level for all pore pressure transducers and total pressures.

G-level	90	100	110	120	130
PPT_01	1.18	1.17	1.15	1.14	1.13
PPT_02	1.21	1.21	1.19	1.19	1.16
PPT_03	2.52	2.41	2.32	2.24	2.16
PPT_05	1.08	1.08	1.07	1.07	1.07
PPT_06	1.05	1.04	1.03	1.03	1.03
PPT_07	1.44	1.42	1.41	1.39	1.39
PPT_08	1.13	1.13	1.12	1.11	1.10
PPT_09	1.23	1.21	1.19	1.17	1.15
PPT_10	1.10	1.09	1.08	1.07	1.07
PPT_11	1.12	1.12	1.06	1.00	0.95
PPT_stp_L	1.01	1.01	1.01	1.01	1.01
PPT_stp_R	1.06	1.06	1.05	1.05	1.04
TP_03	0.89	0.89	0.88	0.88	0.88
TP_04	1.00	0.99	1.00	1.00	1.00
TP_05	0.93	0.92	0.93	0.93	0.93
TP_06	0.86	0.85	0.85	0.85	0.85
TP_07	0.35	0.36	0.37	0.37	0.38

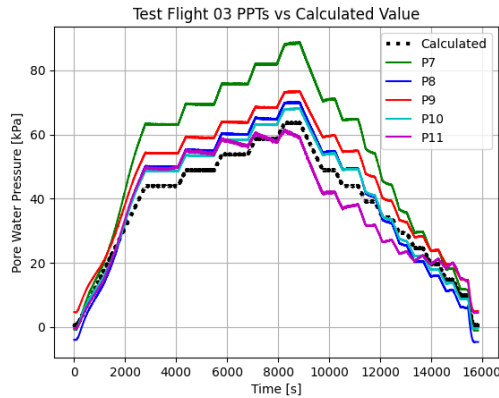


Figure 3.2 Sensor data of PPT 7 to versus factors used.

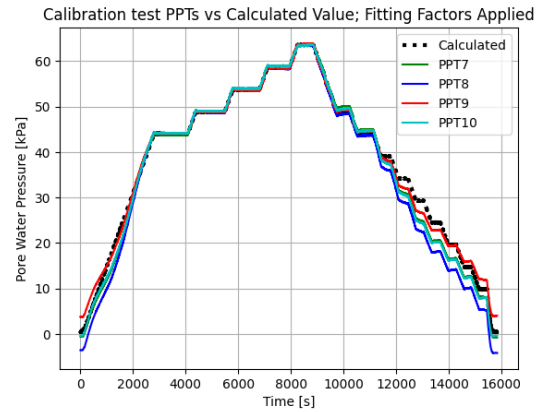


Figure 3.3 Calibrated pore pressures and fitting the theoretical pore water pressure value.

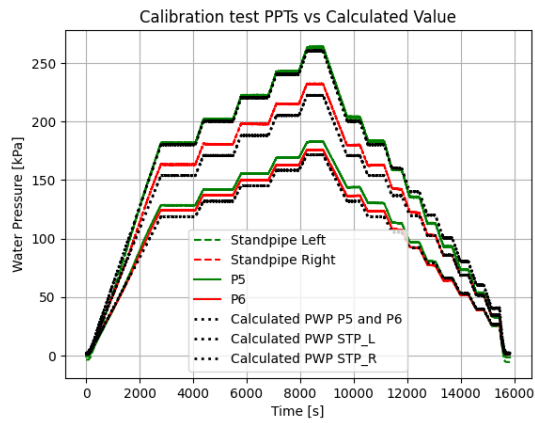


Figure 3.4 Sensor data of PPT 5 and 6 and standpipe left and right versus the theoretical pore water pressure value for PPT 5 and 6.

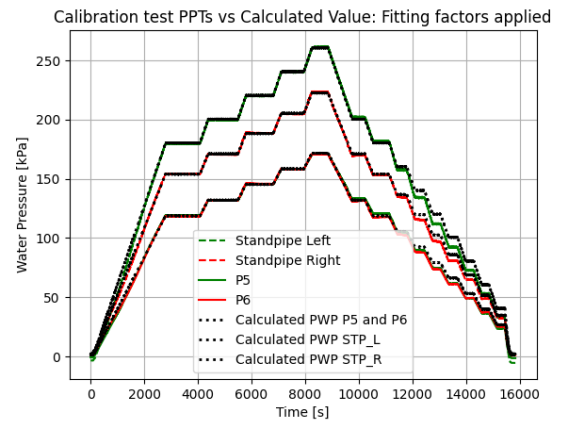


Figure 3.5 Calibrated pore pressures.

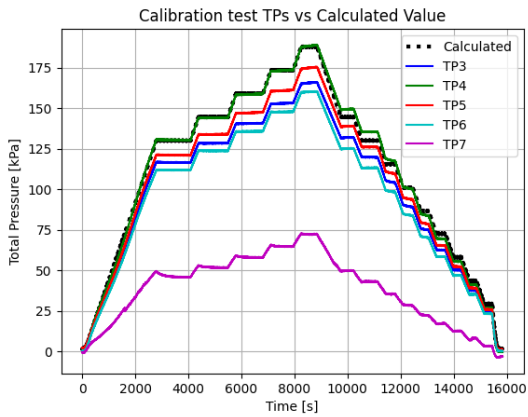


Figure 3.6 Sensor data of TP 3 to 7 versus the theoretical total pressure value for these sensor locations.

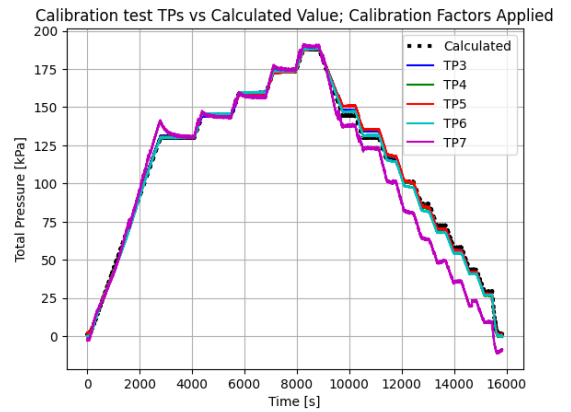


Figure 3.7 Calibrated total pressures.

4 Overview test characteristics

Test 1 and 2 are meant to reproduce test 10 of the POD series, and the consecutive tests had only minimal changes compared to that baseline. Therefore certain characteristics and outcomes of all tests are outlined in Table 4.1 below. A clear difference was found in the obtained density of the dike sand body. In this test series it was possible to use laser scanning methods to obtain the volume of the dike body, see Table 4.2, whereas this was not the case in the POD series. Therefore, the volume calculation methods that were used in the previous series, the conventional method and the camera video method, were also used to re-calculate the volume and density of the dike body in test 1, and compared to the value found with the laser scanning method.

The conventional method relies on the geometry of the design of the model (See Figure 4.1) combined with the measured height of the crest of the sand dike, and the width of the strongbox to obtain the volume of the sand dike. Relying on just one measurement and the assumption that the model could be built exactly as designed, it is the most uncertain method to obtain the volume. In the process of the POD series, therefore, another method was used as well, namely using the camera footage of the model in the centrifuge before testing to measure the area of the cross-section on the side and multiplying it with the width of the strongbox. This assumes that the side view of the model is representative of the rest of the dike body. For the laser scanning method, the model is laser scanned after the clay cover layer has been placed and consolidated, as well as after the sand dike body has been added. Using a software like CloudCompare, the distance between the point clouds obtained from these scans can be computed and converted to a total volume of the sand dike.

Table 4.3 shows the values calculated using the different methods. The camera video method shows very similar results to the laser scanning method, therefore these values can be mutually compared.

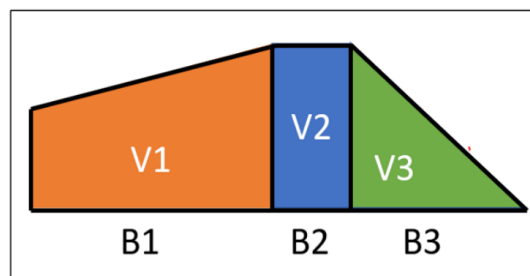


Figure 4.1 Geometry of the design of the cross-section of the sand dike body.

Table 4.1 Overview of parameters and phenomena in the tests in this series and reference test 10 from the previous series.

Phenomenon/parameter	Test number						
	10*	1	2	3	4	5	6
Cover layer thickness [mm]	28.8	31.7	32.0	33.7	32.0	31.6	32.0
Crest height [mm]	88.6	92.3	91.7	89.7	91.0	92.4	91.3
g-level at applying uplift conditions	80	80	80	130	80	80	80
Head p5 at uplift [m]	0.17	0.20	0.20	0.20	0.21	0.21	0.22
Head p5 above crest	No	No	No	No	No	No	No
Uplift cover layer according to D2 [mm]	0.15	0.28	1.09	-	0.55	0.14	0.89
Uplift cover layer according to D3 [mm]	0.25	-0.53	2.58	1.20	0.64	0.86	-0.47
Uplift cover layer according to D4 [mm]	0.50	-0.85	2.41	-0.22	-0.27	0	-0.44
Angle diagonal crack [degrees]	65	62	59	62	49	75	Top: 40 Bottom:77
Lateral cracks	no	yes	yes	yes	yes	no	yes
Sand-boils from diagonal crack	yes	yes	yes	yes	yes	yes	yes
Sand-boils from lateral cracks	no	no	yes	yes	no	no	no
Piping/erosion sand layer	slight	strong	slight	strong	strong	strong	strong
g-level at failure	91	113	112	130	110	113	110
Thorvane value [kg/cm ²]	5 - 6	5,7	6,5	7	7	7,6	7,5
Density [g/cm ³]	1.64**	1.72	1.75	1.74	1.70	1.81	1.73

* Part of the POD test series. repeated here for comparison.

** Based on the density value calculated using the 2023 camera video method.

Table 4.2 Relative density obtained from laser scans.

Test	Mass Sand [g]	Total volume [mm ³]	Density [g/cm ³]	Relative density	Void ratio
Test 1	4085	2371140	1.72	109	0.54
Test 2	4071	2322327	1.75	116	0.51
Test 3	4129	2370000	1.74	114	0.52
Test 4	4148	2443976	1.70	102	0.56
Test 5	4062	2246120	1.81	130	0.46
Test 6	4009	2321790	1.73	110	0.53

Table 4.3 Density calculations for test 1 using 2023 density calculation methods and comparing to test 10.

Test	Height [mm]	Mass Sand [g]	B1 [mm]	B2 [mm]	B3 [mm]	V1 [mm ³]	V2 [mm ³]	V3 [mm ³]	V-total [mm ³]	Density [g/cm ³]	Dr [%]	Void ratio
Camera video method												
Test 10	73.01	3855	97.17	22.61	119.18	1145624	330118.9	870177.4	2345920	1.64	87	0.61
Test 1	77.4516	4085	92.75	22.20	106.21	1211852	343843.7	822579.9	2378275	1.72	107	0.54
Conventional method												
Test 10	79.22	3855	90	30	110	1223460	475320	792200	2490980	1.55	59	0.71
Test 1	82.33	4085	90	30	110	1361970	493980	905630	2761580	1.48	36	0.79

5 Test 1: reproduction

5.1 General observations

Test 1 was meant to be a reproduction of Test 10 in the 2023 Reevediep centrifuge test series. The model was built the same, and the test was conducted following the same steps as the previous test. At a g-level of 80 uplift was induced and after increasing the g-level incrementally, failure was reached at a g-level of 113. The failure plane was similar as what was found in the previous test series, and the hinterland also showed similar behaviour. Nevertheless, there is a significant difference in g-level at dike failure between test 10, which failed at 91 g and test 1, which failed at 113 g.

5.2 Consolidation

The clay slurry was poured into the strongbox and consolidated at 1g at a force of 7kN. This is the same force as was used for test 10 in the previous series, which we aimed to reproduce. Figure 1 and Figure 2 show very similar force over time, going to 7 kN with 1 N/s. Since the area of the strongbox and thus the consolidation plate is 0.174 m² (0.2 mx0.87 m), there is a stress of 40.22 kPa on the clay layer.

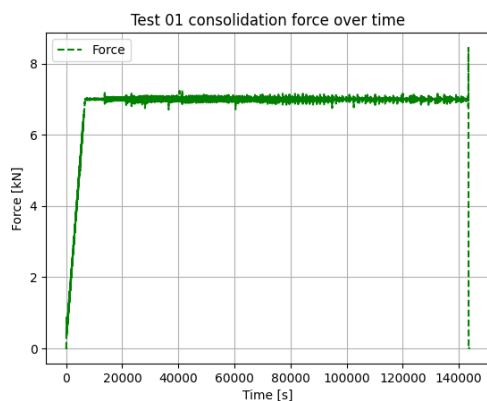


Figure 5.1 Consolidation curve of the clay prior to testing of reference test 10 from the previous series, force over time.

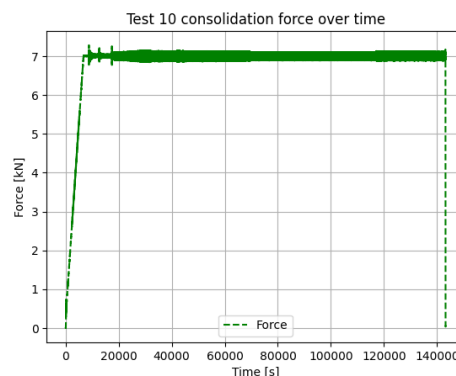


Figure 5.2 Consolidation curve of the clay to testing of test 1, force over time.

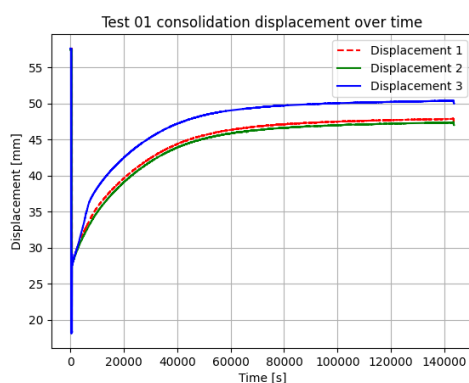


Figure 5.3 Consolidation curve of the clay prior to testing of test 1, displacement over time.

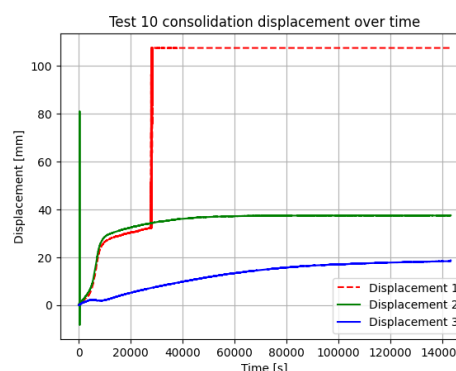


Figure 5.4 Consolidation curve of the clay prior to testing of reference test 10 from the previous series, displacement over time.

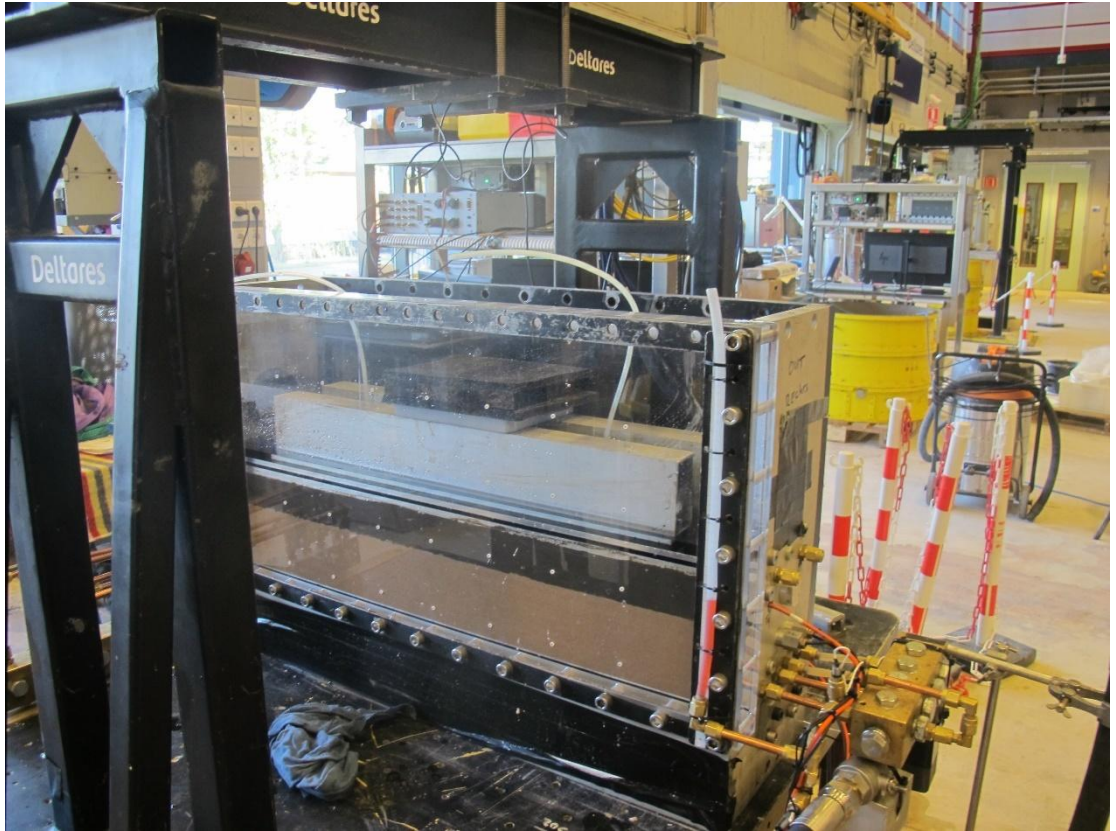


Figure 5.1 Set-up of the consolidation process of the clay cover, prior to testing in the strongbox.

A crack formed after removing the consolidation plate. It was fixed by filling it with Cebo Drill Grout using a syringe. It is a low-permeability, plastic material when it hardens and was used in a similar situation with a good outcome in Test 2 in the previous series of centrifuge tests. Therefore, no adverse effects of the crack were expected.

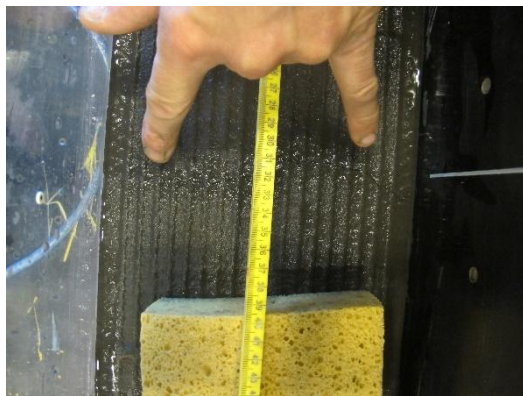


Figure 5.2 Crack observed in clay cover layer after removing consolidation plate.

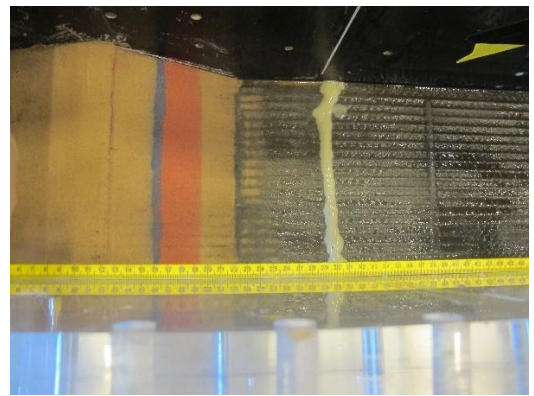


Figure 5.3 Crack filled with drill grout.

5.3 Centrifuge test

5.3.1 Preliminary analysis and commentary on the data

The hydraulic head in the sand layer was raised by stepwise raising the plunger. The insured 33 kPa increase water pressure was reached. A lift of 22 mm of the plunger resulted a 15 kPa increase. Therefore, for each mm of lifting there is a 0.69 kPa increase in water pressure so the plunger was lifted by 57 mm to reach an increment of 33 kPa in water pressure. It should be noted that in test 10 a lift of 85 mm was needed to reach the same pressure increment. An additional lift of 10 mm was applied, bringing the total to 67 mm, to assure a visible uplift of the cover layer. Then, the g-level was increased towards the level of 91 which was the g-level at failure for test 10, but no failure occurred in this test until the g-level was further increased to 113. Figures 5.8 to 5.13 show data from the sensors in the strongbox. The PPTs and TPs are calibrated according to the methods laid out in **Error! Reference source not found. Error! Reference source not found.** The DCDTs were corrected (nulled) based on their respective starting value at t=0.

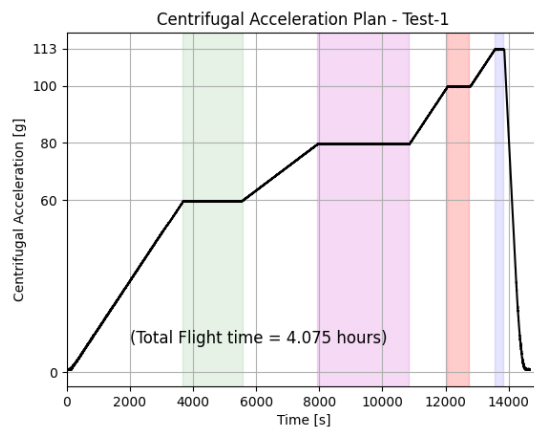


Figure 5.4 Centrifugal acceleration plan of Test 1.

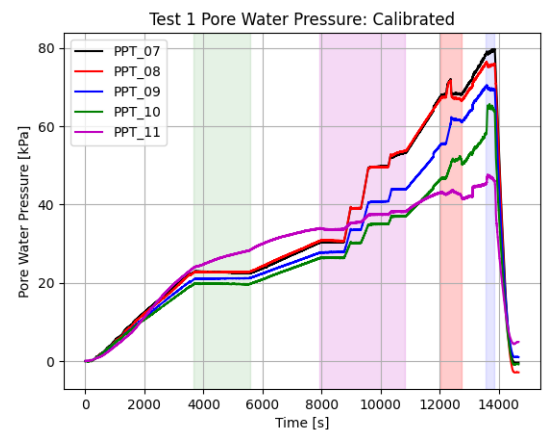


Figure 5.5 Pore water pressures at locations P7-P11 calibrated.

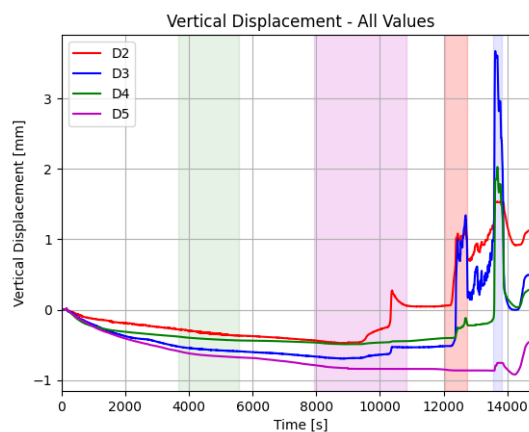


Figure 5.6 Vertical displacement of D2-D5, corrected.

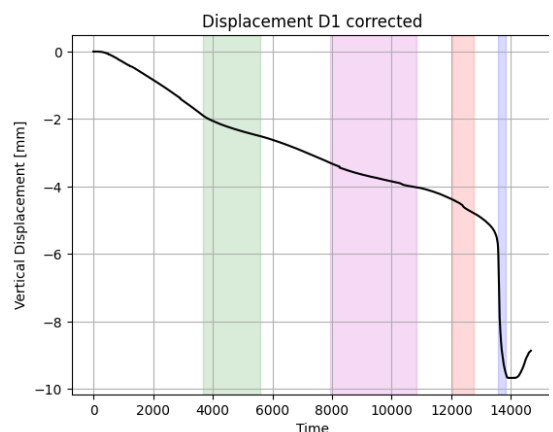


Figure 5.7 Vertical displacement of D1, corrected.

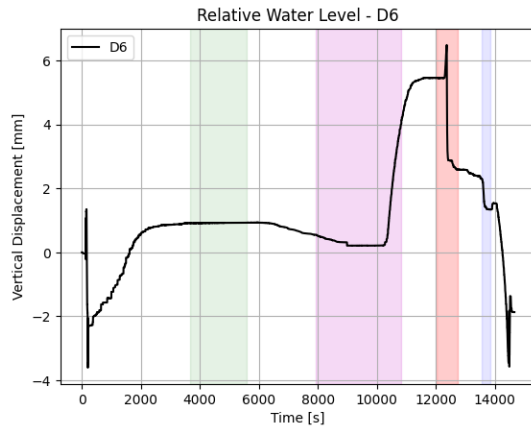


Figure 5.8 Relative water level according to D6, a floating sensor.

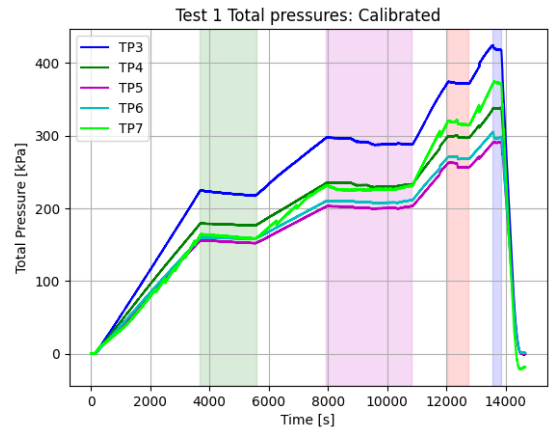


Figure 5.9 Total pressures measured at the bottom of the strongbox at locations TP3-TP7 (left to right).

5.3.2 Observations, notes and remarks

Pore water pressure values are similar to what was observed in reference test 10, but do suggest that the water on top of the clay cover layer and water in the sand were connected, already from the start of the test, since the PWP levels represent a water height that is higher than expected if only the water height in the sand was measured and coincide with the water height on top of the clay.

There was a gradient of the head in the sand from the start of the test until the head was increased at 80 g. The water level at the left standpipe was higher than on the right standpipe, and the gradient was seen in camera footage from colour difference in the sand. The free water depth on the cover clay layer was also larger than in reference test 10, since test 10 had extra height of the sand layer, making the top of the clay layer closer to the outlet which was at a fixed height. There is no current hypothesis on the influence of the higher free water depth on top of the clay layer on the stability of the dike.

5.3.3 Uplift

Uplift was initiated at a g-level of 80, when the hydraulic head was 21.1 cm according to the standpipe visible on camera footage, and 20 cm according to PPT 5 as shown in **Error! Reference source not found.** below. Uplift was most present at D2 and D3 as shown in **Error! Reference source not found.**, but reached a maximum length of 27.73 cm at a g-level of 100.

Table 5.1 Overview of uplift values for test 1 from photo analysis.

	G-level	Hydraulic head [cm]	Max uplift length [cm]	Max uplift height [mm]
Initial uplift	80	21.1		
Max uplift length @ 80g	80	21.8	14.26	~0.1
Max uplift length @ 100g	100	23.8	27.73	2.4

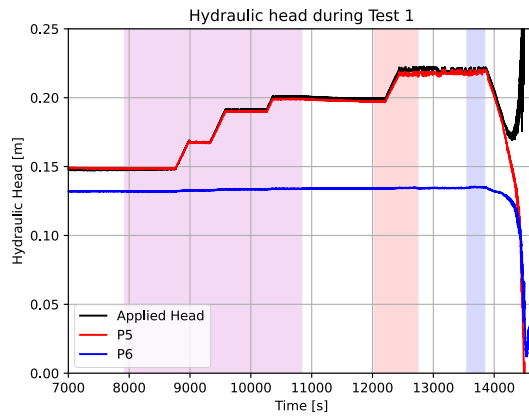


Figure 5.10 Hydraulic head during uplift and failure back calculated from pore water pressure transducers Standpipe left, PPT5 and PPT6, corrected for the position of the sensors.

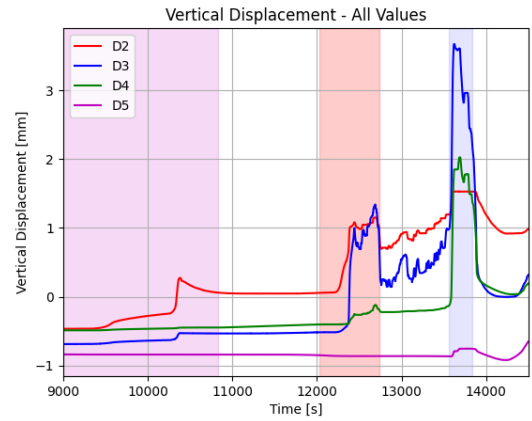


Figure 5.11 Vertical displacement during uplift and failure.

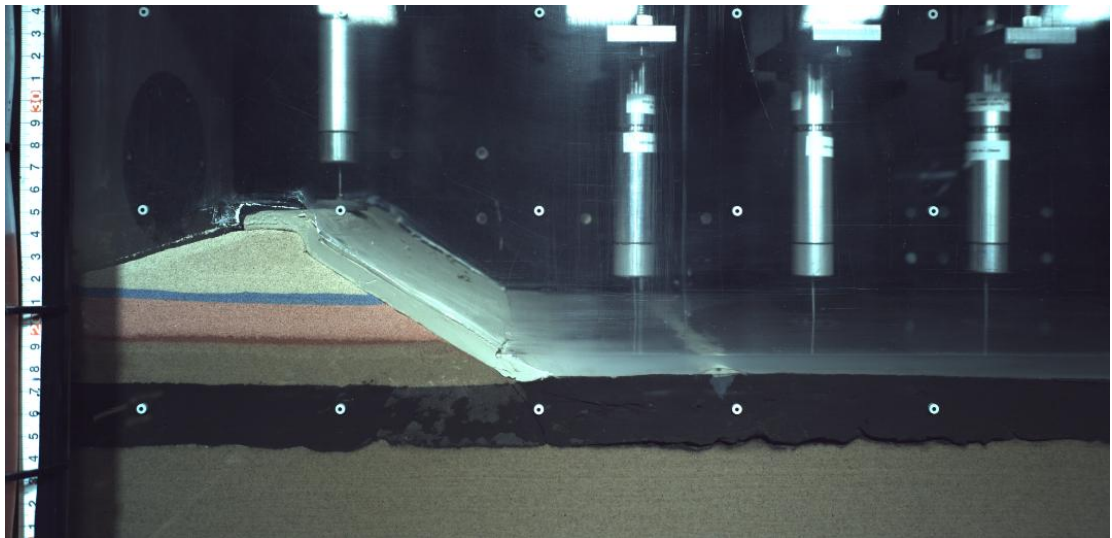


Figure 5.12 Maximum uplift of the clay cover layer.

5.3.4 Failure

Failure occurred at a g-level of 113. As seen in Figure 5.13, there is a large sliding plane and a smaller one on its right side. The clay cover layer is lifted up between D2 and D3, but no cracking of the layer occurred due to lateral pressure of the failing dike body.

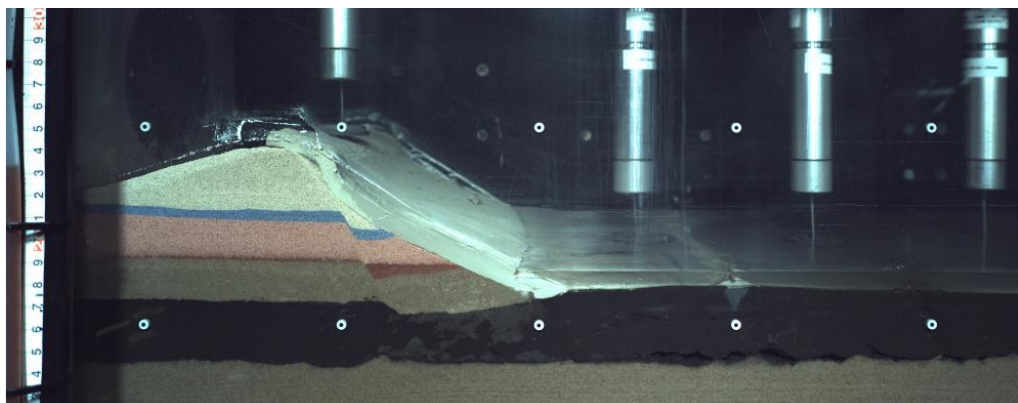


Figure 5.13 Failure of the dike body during the experiment.

5.4 Post-test observations

5.4.1 Sliding planes, sand-boils, piping

The two sliding planes identified in Figure 5.13 are also recognised in the clay layer after excavation of the dike as seen in Figure 5.14 below. Sand boils appeared at the diagonal crack at the toe and at 40 cm from the left side of the strongbox (**Error! Reference source not found.** and **Error! Reference source not found.**). Full excavation of the clay layer shows sand erosion under the clay (see Figure 5.17), including erosion around the toe and at 40 cm, where the other sand boil was found.

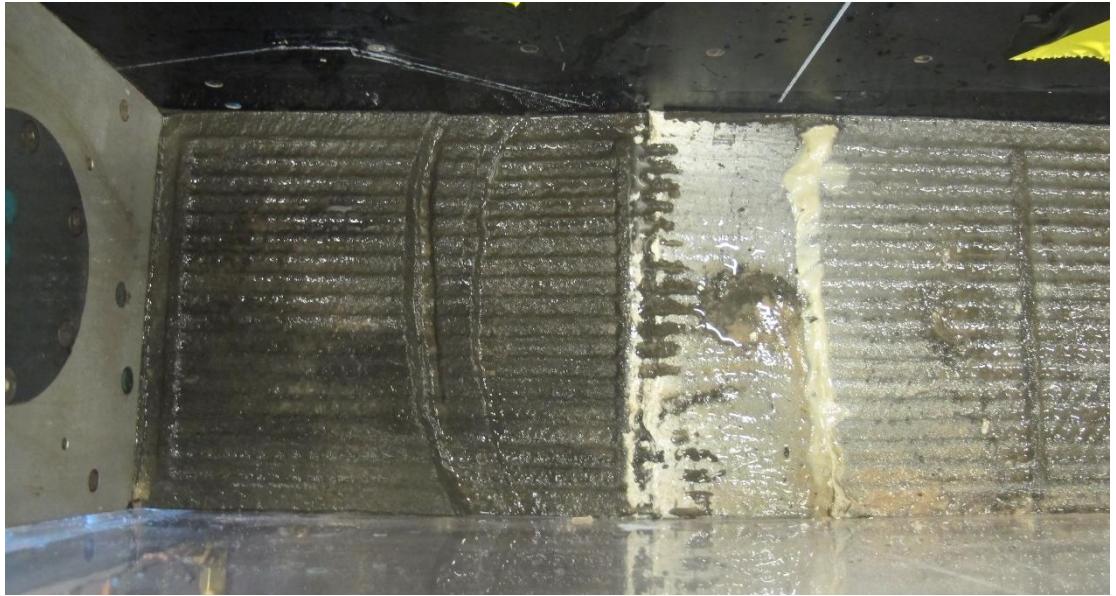


Figure 5.14 Sliding planes visible in the clay after removing the sand dike body.

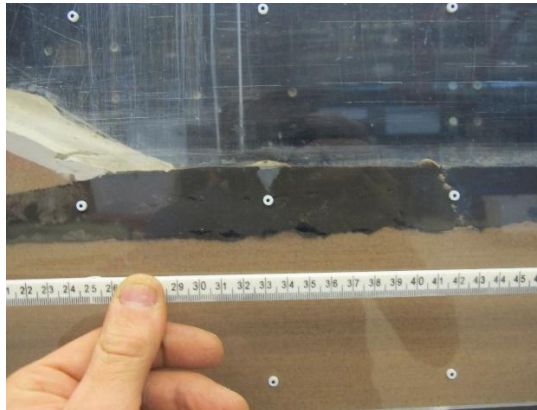


Figure 5.15 Close-up picture of the cover layer showing cracks, a sand boil and displacement.



Figure 5.16 Close-up picture of the excavated sand boil at 40 cm from the left side of the strongbox.



Figure 5.17 Sand erosion visible after excavation of the clay cover layer.

5.4.2 Laser scan

The dike model was laser scanned before and after the experiment. In Figure 5.18, the model after the experiment is shown, with a colour projection showing the displacement compared to the laser scan before the test. Blue shows sinking (at the crest) and red shows upward displacement (at the toe).

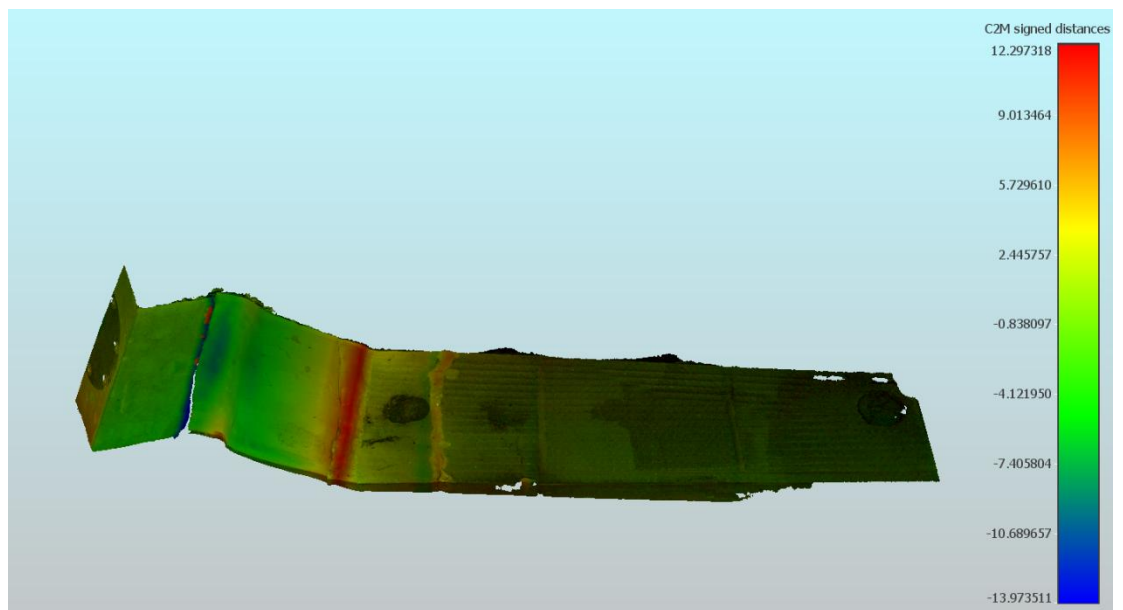


Figure 5.18 Laser scan of dike body with clay layer after failure of the dike. Distance computed [mm] in reference to the dike before failure. Blue shows sinking (at the crest) and red shows upward displacement (at the toe).

6 Test 2: reproduction

6.1 General observations

Test 2 was a reproduction of test 1, thereby aiming to reproduce test 10 of the POD series. Consolidation force was applied more slowly this time, and the consolidation plate was taken off more slowly, meaning to avoid cracking of the clay again, which was successful. The test was conducted in the same way as test 1, and very similar patterns were found. Uplift occurred at 80 g, with a 57 mm head increase, and failure happened at 112 g.

6.2 Consolidation

The consolidation force was applied with 0.1 N/s until 7000 N, which is a slower increase, as shown in **Error! Reference source not found.** and longer overall consolidation time than applied in test 1. This time, no cracking of the surface occurred. This method will be used in all further tests. Consolidation data of the other tests is available but not plotted from this chapter on unless specifically relevant.

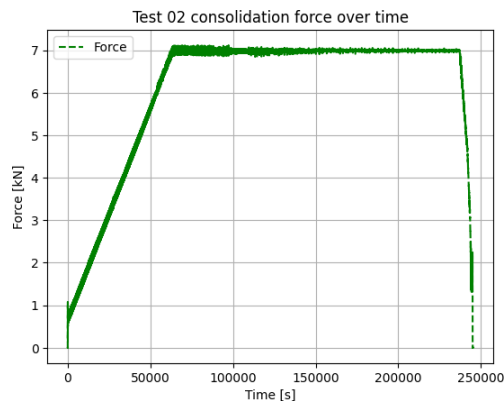


Figure 6.1 Consolidation curve of test 2, force over time.

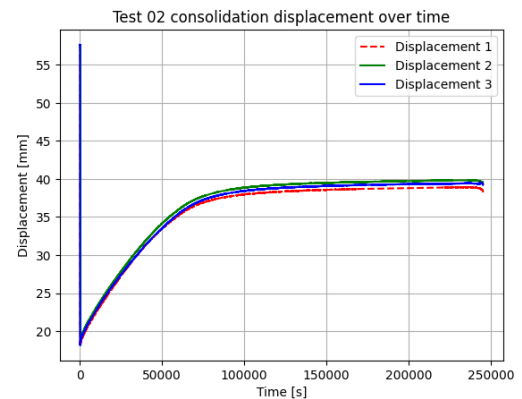


Figure 6.2 Consolidation curve over of test 2, displacement over time.

6.3 Centrifuge test

6.3.1 Preliminary analysis and commentary on the data

Test 2 follows same pattern as test 1. At 80 g, uplift is instigated by applying a hydraulic head increase of +57mm in three steps. After uplift, a crack at the toe appeared.

PPT10 shows a drop in pressure around the peak of the vertical displacement in D3 and D4, at about 10500 seconds in the experiment. At the location of PPT10, a sand boil was found after the experiment which could explain the sudden drop in pressure.

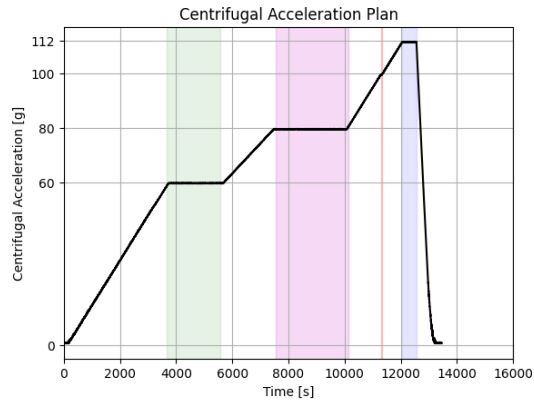


Figure 6.3 Centrifugal acceleration plan of Test 2.

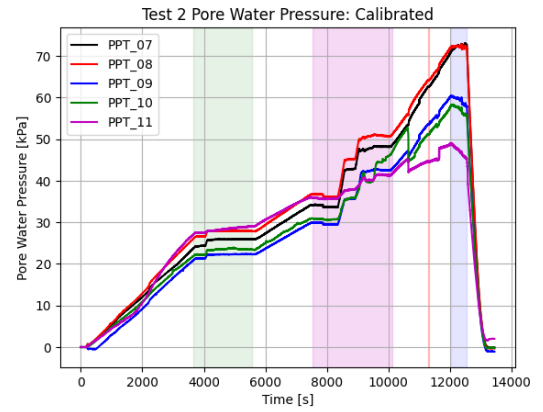


Figure 6.4 Pore water pressures at locations P7-P11 calibrated.

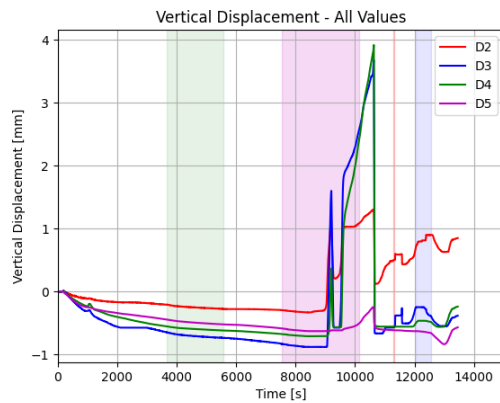


Figure 6.5 Vertical displacement of D2-D5, corrected.

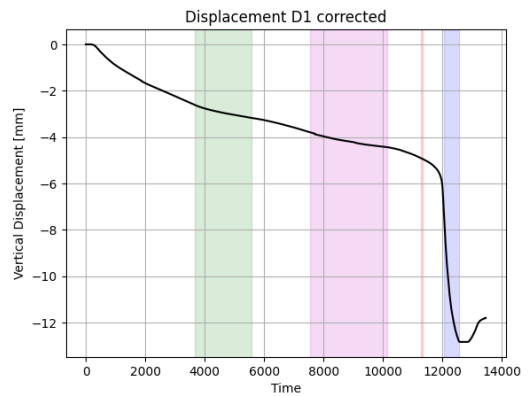


Figure 6.6 Vertical displacement of D1, corrected.

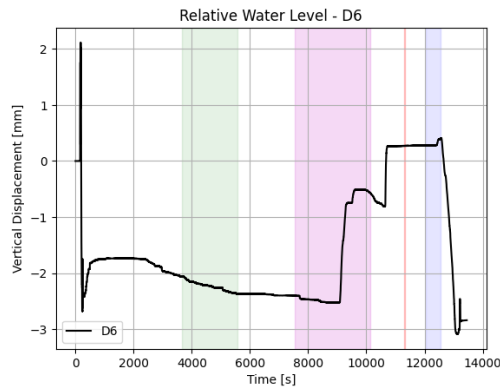


Figure 6.7 Relative water level according to D6, a floating sensor.

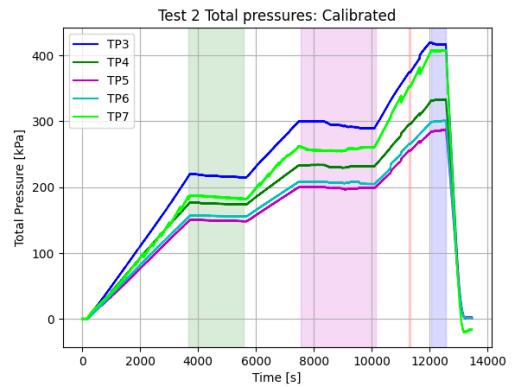


Figure 6.8 Total pressures measured at the bottom of the strongbox at locations TP3-TP7 (left to right).

6.3.2 Observations, notes and remarks

Vertical displacement sensors show larger amplitudes than in test 1, although the parameters of these two tests are the same. It seems that maximum displacement of sensors D3 and D4 was not reached before the end of the waiting time at 80g.

6.3.3 Uplift

As shown in Table 6.1, the first signs of uplift are already visible after increasing the hydraulic head for the first time, see **Error! Reference source not found.** Maximum uplift length is reached after the third hydraulic head increased, still at 80g. The uplift length is longer than found in Test 1 and as seen in **Error! Reference source not found.**, sensor D4 shows significant uplift.

Table 6.1 Overview of uplift values for test 2 from photo analysis.

	g-level	Hydraulic head [cm]	Max uplift length [cm]	Max uplift height [mm]
Initial uplift	80	19.4		
Max uplift length @ 80g	80	22.4	40.59	3.8

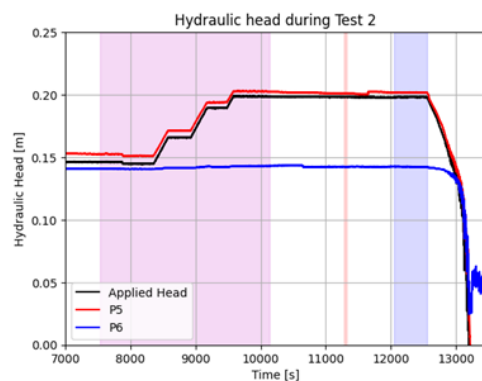


Figure 6.9 Hydraulic head during uplift and failure back calculated from pore water pressure transducers Standpipe left, PPT5 and PPT6, corrected for the position of the sensors.

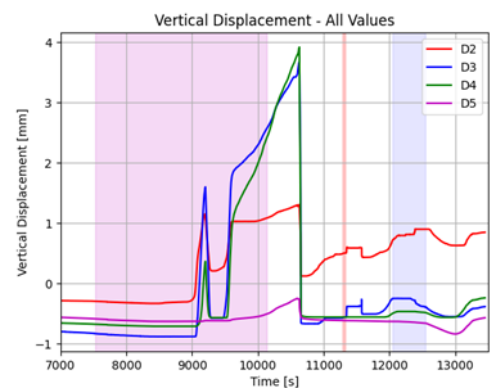


Figure 6.10 Vertical displacement during uplift and failure.

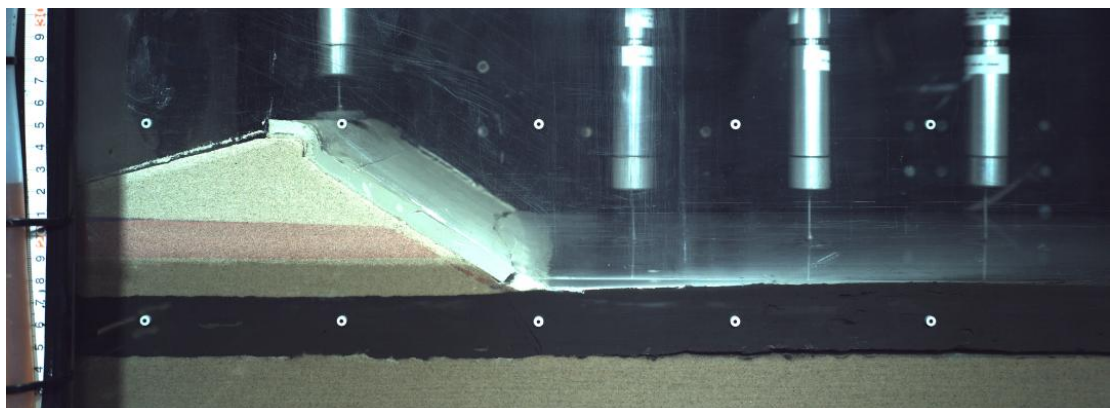


Figure 6.11 Maximum uplift of the clay cover layer.

6.3.4 Failure

Failure occurred at 112 g. Two sliding planes are visible in the side camera footage as shown in Figure 6.12. The diagonal crack at the toe that was still visible in Figure 6.11 has been closed after failure and the cover layer is lifted up around D3. No cracking of the cover layer at the surface is seen.

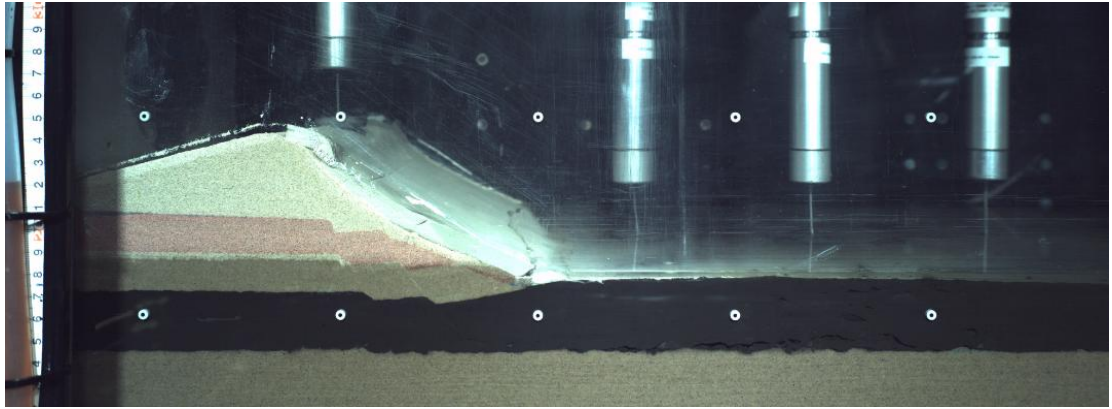


Figure 6.12 Failure of the dike body during the experiment.

6.4 Post-test observations

6.4.1 Sliding planes, sand-boils, piping

Error! Reference source not found. and **Error! Reference source not found.** show multiple sliding planes in a similar shape as seen in test 1. Several sand boils were found, mostly along the back wall, and the clay layer had many lateral cracks.

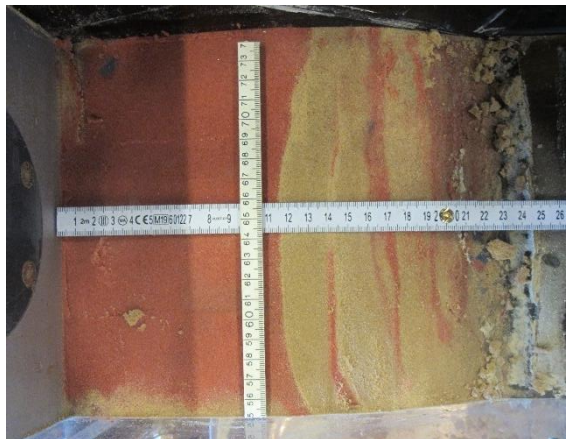


Figure 6.13 Sliding planes visible in the coloured sand layers after partial excavation of the dike.



Figure 6.14 Sliding planes visible in the clay under the dike after excavation

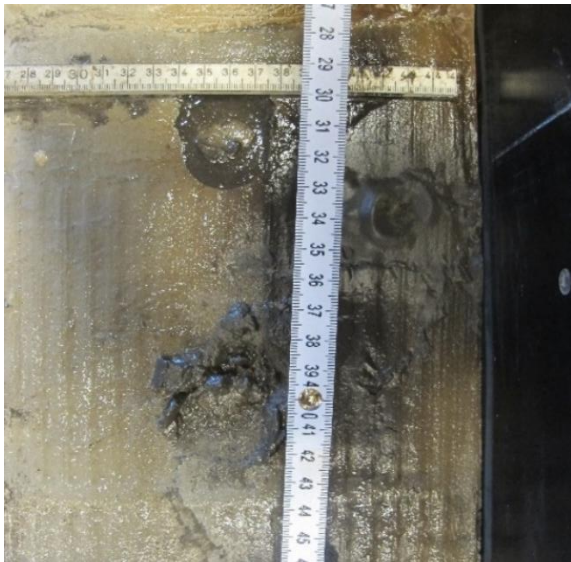


Figure 6.15 Sand boil at 33 cm, near the toe, at the back wall.

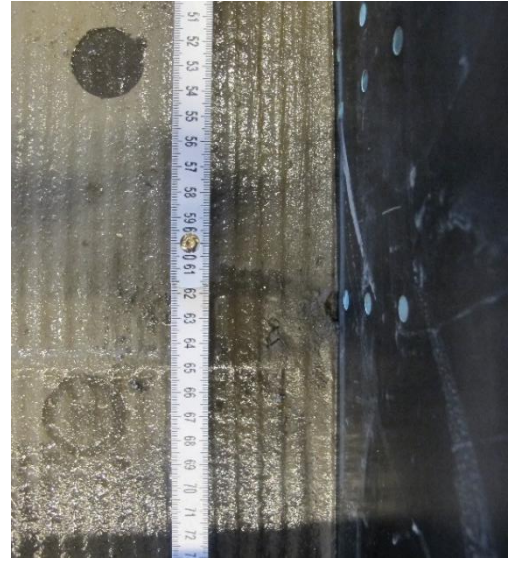


Figure 6.16 Sand boil at 65 cm from left side of strongbox at the back wall.

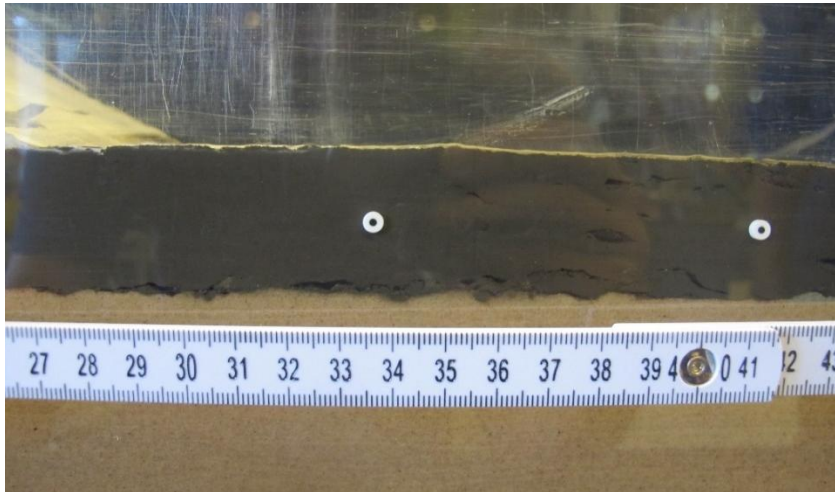


Figure 6.17 Lateral cracks in the clay cover layer.



Figure 6.18 Sand boil at 37 cm from left side of the strongbox, seen after partial excavation of the clay layer. Lateral crack visible at top of the picture



Figure 6.19 Sand erosion visible in the sand under the clay layer, especially along the back wall.

6.4.2 Laser scan

Comparing laser scans from before and after the experiment show similar results as found in Test 1. At the crest there is negative displacement, settlement, and at the toe there is positive displacement.

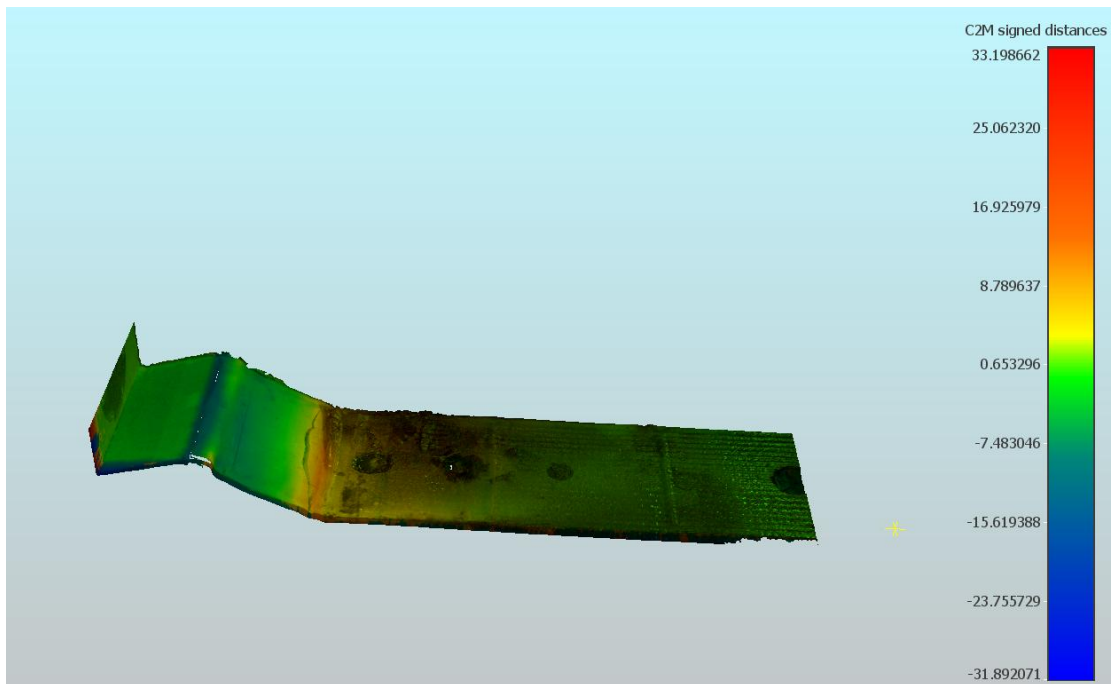


Figure 6.20 Laser scan of dike body with clay layer after failure of the dike. Distance [mm] computed in reference to the dike before failure. Blue shows sinking (at the crest) and red shows upward displacement (at the toe).

7 Test 3: without uplift

7.1 General observations

This experiment aims to assess the influence of the uplift phenomenon on slope stability. The model and test plan was the same as in test 1 and 2, however instead of increasing the free water head at 80 g, the head was kept the same and there was a wait time of 15 minutes which is the time it normally takes to increase head and stabilise the sensors. Then, g-level was increased until failure occurred or the maximum g-level was reached. At the maximum possible g-level of 130, still no failure was detected. Since uplift is the only significant difference between test 3 and test 1 and 2, the lack of failure until 130 g suggests that uplift negatively affects the stability of the slope. To verify this, after a wait time at 130 g, the head was increased, which ultimately resulted in failure of the slope.

7.2 Centrifuge test

7.2.1 Preliminary analysis and commentary on the data

Uplift and failure occurred at the same g-level. PPT sensor data shows an almost round curve after the uplift is applied and failure is instigated, whereas the DCDTs show two peaks at D3 and D4. Total pressures all show an increasing trend in the 130 g-level period, except for TP3, where there is a decrease in pressure.

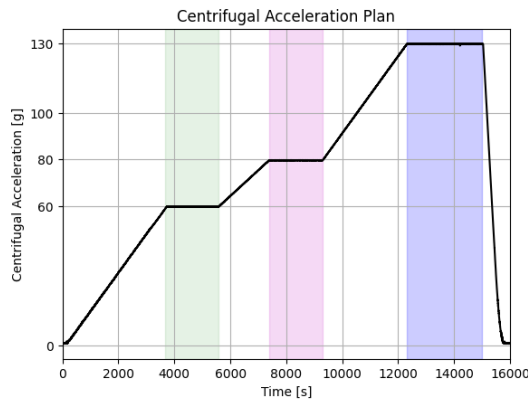


Figure 7.1 Centrifugal acceleration plan of Test 2.

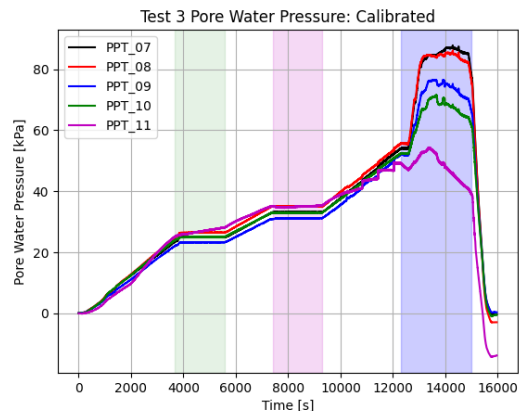


Figure 7.2 Pore water pressures at locations P7-P11 calibrated

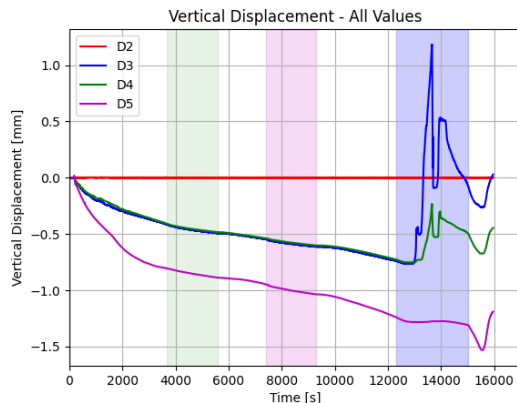


Figure 7.3 Vertical displacement of D2-D5, corrected.

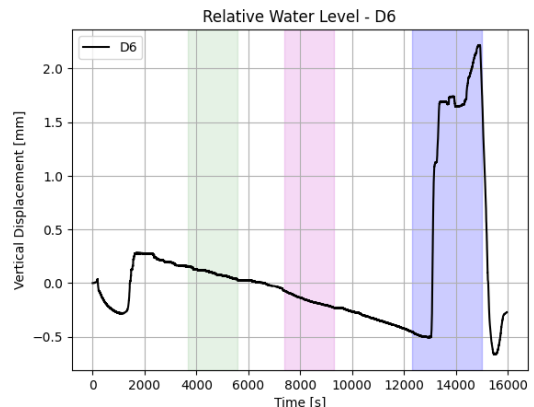


Figure 7.4 Relative water level according to D6, a floating sensor.

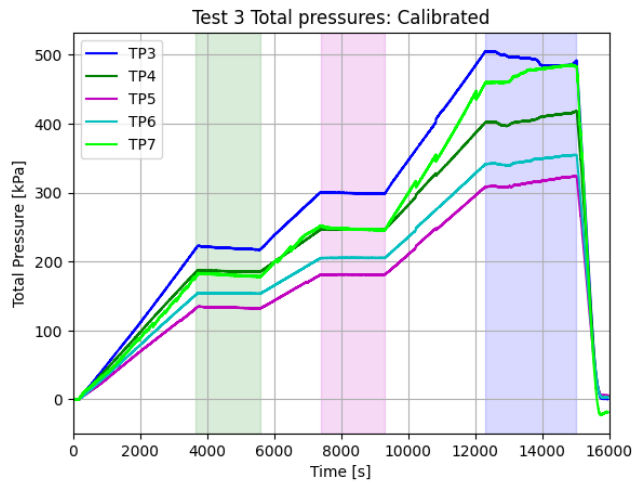


Figure 7.5 Total pressures measured at the bottom of the strongbox at locations TP3-TP7 (left to right).

7.2.2 Observations, notes and remarks

Sensors D1 and D2 were stuck or unconnected so there is a gap in the sensor data. When no failure was observed at 130 g, the conditions for uplift were applied. However, the dike did not fail immediately after applying the hydraulic head. While deciding what to do, and waiting longer than usual, the dike ultimately collapsed. This raises the question whether other tests would have had failure of the dike at a lower g-level if the waiting time had been longer.

7.2.3 Uplift

This test was originally planned without uplift. At 130 g, the head was increased anyway, showing initial uplift halfway through applying the second step, see Figure 7.6, at around 13000 seconds.

Table 7.1 shows that the maximum uplift length was 39.18 cm, which is similar to test 2. Figure 7.7 shows that uplift is found at D3 and D4, which supports the long uplift length derived from photo analysis. After initial uplift occurred, a sand boil formed from the crack at the toe and the toe of the dike started eroding more rapidly.

Table 7.1 Overview of uplift values for test 3 from photo analysis.

	G-level	Hydraulic head [cm]	Max uplift length [cm]	Max uplift height [mm]
Initial uplift	130	20.1		
Maximum uplift	130	20	39.18	3.6

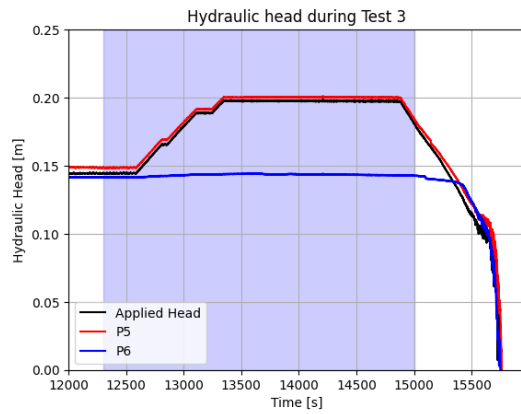


Figure 7.6 Hydraulic head during uplift and failure back-calculated from pore water pressure transducers Standpipe left, PPT5 and PPT6, corrected for the position of the sensors

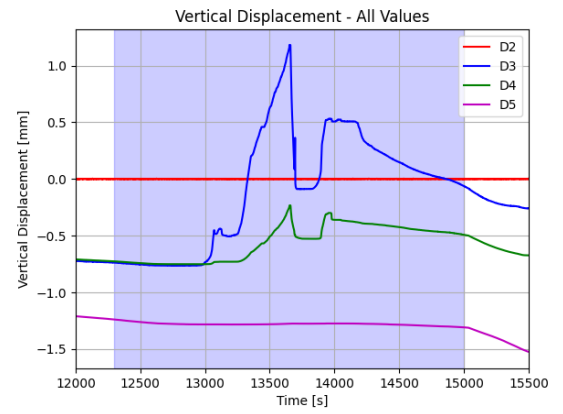


Figure 7.7 Vertical displacement during uplift and failure.

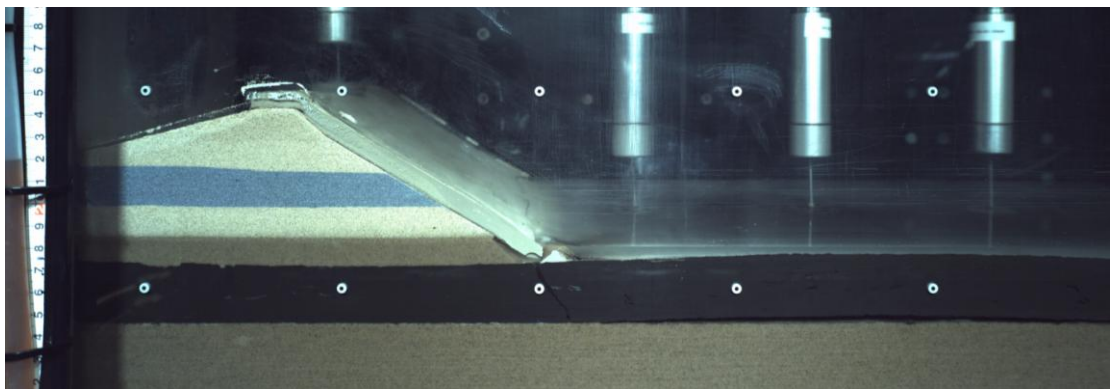


Figure 7.8 Maximum uplift of the clay cover layer.

7.2.4 Failure

Figure 7.9 shows two sliding planes and an eroded toe. The deformation of the dike body did not move the clay layer enough to fully close the crack at the toe. Around D3, the cover layer is lifted up but no cracks formed at the surface.

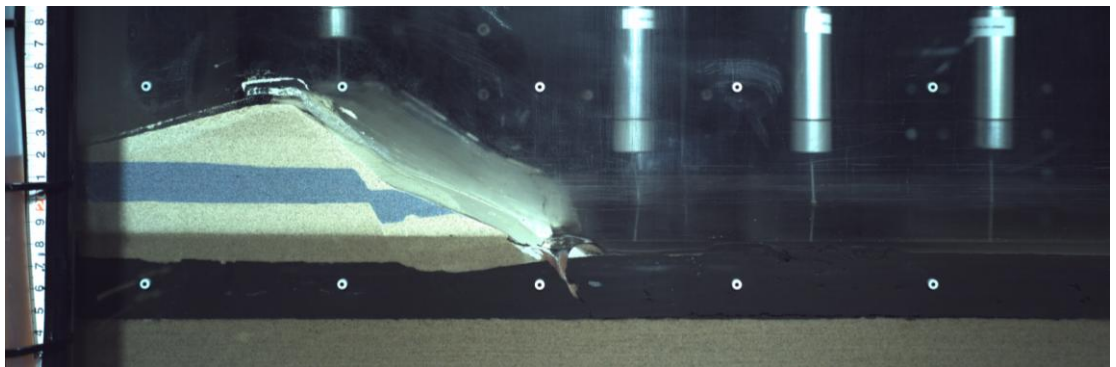


Figure 7.9 Failure of the dike body during the experiment.

7.3 Post-test observations

7.3.1 Sliding planes, sand-boils, piping

Partial excavation of the sand dike body shows two sliding planes in **Error! Reference source not found.**. Some sand boils are also visible along the glass front wall and around 40 cm. Lateral cracks and lamination are shown in *Figure 7.11*. *Figure 7.12* shows sand erosion between 27 and 47 cm from the left side wall. In *Figure 7.13* some more erosion in the sand is shown along the glass front wall.

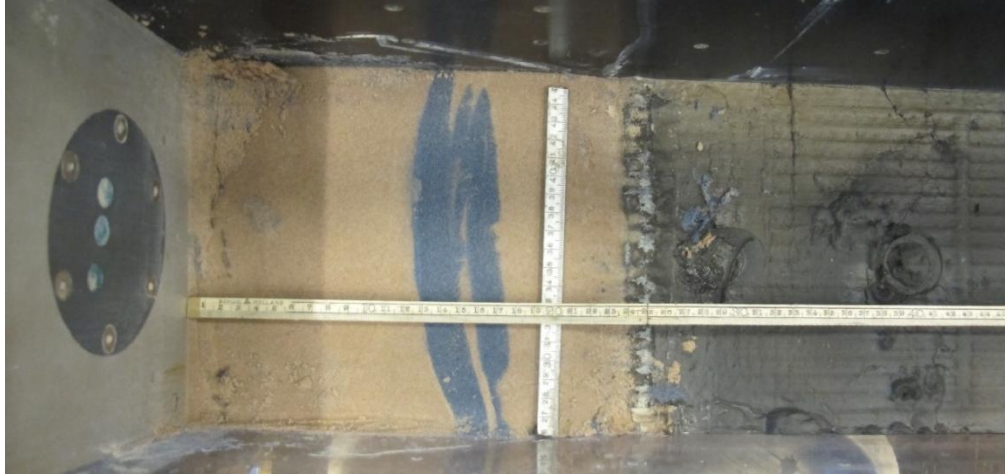


Figure 7.10 Sliding planes visible in the partially excavated coloured sand layer. Sand boils visible at 40 cm and along the glass side wall.



Figure 7.11 Lateral cracks in the clay layer.



Figure 7.12 Sand erosion between 27 cm and 47 cm from the left side.



Figure 7.13 Sand erosion below the clay layer.

7.3.2

Laser scan

This laser scan analysis shows some more negative vertical displacement, settlement, at the inner crest of the levee and in at the centre. This is in line with the shape of the sliding planes, which is curved. There is a second band of red for positive vertical displacement after the toe, which is supported by the findings in the LVDT sensor data.

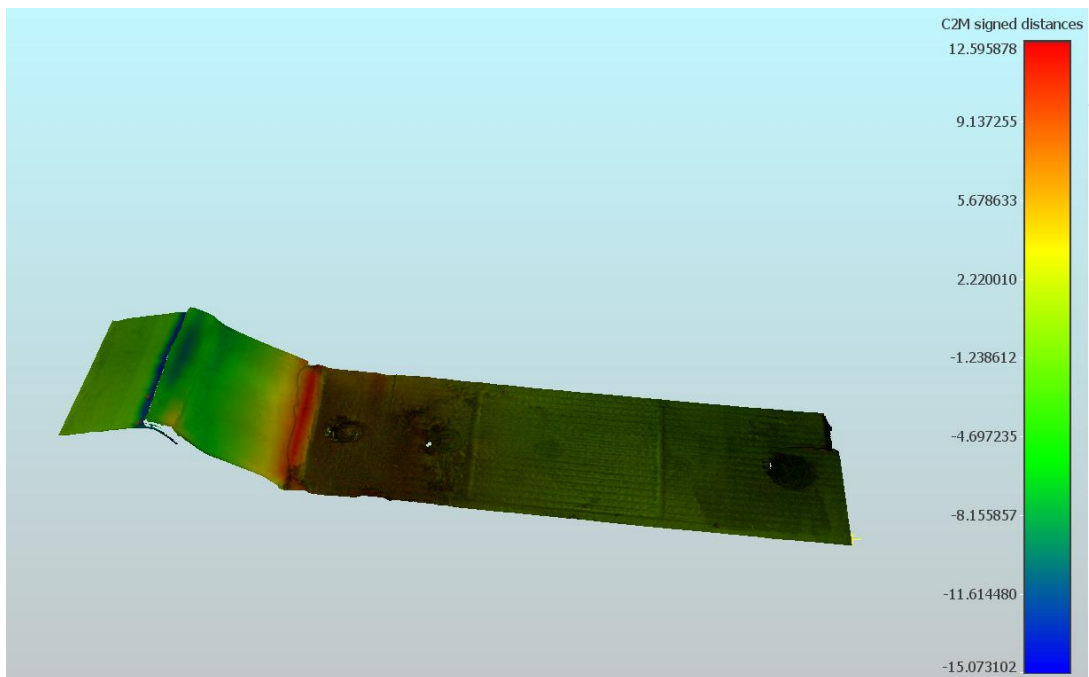


Figure 7.14 Laser scan of dike body with clay layer after failure of the dike. Distance [mm] computed in reference to the dike before failure. Blue shows settlement at the crest and red shows upward displacement at the toe.

8 Test 4: ditch close – narrow

8.1 General observations

This test was conducted with ditch configuration close – narrow. The length of the uplifted zone was constricted by the location of the ditch. The g-level at which failure was observed was similar to that in test 1 and 2. The narrow ditch did not seem to have a significant impact on the stability of the levee. The largest vertical displacement is seen at D3, which is located at the bottom of the ditch.

8.2 Centrifuge test

8.2.1 Preliminary analysis and commentary on the data

Pore water pressure and total pressure look very similar to what was seen in the previous 3 tests. The incorporation of the ditch is mainly reflected in sensor data from the DCDTs, *Figure 8.3*. Failure occurred at 110 g, which is very similar to test 1 and 2, which could mean that a small ditch near the toe of the levee does not influence the stability of the dike body significantly.

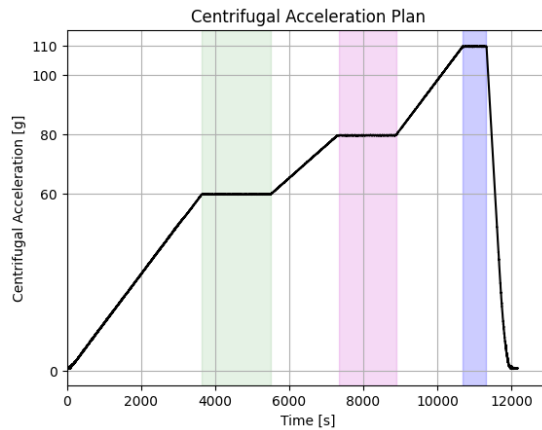


Figure 8.1 Centrifugal acceleration plan of Test 4.

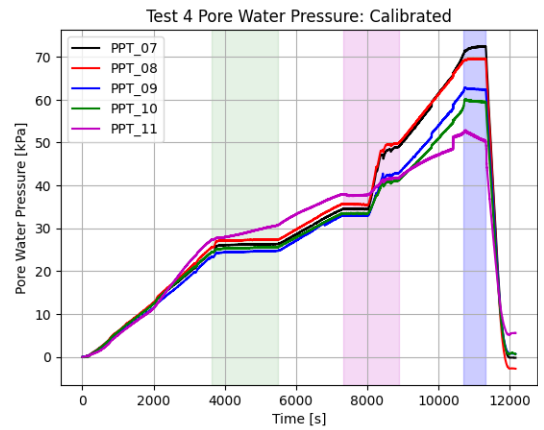


Figure 8.2 Pore water pressures at locations P7-P11 calibrated.

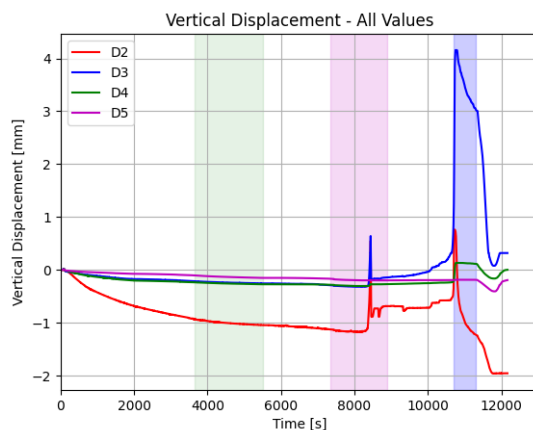


Figure 8.3 Vertical displacement of D2-D5, corrected.

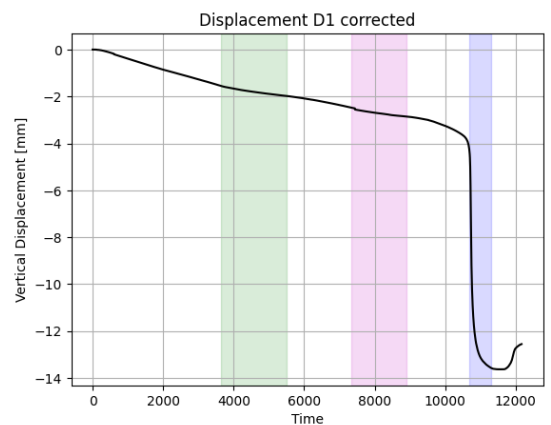


Figure 8.4 Vertical displacement of D1, corrected.

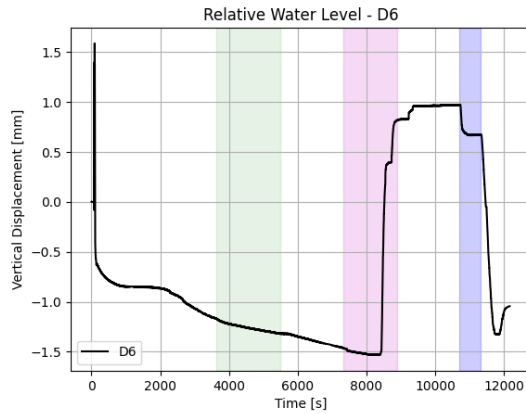


Figure 8.5 Relative water level according to D6, a floating sensor.

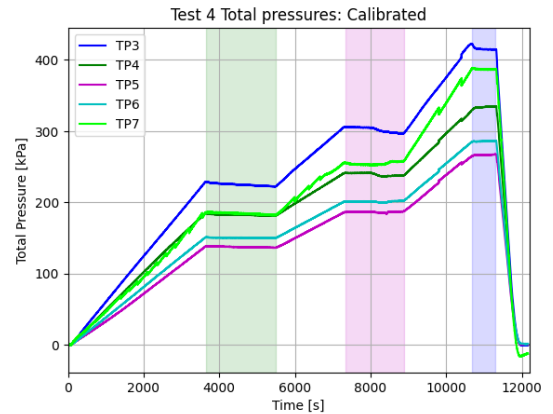


Figure 8.6 Total pressures measured at the bottom of the strongbox at locations TP3-TP7 (left to right).

8.2.2 Observations, notes and remarks

The largest vertical displacement is found at D3, which is located on the right side of the ditch. When looking at Figure 8.10, even more vertical displacement would have been found closer to the ditch on the right side.

8.2.3 Uplift

Uplift occurred after applying the second step of hydraulic head increase. The maximum uplift length was 17.58 cm. There is a sharp peak at D2, which is at the bottom of the ditch.

Table 8.1 Overview of uplift values for test 4 from photo analysis.

	G-level	Hydraulic head [cm]	Max uplift length [cm]	Max uplift height [mm]
Initial uplift	80	19.7		
Maximum uplift	80	22.7	17.58	2.0

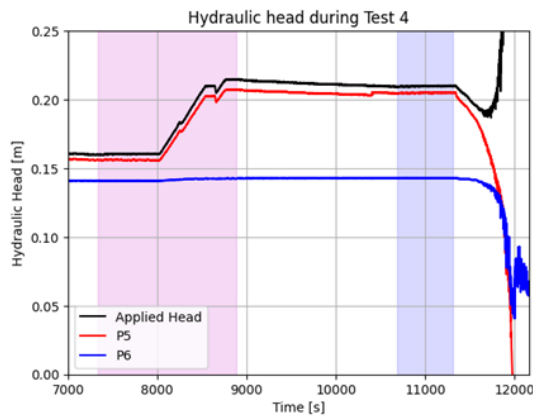


Figure 8.7 Hydraulic head during uplift and failure back-calculated from pore water pressure transducers Standpipe left, PPT5 and PPT6, corrected for the position of the sensors.

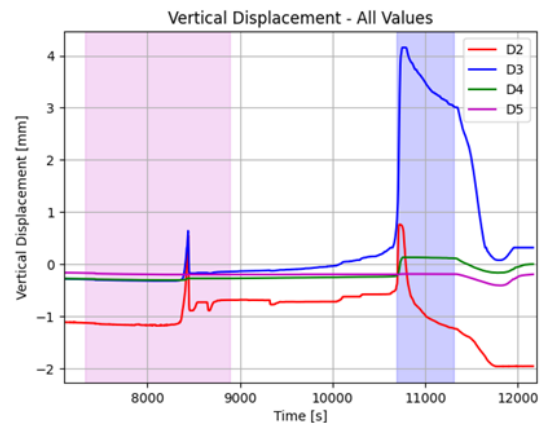


Figure 8.8 Vertical displacement during uplift and failure

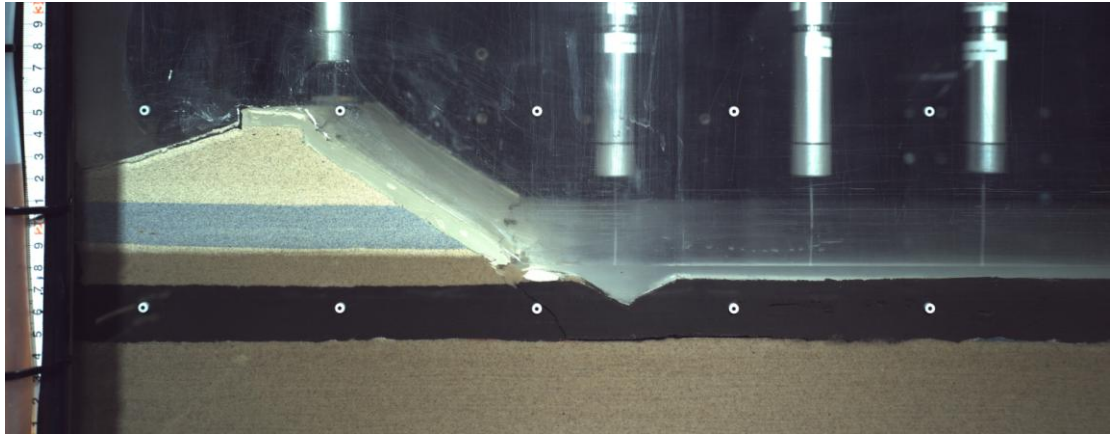


Figure 8.9 Maximum uplift of the clay cover layer.

8.2.4 Failure

The dike body failed at 110 g, in multiple clearly recognisable sliding planes. The failure of the dike body drove lateral movement in the clay layer and caused the right side of the ditch to lift up significantly, and form a crack at the surface. The diagonal cracks at the toe were almost completely closed. Besides the deformations near the ditch, differences in the failure modes found in test 1, 2 and 3 seem to be small.

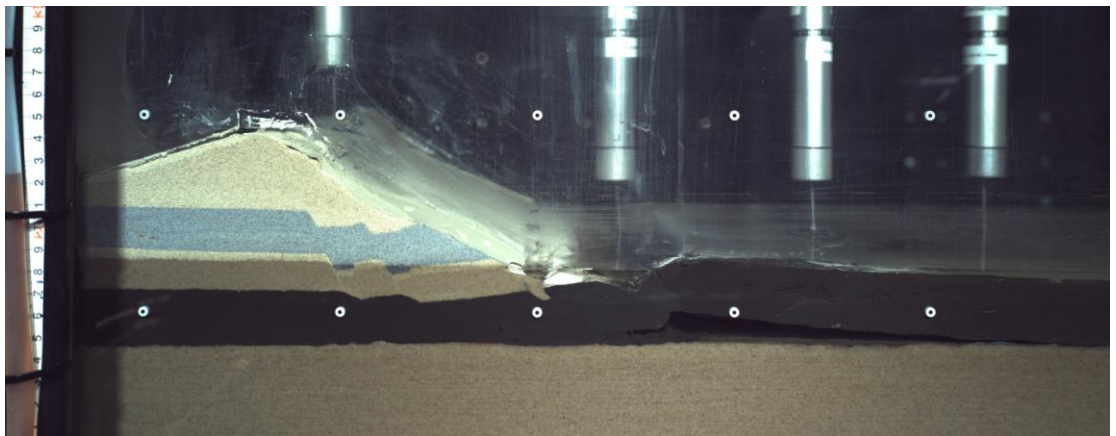


Figure 8.10 Failure of the dike body during the experiment.

8.3 Post-test observations

8.3.1 Sliding planes, sand-boils, piping

Two distinctive sliding planes can be distinguished from the excavated dike body shown in Figure 8.11 and Figure 8.12. The sand boil at the toe already seen from the side camera is clearly recognisable after excavating the clay layer, and shown in Figure 8.15. Another sand-boil was discovered at a 40 cm distance from the left side wall, as shown in Figure 8.13. Figure 8.14 shows erosion in the sand below the clay.



Figure 8.11 Sliding planes visible in the partially excavated sand dike.



Figure 8.12 Sliding planes visible in the clay layer.



Figure 8.13 Sand erosion patterns in the hinterland, at the location of a sand boil (at 40 cm).



Figure 8.14 Sand erosion under the dike body.

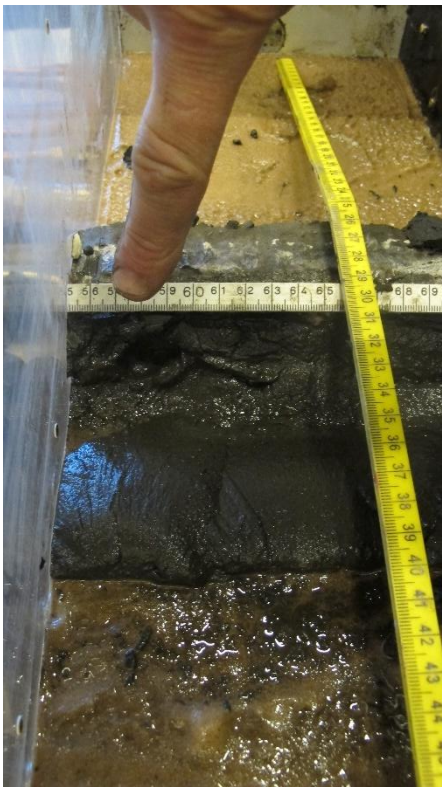


Figure 8.15 Front view of partially excavated sand-boil at the ditch.



Figure 8.16 Sand erosion at dike toe.



Figure 8.17 Lifted ditch bottom after dike failure.

8.3.2 Laser scan

Figure 8.18 shows the difference in elevation by the laser scans prior and after the test.

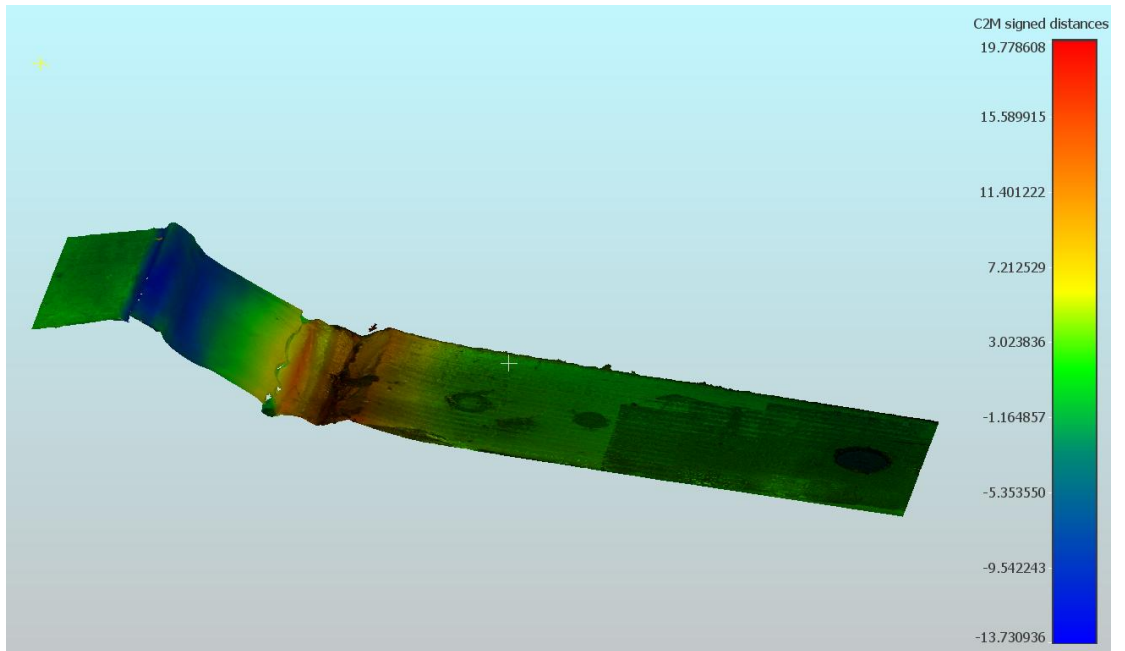


Figure 8.18 Laser scan of dike body with clay layer after failure of the dike. Distance [mm] computed in reference to the dike before failure. Blue shows settlement (at the crest) and red shows upward displacement (at the toe).

9 Test 5: ditch far – wide

9.1 General observations

This test was conducted with ditch configuration far- wide. Uplift was found, and again the length of the uplifted zone was confined by the edge of the ditch. The dike failed at a g-level of 112, similar to the previous tests in this series, including those without a ditch. After failure, the bottom of the ditch lifted up and cracked in the middle.

9.2 Centrifuge test

9.2.1 Preliminary analysis and commentary on the data

The results of this experiment were in line with expectations and results of the previous tests in this series. The magnitude of the vertical displacements seems to be lower than in test 4, with a maximum of 1.5 mm at D3, where test 4 saw a maximum uplift of 4 mm at D3.

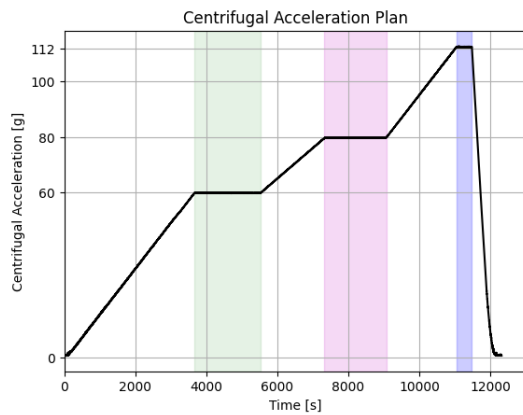


Figure 9.1 Centrifugal acceleration plan of Test 5.

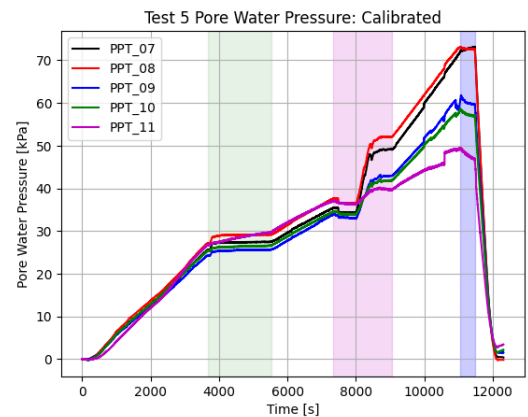


Figure 9.2 Pore water pressures at locations P7-P11 calibrated.

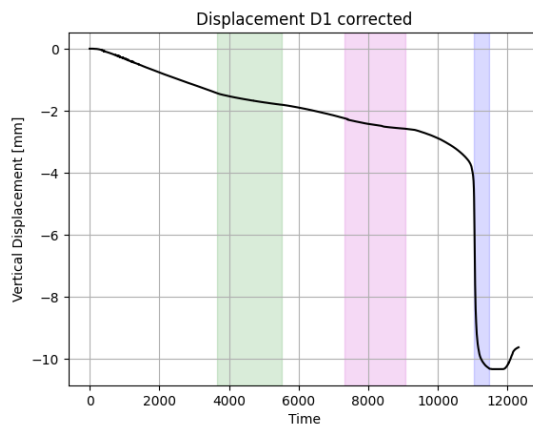


Figure 9.3 Vertical displacement of D1, corrected.

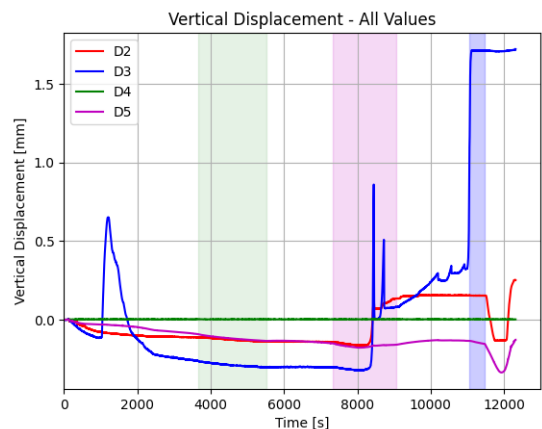


Figure 9.4 Vertical displacement of D2-D5, corrected.

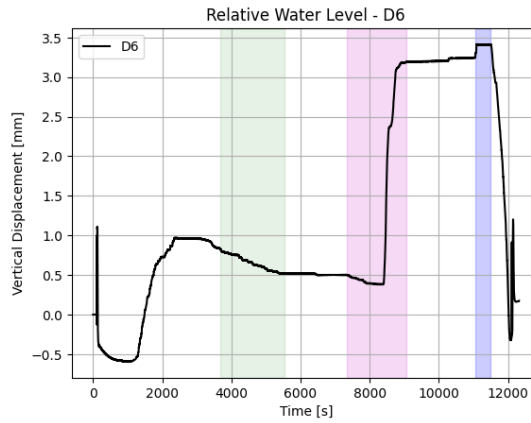


Figure 9.5 Relative water level according to D6, a floating sensor.

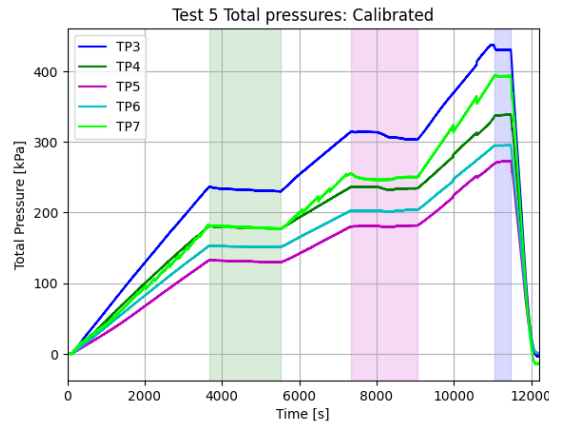


Figure 9.6 Total pressures measured at the bottom of the strongbox at locations TP3-TP7 (left to right).

9.2.2 Observations, notes and remarks

There was a sand boil at the diagonal crack at the toe, as well as at the left side of the ditch. Sensor D3 was moved to the bottom of the ditch, more to the right side of the strong box than normal, and D4 was not connected. A spike at D3 is noticed at about 1000 seconds, see Figure 9.4, but this did not seem to be connected to any failure phenomena observed in other sensor data or camera footage.

9.2.3 Uplift

Uplift initiated after the first step of hydraulic head increase, and reached the maximum length after 8792 seconds. This can be recognised in the vertical displacements shown in Figure 9.8. The end of the uplifted area coincides with the right side of the ditch, as can be seen in Figure 9.9.

Table 9.1 Overview of uplift values for test 5 from photo analysis.

	g-level	Hydraulic head [cm]	Max uplift length [cm]	Max uplift height [mm]
Initial uplift	80	19.8 - 20.5		
Maximum uplift	80	23.1	26.86	3.7

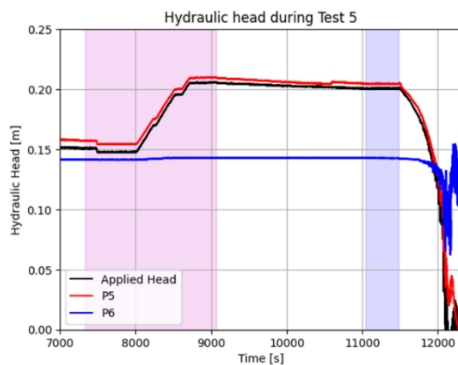


Figure 9.7 Hydraulic head during uplift and failure back-calculated from pore water pressure transducers Standpipe left, PPT5 and PPT6, corrected for the position of the sensors.

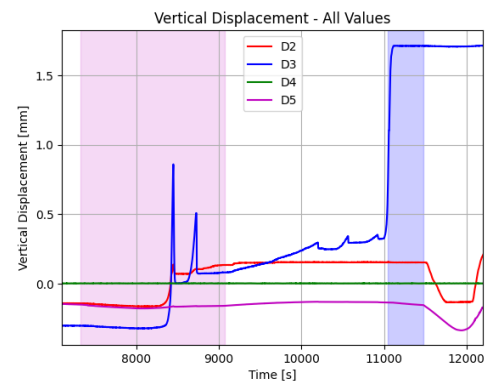


Figure 9.8 Vertical displacement during uplift and failure

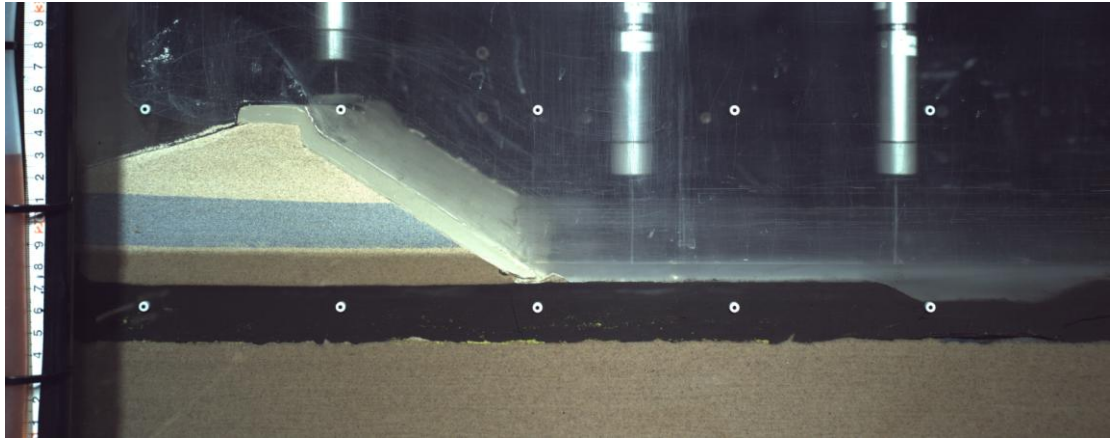


Figure 9.9 Maximum uplift of the clay cover layer.

9.2.4 Failure

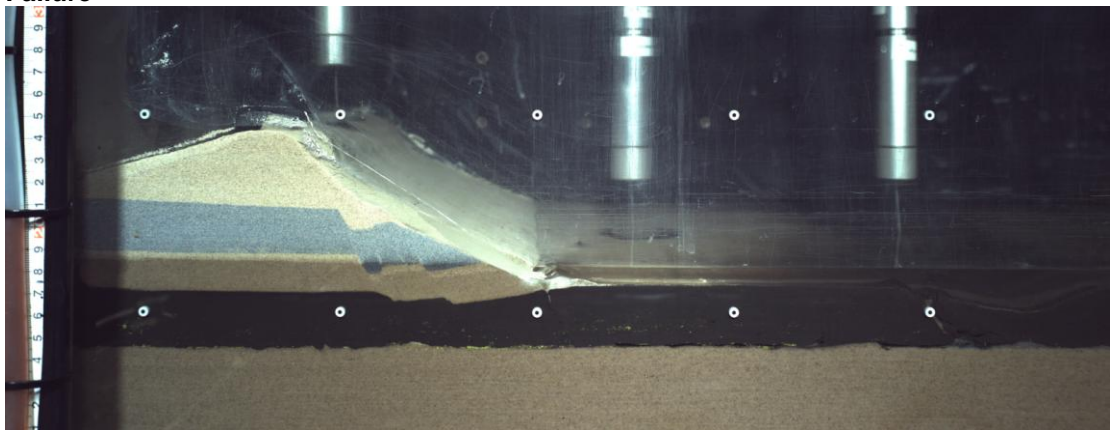


Figure 9.10 Failure of the dike body during the experiment.

9.3 Post-test observations

9.3.1 Sliding planes, sand-boils, piping

Post-test excavation of the model show multiple sliding planes, Figure 9.11 and Figure 9.12 in a similar shape as found in the previous tests in this series. A sand-boil at the ditch, Figure 9.13 and Figure 9.14, was found, as well as sand erosion under the clay layer, Figure 9.15 and Figure 9.16.

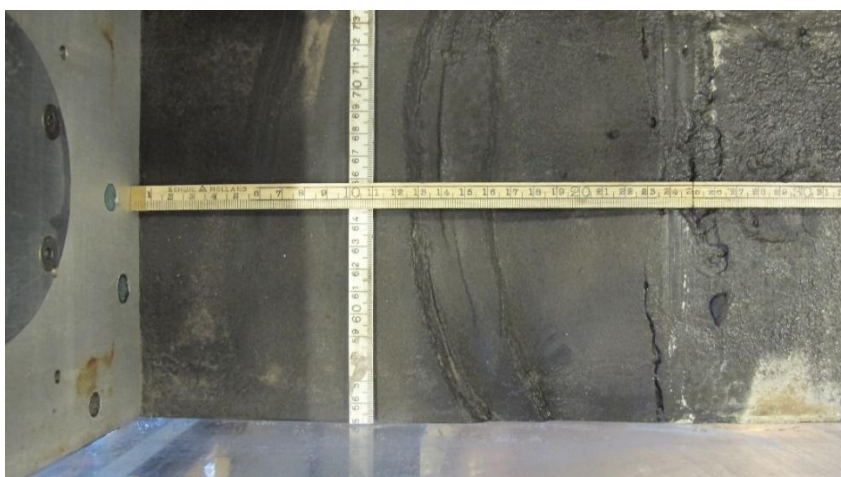


Figure 9.11 Sliding planes in the clay layer.



Figure 9.12 Sliding planes in the partially excavated sand dike.



Figure 9.13 Side view of the ditch after failure, clearly showing a large crack and sand boil on the left side.



Figure 9.14 Top view of the ditch after failure. Sand boils visible along the width of the ditch (at about 46 cm).



Figure 9.15 Sand erosion under the clay layer at the ditch location.



Figure 9.16 Sand erosion under the clay layer under the dike.

9.3.2 Laser scans

Figure 9.17 clearly shows upward vertical displacement at the toe and ditch bottom.

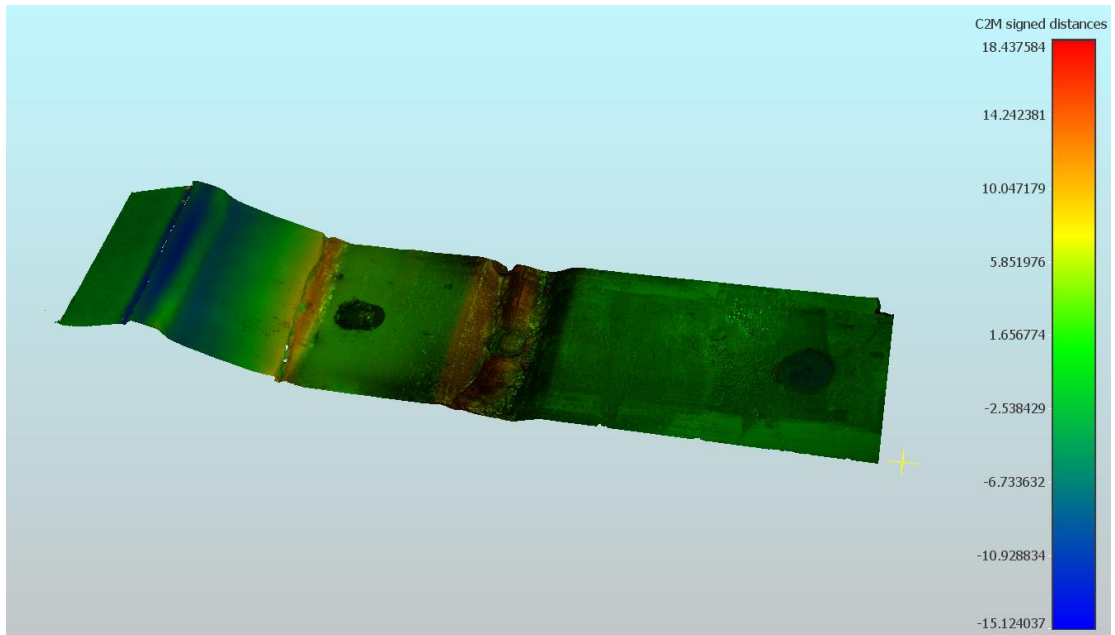


Figure 9.17 Laser scan of dike body with clay layer after failure of the dike. Distance [mm] computed in reference to the dike before failure. Blue shows settlement (at the crest) and red shows upward displacement (at the toe).

10 Test 6: ditch close – wide

10.1 General observations

This test was executed with the ditch configuration close – wide. This was expected to be the most impactful configuration, and therefore the early stages of the test were conducted more slowly, to prevent premature failure. However, again no failure occurred at a significantly lower g-level than in the previous tests. After failure at 110 g, the clay layer moved laterally and lifted the bottom of the ditch, leading to cracking of the ditch bottom.

10.2 Centrifuge test

10.2.1 Preliminary analysis and commentary on the data

The sensor data is very similar to the previous tests in this series. Since this experiment had the most risky ditch configuration, the initial increase of g-level towards 60 g and onwards was done at a slower pace to prevent premature failure. The most apparent sensor measurement outcome is found at the vertical displacement of D2, which is shown in Figure 10.3 and Figure 10.8.

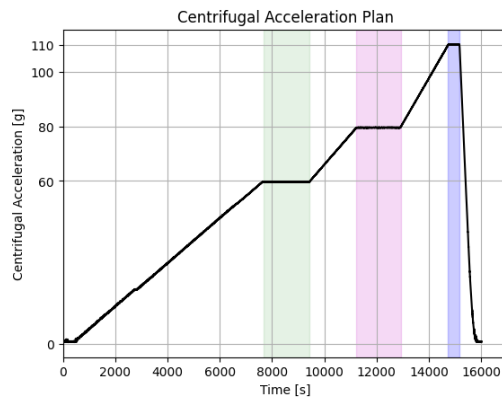


Figure 10.1 Centrifugal acceleration plan of Test 6.

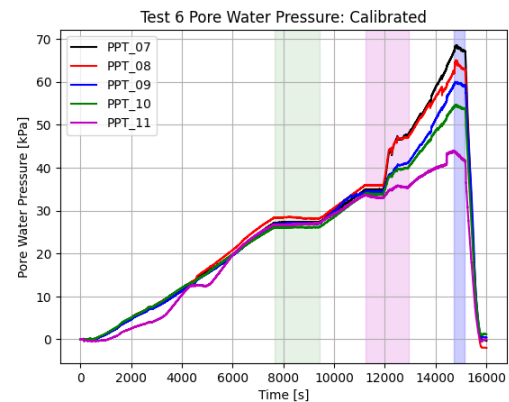


Figure 10.2 Pore water pressures at locations P7-P11 calibrated.

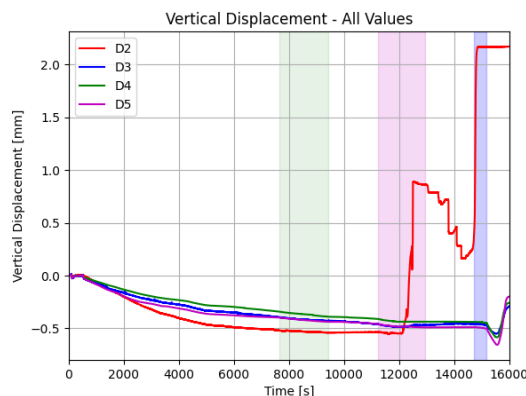


Figure 10.3 Vertical displacement of D2-D5, corrected.

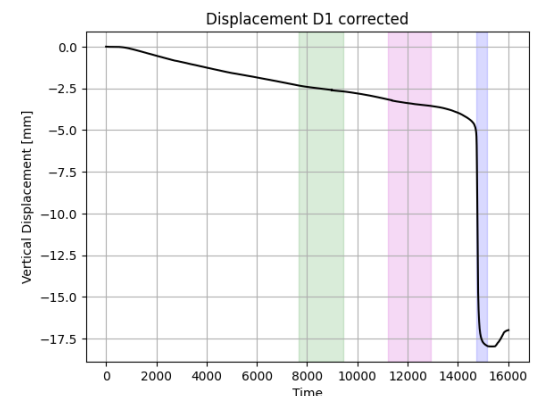


Figure 10.4 Vertical displacement of D1, corrected.

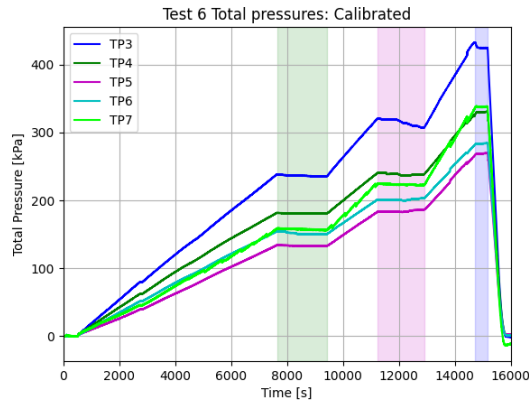


Figure 10.5 Total pressures measured at the bottom of the strongbox at locations TP3-TP7 (left to right).

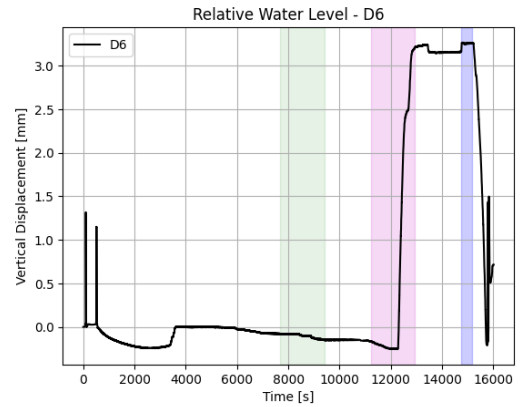


Figure 10.6 Relative water level according to D6, a floating sensor.

10.2.2 Observations, notes and remarks

Figure 10.2 shows PPT11 behaving slightly non-linear in the 0-60 g-level increase phase but regains balance after the consolidation phase.

10.2.3 Uplift

In this test the initial signs of uplift showed at 12040 seconds into the experiment, already during the first step of hydraulic head increase. Maximum uplift was reached after 12701 seconds, around the third step. The maximum uplift length reached only 10.49 cm, and as seen in Figure 10.9, the end of the uplifted area coincides with the right end of the ditch. The vertical displacement sensors also show uplift only at D2, which was positioned at the bottom of the ditch, see Figure 10.8.

Table 10.1 Overview of uplift values for test 6 from photo analysis.

	G-level	Hydraulic head [cm]	Max uplift length [cm]	Max uplift height [mm]
Initial uplift	80	18.6		
Maximum uplift	80	22.7	10.49	2.8

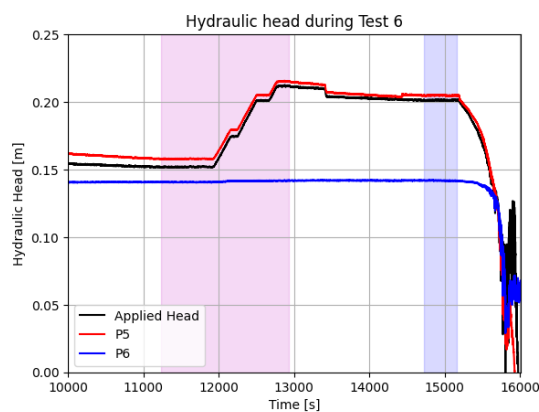


Figure 10.7 Hydraulic head during uplift and failure back-calculated from pore water pressure transducers Standpipe left, PPT5 and PPT6, corrected for the position of the sensors.

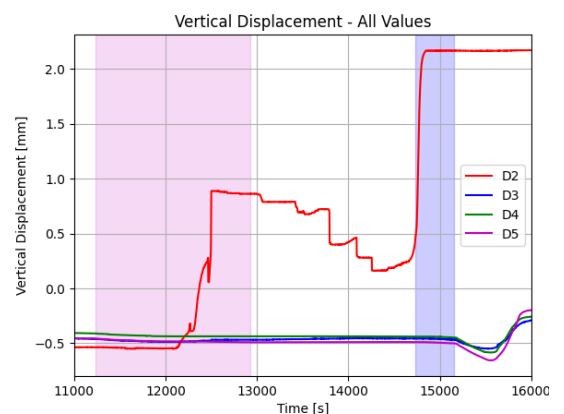


Figure 10.8 Vertical displacement during uplift and failure.

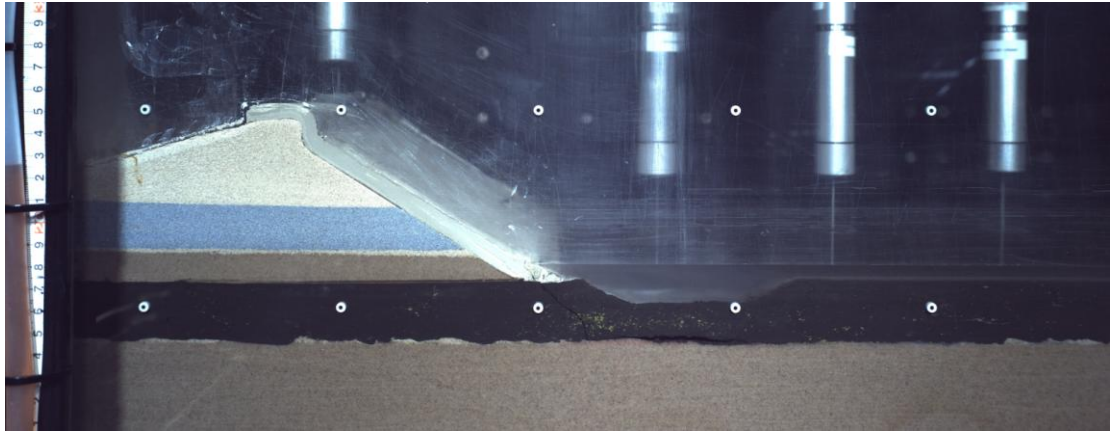


Figure 10.9: Maximum uplift of the clay cover layer.

10.2.4 Failure

At 110g, the dike collapsed. As shown in Figure 10-10, there are multiple sliding planes, and they look similar to the previous tests in this series. No premature failure happened due to the presence of the wide ditch nearby. Lateral movement in the clay layer due to collapse of the dike body is clearly visible, due to the bottom of the ditch being lifted upwards.

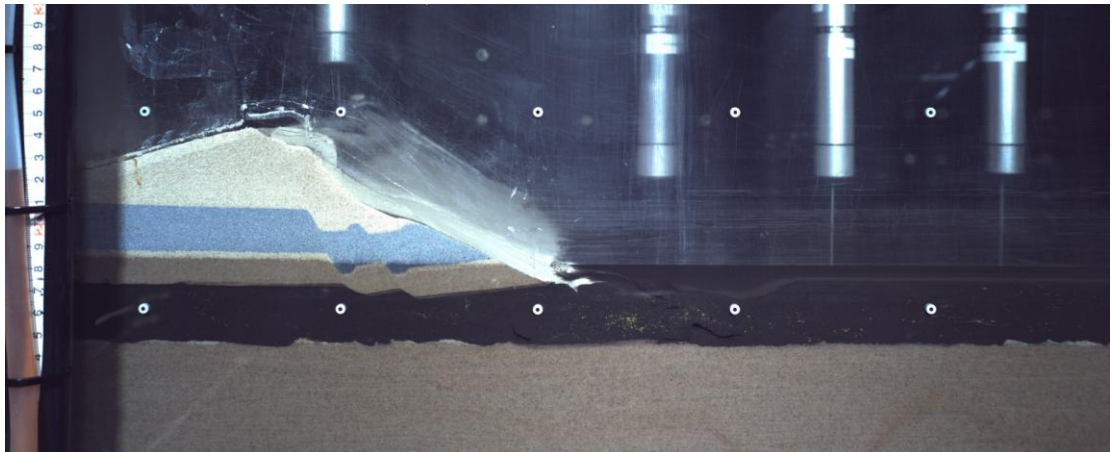


Figure 10.10 Failure of the dike body during the experiment.

10.3 Post-test observations

10.3.1 Sliding planes, sand-boils, piping

Similar to all tests in this series, two distinctive sliding planes are recognisable in the sand and clay layer after partial excavation. From closer inspection and after removing the free water on top of the clay layer, it is also clear that the bottom of the ditch cracked in the end after being pushed upwards, see Figure 10.13.



Figure 10.11 Sliding planes visible in the clay after excavation of the sand dike.



Figure 10.12 Sliding plane visible in the partially excavated sand dike.

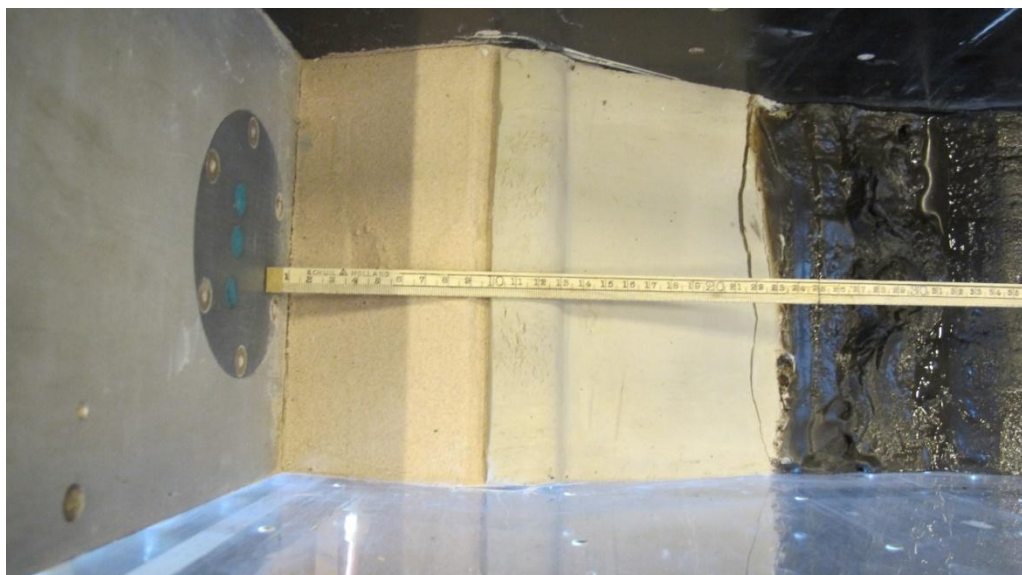


Figure 10.13 Top view of dike after failure, after taking off the fingerling clay layer. The deformed ditch is visible on the right side.



Figure 10.14 Side view of dike toe after failure. Diagonal crack has partially been pressed closed.



Figure 10.15 Side view of ditch after failure. Lateral crack along the bottom and remnant of diagonal crack on the left side are visible.



Figure 10.16 Top view of sand layer after removal of dike and cover layer.

10.3.2

Laser scans

Figure 10.17 shows clear upwards displacement of the bottom of the ditch as mentioned earlier.

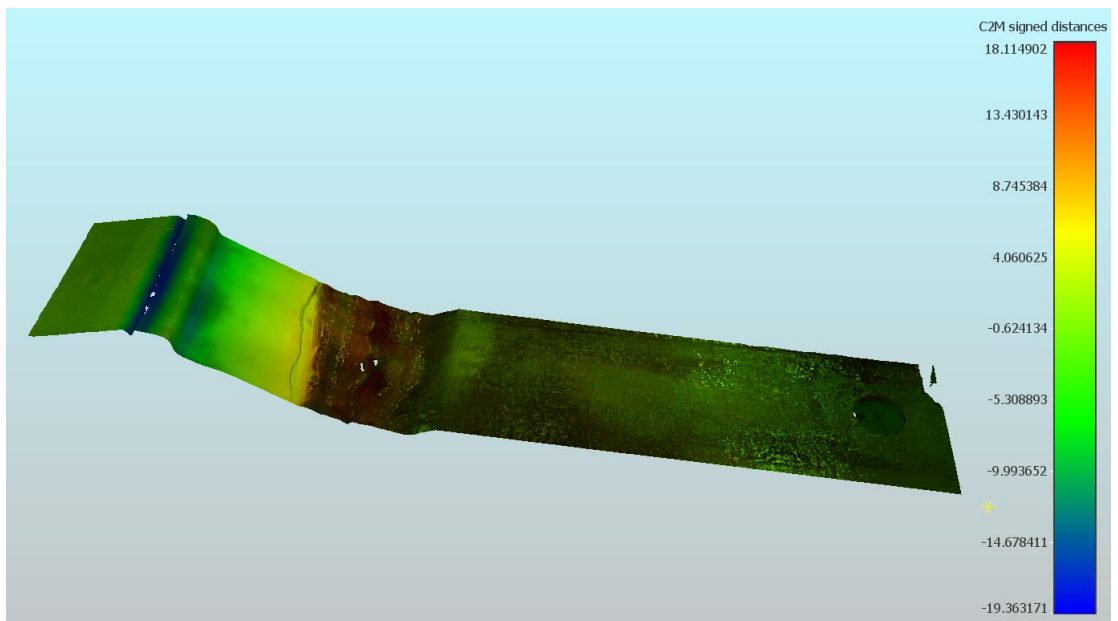


Figure 10.17 Laser scan of dike body with clay layer after failure of the dike. Distance [mm] computed in reference to the dike before failure. Blue shows settlement (at the crest) and red shows upward displacement (at the toe).

A Design and prediction

A.1 Introduction

This section describes the numerical analysis related to the centrifuge tests described in this report. The aim of the calculations is two-fold:

- Design of the centrifuge test.
- Hindcast of the results.

The tests follow a series earlier conducted tests and a basic understanding of the tests and their results is already available. The presence of ditch in the model requires additional numerical analysis. The design calculations should indicate the optimal position and dimensions of the ditch. The position and dimensions should be such that impact of the presence of a ditch is to be expected. However, premature failure should be avoided. Premature failure is defined as failure while spinning up, before the uplift pressure is applied in the test. Besides the position and dimensions of the ditch, the rate of spinning up and optional consolidation periods are design parameters that can be used to avoid premature failure.

A.2 Model Geometry

The basic geometry will be the geometry applied in test 11 of the Reevediep series. Figure A.1 sketches the geometry. N.B. it should be noted that the configuration of test 10 is used in the experimental study for the duplicate test to study the reproducibility. The numerical analysis uses Test 11 since it has been used for the hindcast of the first series and the basic geometry should be the same, both clay layer thickness of 30 mm and slope angle of 1(V):1.5(H). The main difference between the two is the preparation technique of the clay. Figure A.1 shows the geometry.

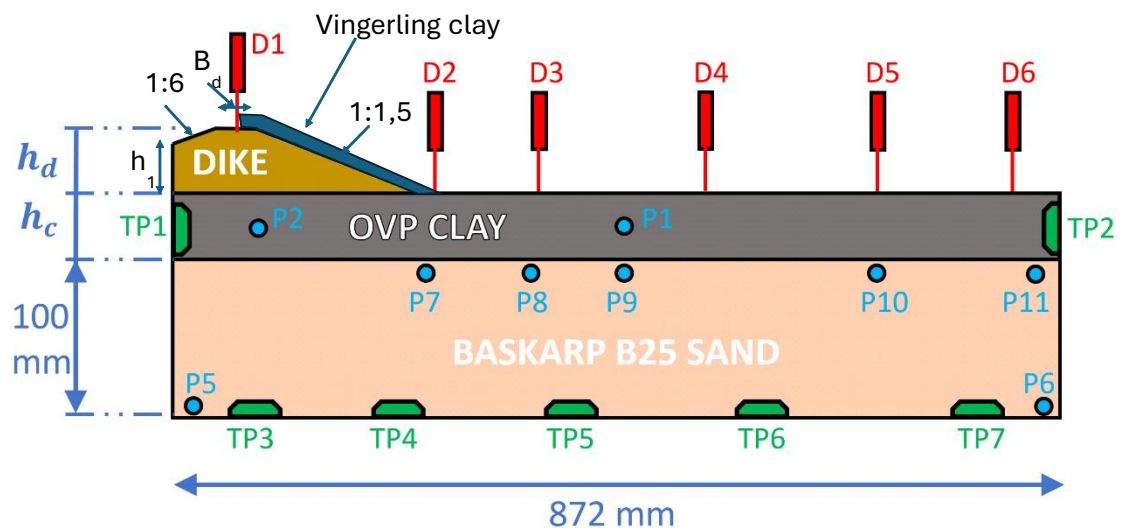


Figure A.1 Sketch geometry.

Based on the geometry above, the following dimensions are used:

- Height cover layer, $h_c = 30$ mm.
- Height dike, $h_d = 80$ mm (exclusive Vingerling clay).
- Width dike crest $B_d = 30$ mm.

- Dike height left boundary, $h_1 = 69$ mm.

Thickness Vingerling clay is 10 mm. The Vingerling clay is meant to prevent erosion due to outflowing pore water. For the FEM analysis, the relevance of the Vingerling clay is to avoid shallow failure.

A.3 Soil parameters

The applied soil parameters are given in Table A.1 to Table A.3. The soil parameters are chosen equivalent to the parameters used in the hindcast of the earlier conducted test series.

Table A.1 Parameters for OVP clay – cover layer soft soil model.

Parameter	Symbol	Unit	Value
Density	γ_{unsat}	kN/m ³	13.36
Saturated density	γ_{sat}	kN/m ³	13.36
Initial void ratio	e_{init}	-	3.00
Compression index	λ^*	-	0.1225
Re-compression index	κ^*	-	0.01149
Cohesion	c'	kN/m ²	3.3
Friction angle	φ'	°	27.7
Dilatancy angle	ψ	°	0
Poisson's ratio	ν'_{ur}	-	0.15
Pre-overburden pressure	POP	kN/m ²	40
permeability	k_x, k_y	m/day	0.4920×10^{-3}
Change in permeability	c_k	-	1,9

Table A.2 Parameters dike body + sand layer, HS model.

Parameter	Symbol	Unity	Dike	Sand layer
Density	γ_{unsat}	kN/m ³	19.6	19.70
Saturated density	γ_{sat}	kN/m ³	15.74	19.70
Initial void ratio	e_{init}	-	0.50	0.50
Reference Young's modulus	E_{50}^{ref}	kN/m ²	50 000	48 000
Reference oedometer stiffness	E_{oed}^{ref}	kN/m ²	40 000	48 000
Unloading – reloading stiffness	E_{ur}^{ref}	kN/m ²	150 000	144 000
Poisson's ratio	ν_{ur}	-	0.20	0.20
Cohesion	c'_{ref}	kN/m ²	0.10	0.10
Friction angle	φ'	°	45.00	38.00
Dilatancy angle	Ψ	°	8.00	8.00
permeability	k_x, k_y	m/day	0.1	0..1

Table A.3 Parameters Vingerling clay, MC model – drained.

Parameter	Symbol	Unity	Value
Density	γ_{unsat}	kN/m ³	15.80
Saturated density	γ_{sat}	kN/m ³	15.80
Initial void ratio	e_{init}	-	0.50
Reference Young's modulus	E'_{ref}	kN/m ²	1.500
Poisson's ratio	ν	-	0.30
Cohesion	c'_{ref}	kN/m ²	30.00
Friction angle	ϕ'	°	20.00
Dilatancy angle	Ψ	°	0.00
permeability	k_x, k_y	m/day	0.1

A.4 Phreatic line – hydraulic heads

The phreatic line is 5 mm above the initial top of the cover layer and runs horizontally. During consolidation this is the general hydraulic head for the entire model. After reaching 80 g, for modelling the uplift situation, the hydraulic head in the sand layer at the left side of the model box will be raised by 60 mm above original top clay layer, 20 mm below original crest dike. At the toe of the dike, the hydraulic head in the sand layer is maximised by the weight of the cover layer, which is 45.9 mm above the bottom of the cover layer, or 15.9 mm above the top of the cover layer. After uplift phase, the hydraulic heads in the model remains unchanged. Figure A.2 shows the applied schematisation.

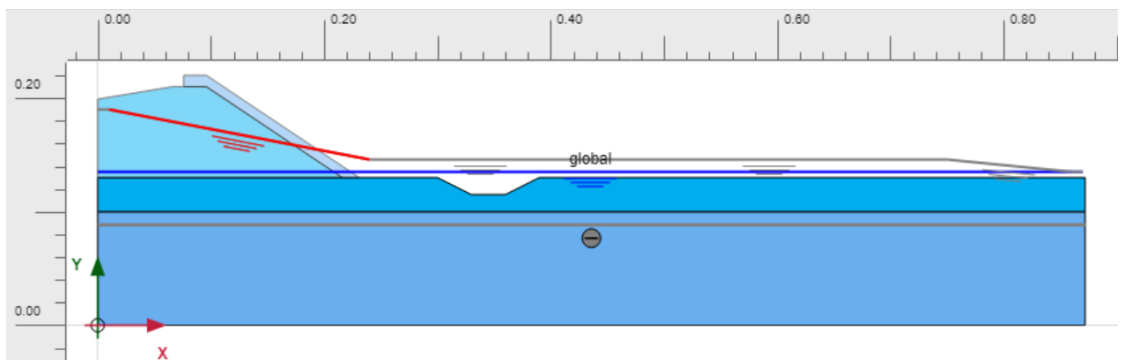


Figure A.2 Schematisation phreatic line and head in sand layer at uplift conditions.

A.5 Test procedure

The centrifuge tests contain multiple steps. The following steps are considered in the FEM analysis:

- Initial stresses at 1 g; containing an even soil body, including two layers, the Aquifer, with thickness of 100 mm at the bottom, and 30 mm thick clay layer is modelled. In the top clay layer, the location of ditch is modelled as already excavated (i.e. no material). K0 procedure is used to initialise stresses.
- The soil body is loaded with 40kPa vertical load, to simulate the loading history of clay layer, the over consolidation, using Plastic calculation type.
- Unloading the 40kPa.
- Activation of the dike body, including the Vingerling clay layer in a undrained situation.
- Stepwise increasing g-level to 80 g, as following:
 - From 1 to 60g in 60 min, calculation type: consolidation; loading type: staged construction).

- 30 min consolidation at 60g.
- From 60g to 80g in 30 min.
- Consolidation at 80g for 15 min.
 - Activating the raised hydraulic head to model uplift, interface is activated, no pore water pressure update. Total time 15 minutes.
 - At 80 g, rise hydraulic head to an elevation equivalent to crest height. (Activate interface, de-activate update pore water pressure → lessons learnt Reevediep tests).

After this step, the g-level is increased stepwise to study dike failure:

- Increase g-level, to 90g in 10 min (with 1 g/min).
- Consolidation at 90g in 5 min.
- Increase g-level, to 110g in 20 min.
- Consolidation at 110g in 5 min.
- Increase g-level, to 130g in 20 min.
- Consolidation at 130g in 5 min.

These steps are shown in Figure A.3. In the PLAXIS model after uplift phase and at the end of each g-level increase/consolidation, a safety calculation is added.

ID	Calculation t...	Loading type...	Pore pressur...	Time interval	Estimated en...	Ignore undr....	Reset displa...	Updated me...	Max steps (D)	First step	Last step
Initial phase [InitialPhase]				0,000 min	0,000 min	<input checked="" type="checkbox"/>	<input type="checkbox"/>	<input type="checkbox"/>	1000	0	0
pre-loading [Phase_3]				2,000 min	2,000 min	<input checked="" type="checkbox"/>	<input type="checkbox"/>	<input type="checkbox"/>	1000	1	122
remove preload [Phase_2]				0,000 min	2,000 min	<input checked="" type="checkbox"/>	<input type="checkbox"/>	<input type="checkbox"/>	1000	123	168
Activate Dike [Phase_1]				2,000 min	4,000 min	<input type="checkbox"/>	<input checked="" type="checkbox"/>	<input type="checkbox"/>	1000	169	171
60g in 60 min [Phase_4]				60,00 min	64,00 min	<input type="checkbox"/>	<input checked="" type="checkbox"/>	<input checked="" type="checkbox"/>	1000	172	200
consolidate 60g [Phase_5]				30,00 min	94,00 min	<input type="checkbox"/>	<input type="checkbox"/>	<input checked="" type="checkbox"/>	1000	201	214
80g in 30min [Phase_6]				30,00 min	124,0 min	<input type="checkbox"/>	<input type="checkbox"/>	<input checked="" type="checkbox"/>	1000	228	252
consolidate 80g [Phase_7]				15,00 min	139,0 min	<input type="checkbox"/>	<input type="checkbox"/>	<input checked="" type="checkbox"/>	1000	215	226
Uplift [Phase_8]				15,00 min	154,0 min	<input type="checkbox"/>	<input type="checkbox"/>	<input type="checkbox"/>	2000	27624	28731
90g in 10min [Phase_9]				10,00 min	164,0 min	<input type="checkbox"/>	<input type="checkbox"/>	<input type="checkbox"/>	6000	253	3723
consolidate 90g [Phase_10]				5,000 min	169,0 min	<input type="checkbox"/>	<input type="checkbox"/>	<input type="checkbox"/>	3000	3724	5385
110g [Phase_11]				20,00 min	189,0 min	<input type="checkbox"/>	<input type="checkbox"/>	<input type="checkbox"/>	8000	28732	34525
consolidate 110g [Phase_13]				5,000 min	194,0 min	<input type="checkbox"/>	<input type="checkbox"/>	<input type="checkbox"/>	8000	5386	6790
130g [Phase_16]				20,00 min	214,0 min	<input type="checkbox"/>	<input type="checkbox"/>	<input type="checkbox"/>	8000	6791	14790
consolidate 130g [Phase_17]				5,000 min	219,0 min	<input type="checkbox"/>	<input type="checkbox"/>	<input type="checkbox"/>	8000	16091	18322
Safety 130g [Phase_18]				0,000 min	219,0 min	<input type="checkbox"/>	<input checked="" type="checkbox"/>	<input type="checkbox"/>	900	18323	19222
Safety 110 [Phase_15]				0,000 min	194,0 min	<input type="checkbox"/>	<input checked="" type="checkbox"/>	<input type="checkbox"/>	500	14791	15290
Safety 90g [Phase_14]				0,000 min	169,0 min	<input type="checkbox"/>	<input checked="" type="checkbox"/>	<input type="checkbox"/>	700	19223	19922
safety_uplift [Phase_12]				0,000 min	154,0 min	<input type="checkbox"/>	<input checked="" type="checkbox"/>	<input type="checkbox"/>	300	15291	15590

Figure A.3 The applied loading phases, their timing and specific conditions regarding drainage and resetting mesh.

A.6 Modelling ditch

In order to study the effect of ditch on the behaviour of embankment, different geometry configurations for the ditch are considered. As shown by Figure A.4 to Figure A.7, four types of wide, small and very small (VSmall) are chosen. Moreover, the depth of the ditch is changed from 15 mm to 7.5 mm. The slope of ditch for the deep configuration (15mm) is kept as 1:2, in the shallow version (7.5 mm depth), the slope is 1:4.

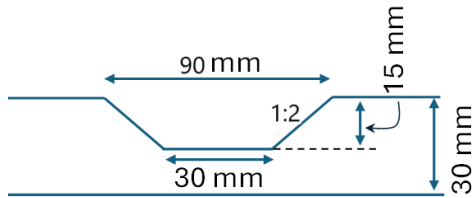


Figure A.4 Sketch Small ditch deep.

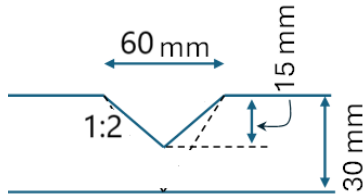


Figure A.5 Sketch VerySmall ditch.

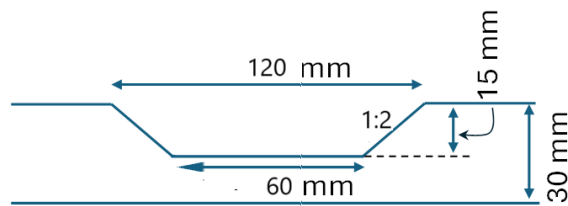


Figure A.6 Sketch Wide ditch deep.

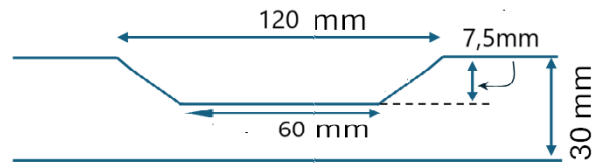


Figure A.7 Sketch Wide ditch shallow.

For the location of ditch compared to the toe of the dike, three predefined situations are considered as:

- 1: Close → edge of ditch at 0.3 m from left model boundary, 7cm from the toe.
- 2: Mid → edge of ditch at 0.4 m from left model boundary, 17cm from the toe.
- 3: Far → edge of the ditch at 0.5 m from left model boundary, 27cm from the toe.

The model is meshed as shown in Figure A.8. Model is discretised into 3700 15-noded elements, i.e., 30670 nodes with the minimum quality of 0,54. The calculations are conducted by PLAXIS 2D, v24.

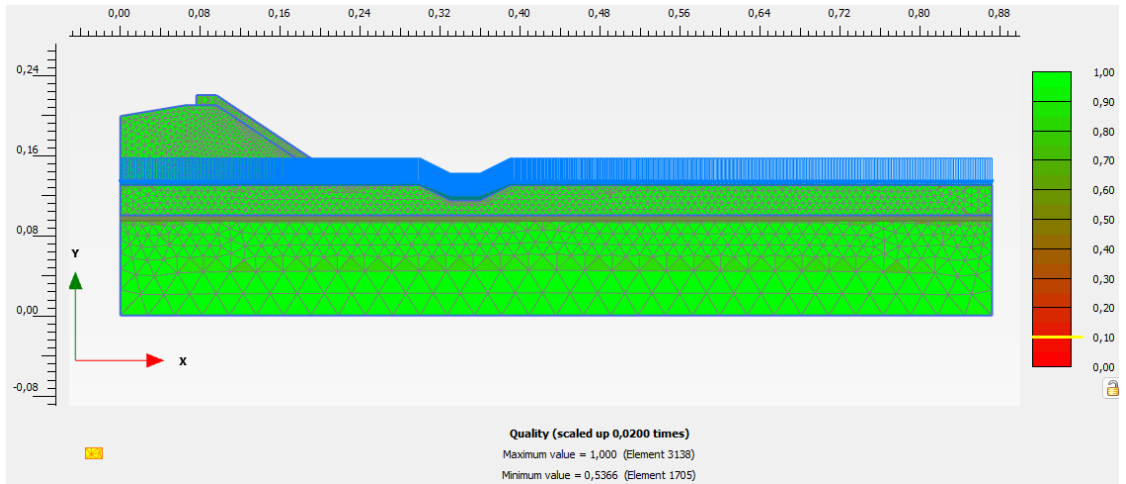


Figure A.8 Mesh discretisation.

A.7 Results

In the following the safety factors for different geometrical configurations of ditch are shown. For comparison calculation for a benchmark model, which does not contain a ditch, are also performed.

In the following, some of the results of the model are represented. The model with Close-small-deep ditch is chosen as the **basis**. In the following some of the outcomes of this model are represented.

The stress distribution after initial phase is represented in Figure A. 9.

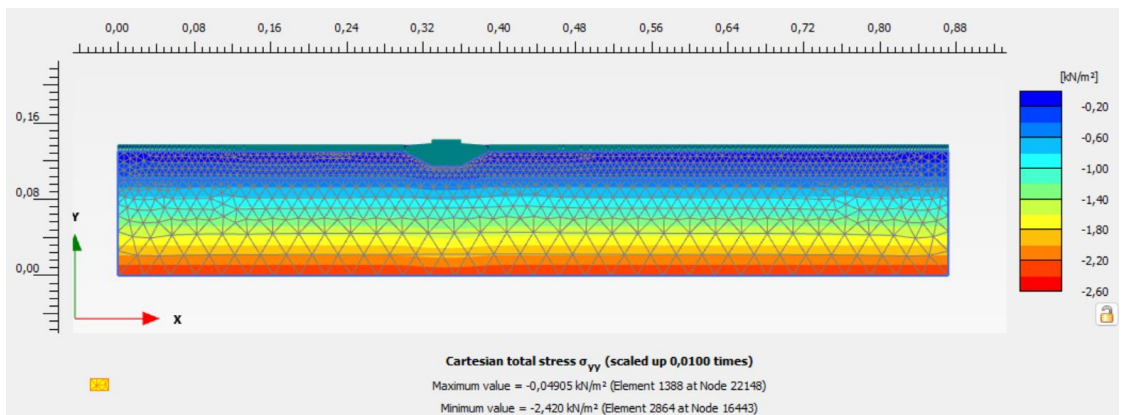


Figure A. 9 Vertical stress at initial phase

The excess pore pressure during the first phases is mainly dissipated before uplift is applied , as shown in Figure A.10 to Figure A.12. Figure A.13 shows the excess pore pressure at the location of P2 under the dike, where the dissipation of excess pore pressure before starting the uplift is indicated.

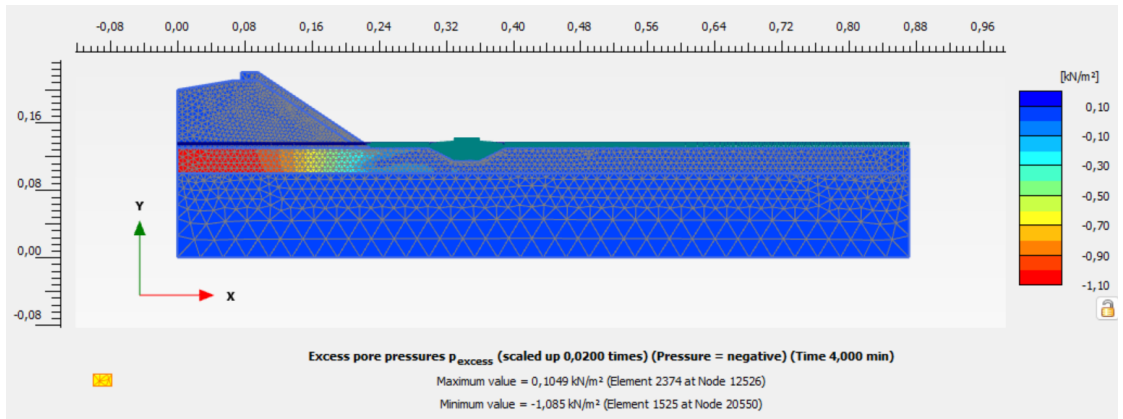


Figure A.10 Excess PWP after activation of dike body.

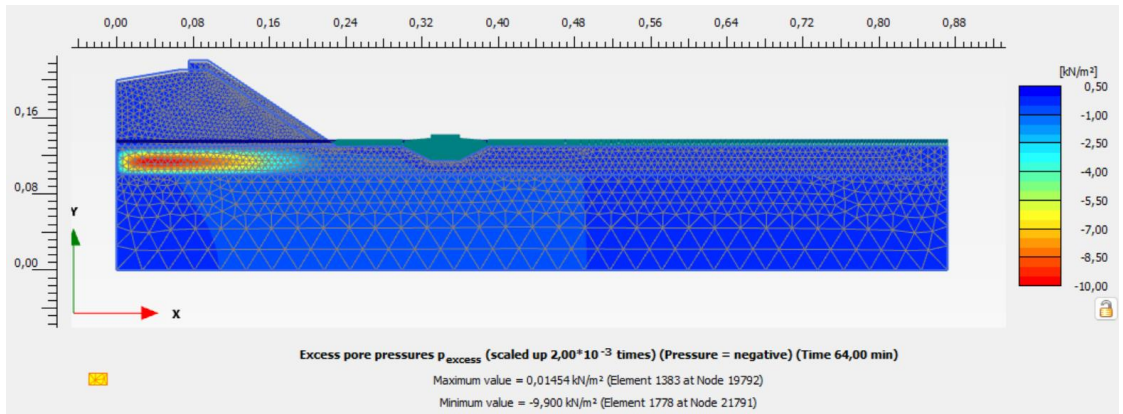


Figure A.11 Excess PWP after consolidation at 60 g.

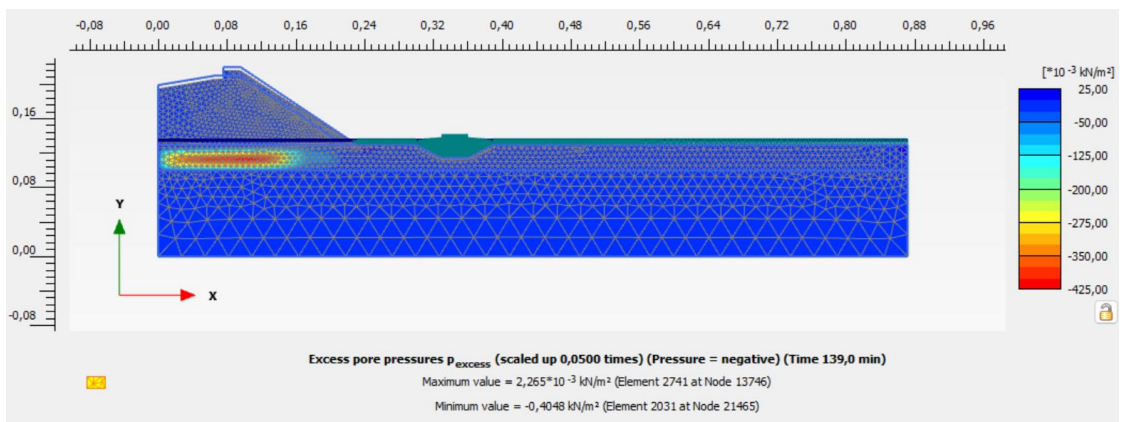


Figure A.12 Excess PWP after consolidation at 80g and before uplift.

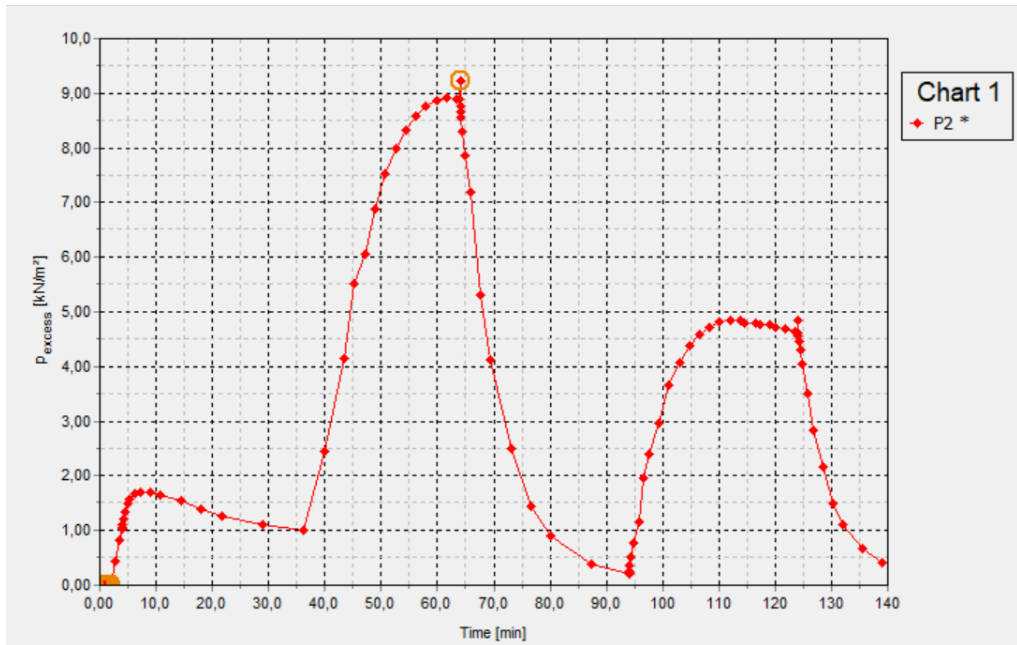


Figure A.13 Excess pore pressure of P2 sensor.

The following figures, Figure A.14 to Figure A.19, show a comparison between calculation with and without a ditch, the benchmark.

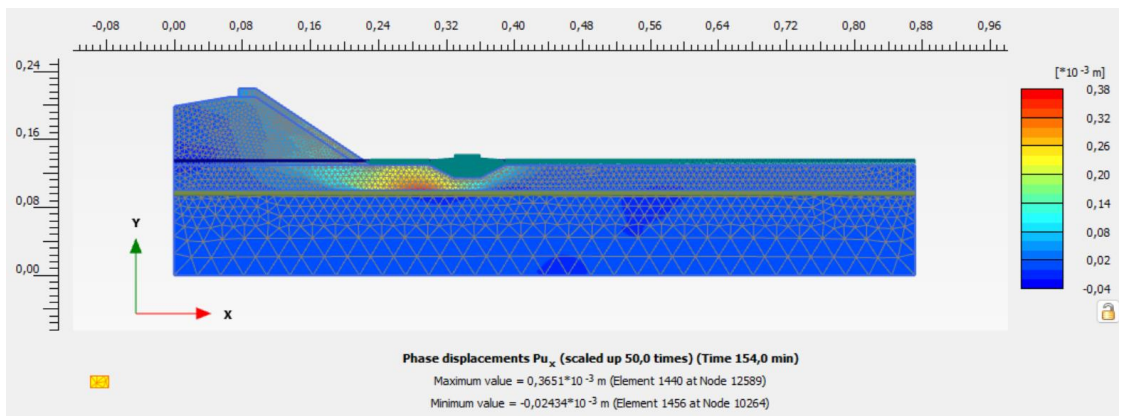


Figure A.14 Vertical phase displacement after Uplift phase.

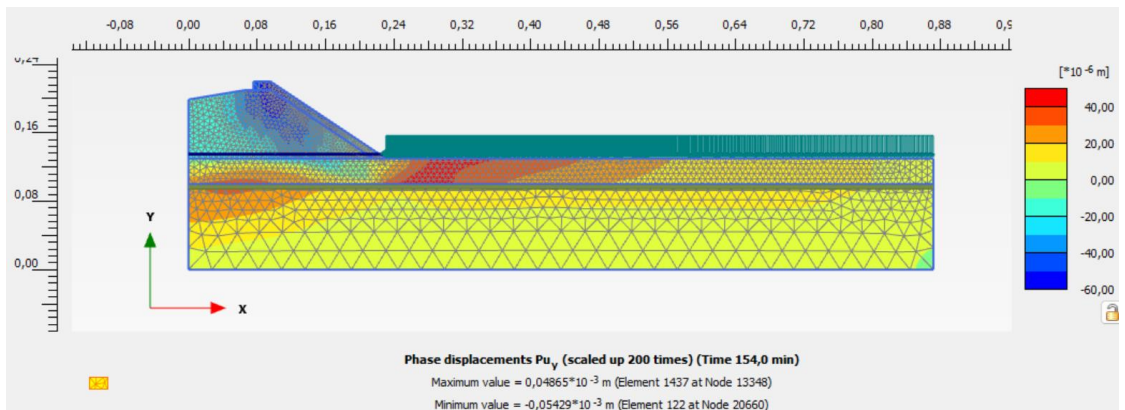


Figure A.15 Vertical phase displacement after Uplift phase (The benchmark model).

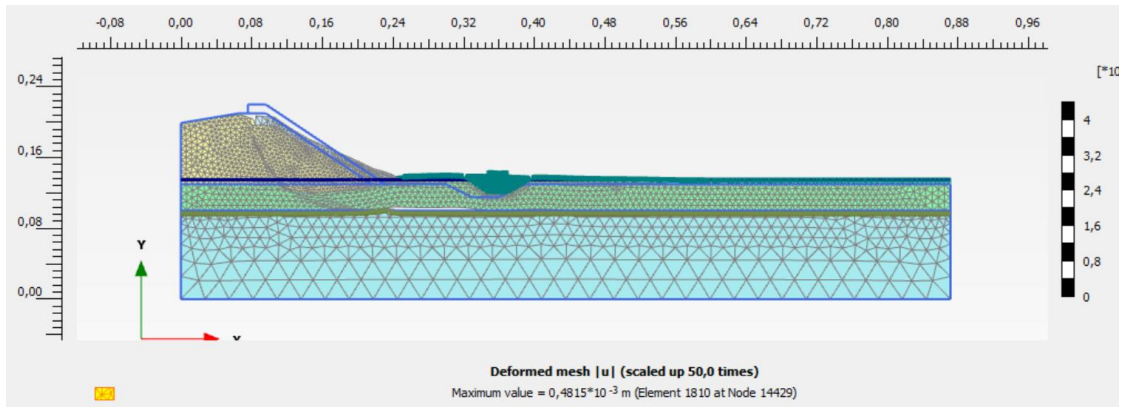


Figure A.16 The basis model after uplift safety phase.

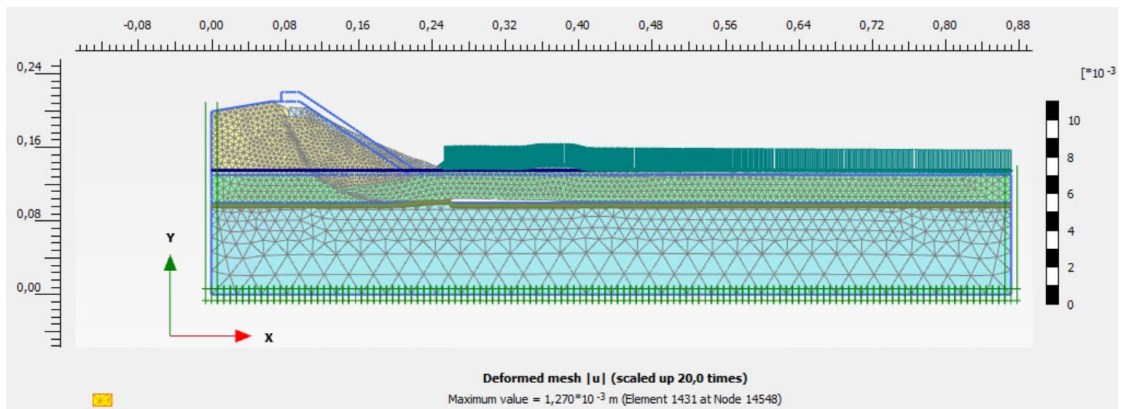


Figure A.17 Benchmark model after uplift safety phase.

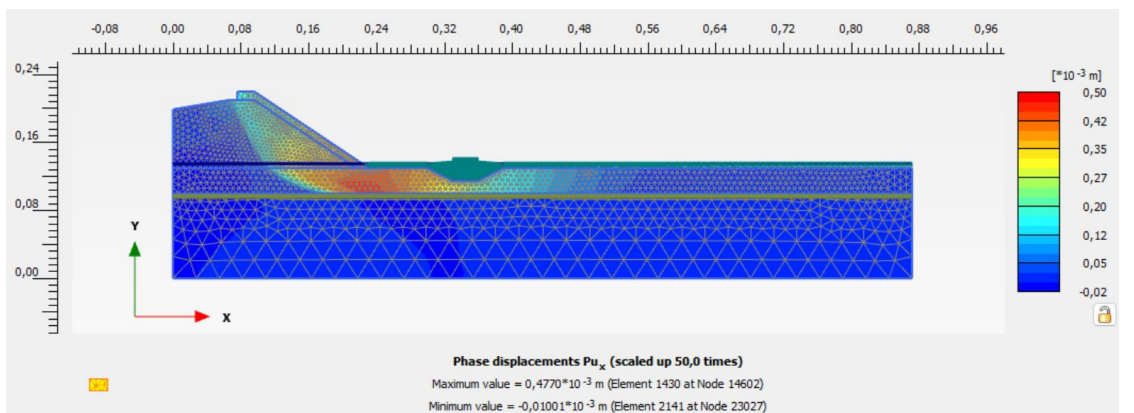


Figure A.18 Basis model after uplift safety phase (horizontal phase displacement).

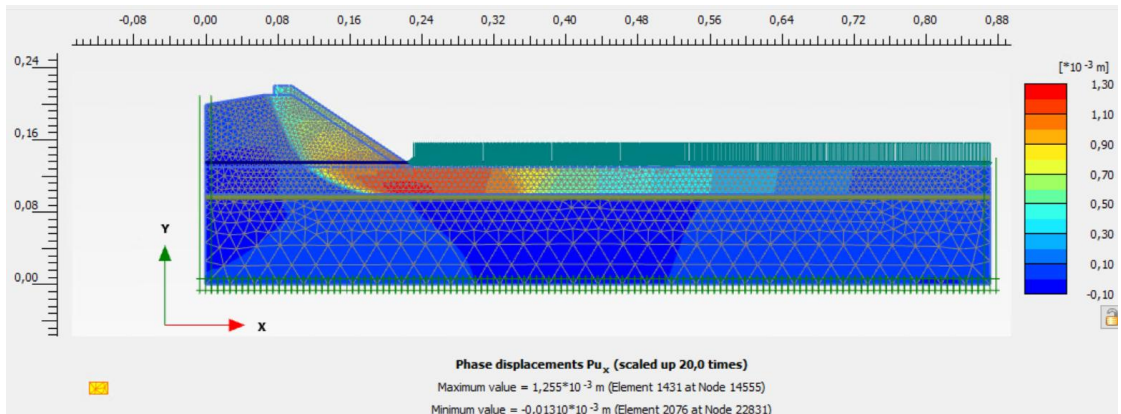


Figure A.19 Benchmark model after uplift safety phase (horizontal phase displacement).

The presence of ditch changes the deformation pattern on the clay cover layer. The horizontal displacement in this layer is not extended much after ditch. The displacement is more concentrated in the area between ditch and toe. This is visualised by Figure A.20 and Figure A.21, which shows the mobilised shear friction along the interface.

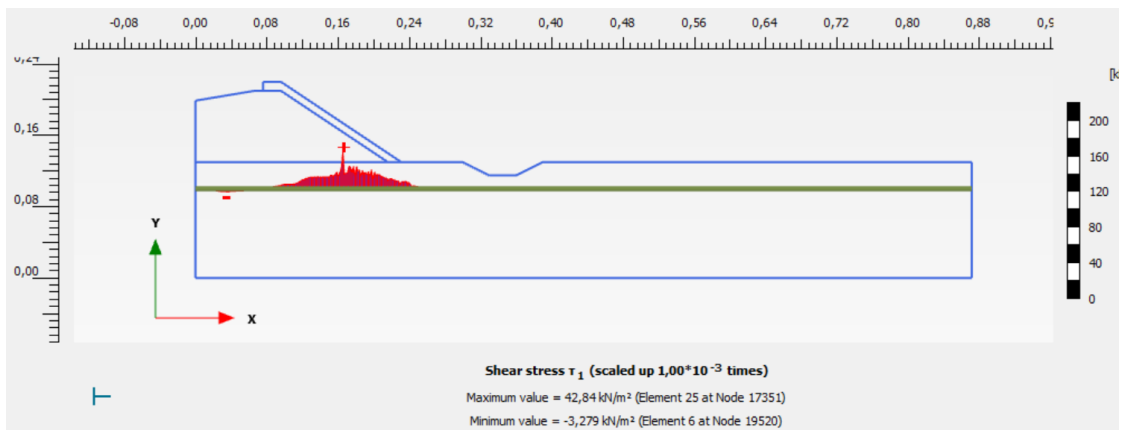


Figure A.20 Relative shear along the interface including ditch.

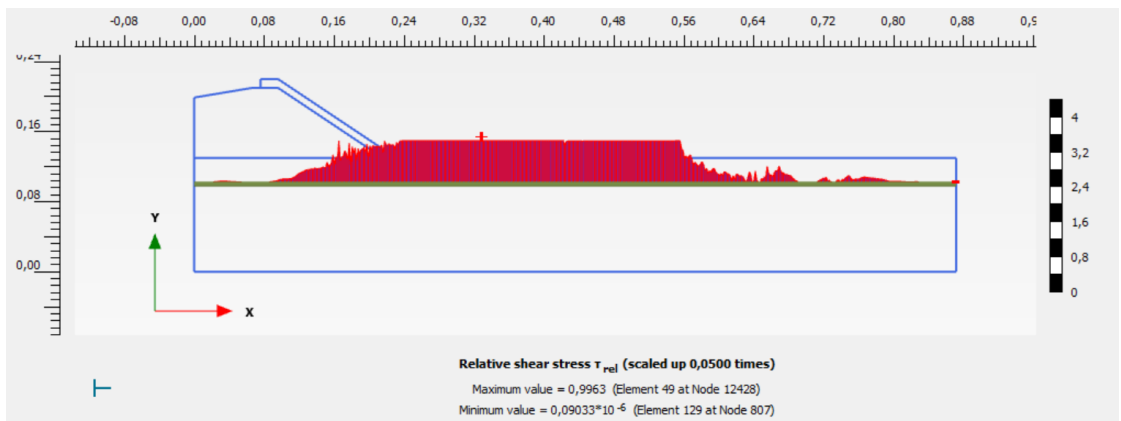


Figure A.21 Relative shear along the interface benchmark calculation.

Figure A.22 shows the results of the $c' - \phi'$ reduction analysis for the different calculation phases. Figure A.23 to Figure A.26 provide an impression of the failure mechanism found for the $c' - \phi'$ reduction analysis for the different phases.

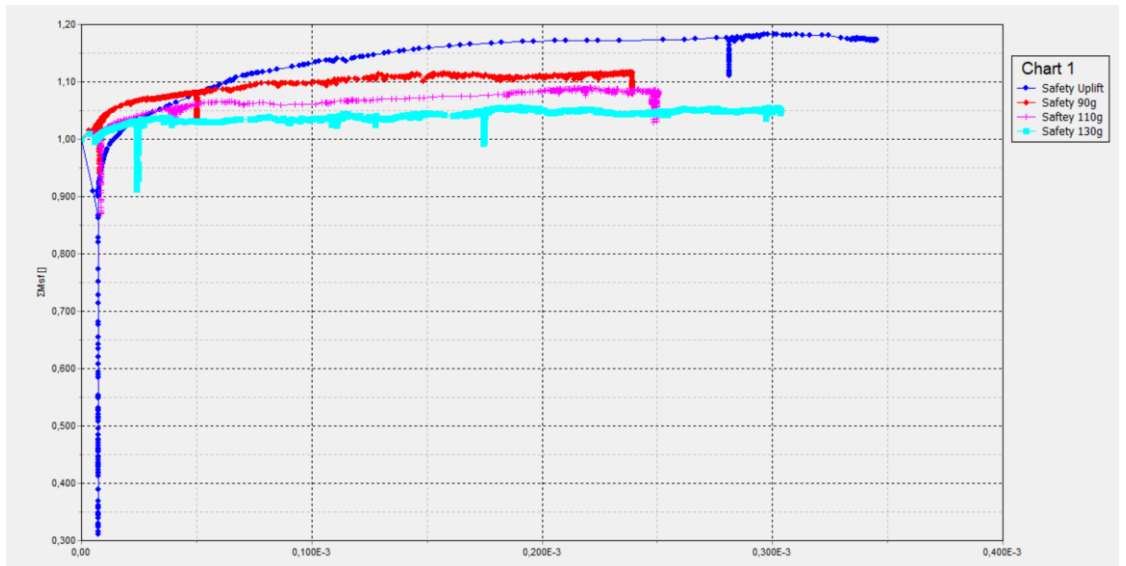


Figure A.22 Safety factor of basis model.

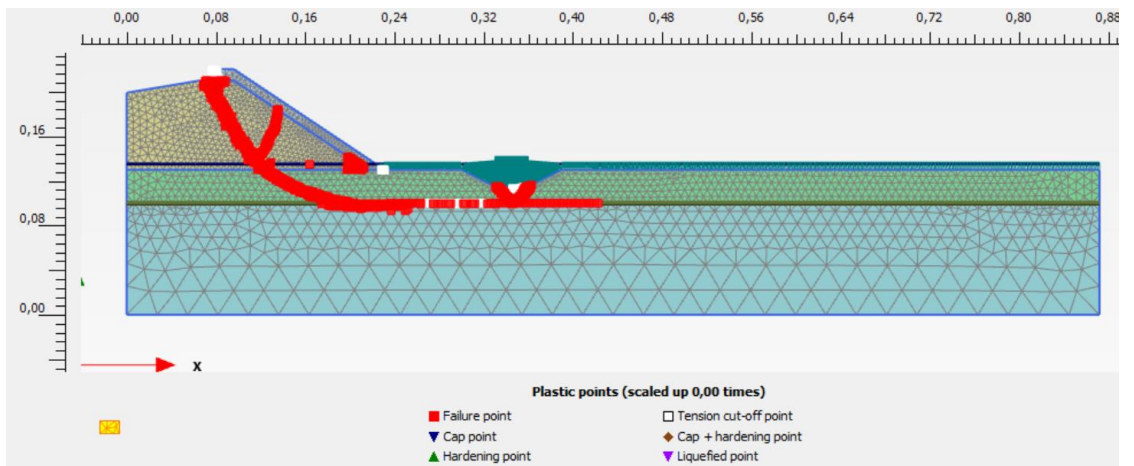


Figure A.23 Impression failure mechanism found after c' - ϕ' reduction at uplift; Plastic points.

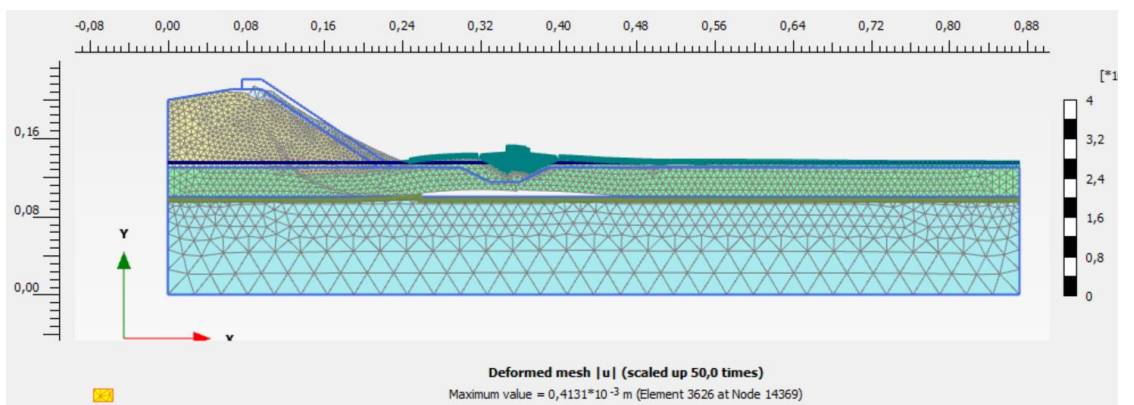


Figure A.24 Impression failure mechanism found after c' - ϕ' reduction when reaching 90g; deformed mesh.

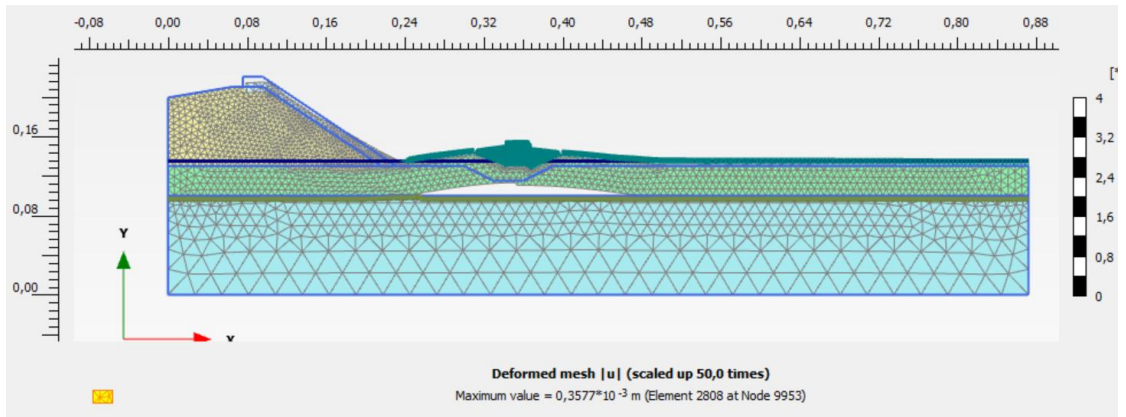


Figure A.25 Impression failure mechanism found after c' - ϕ' reduction when reaching 110g; deformed mesh.

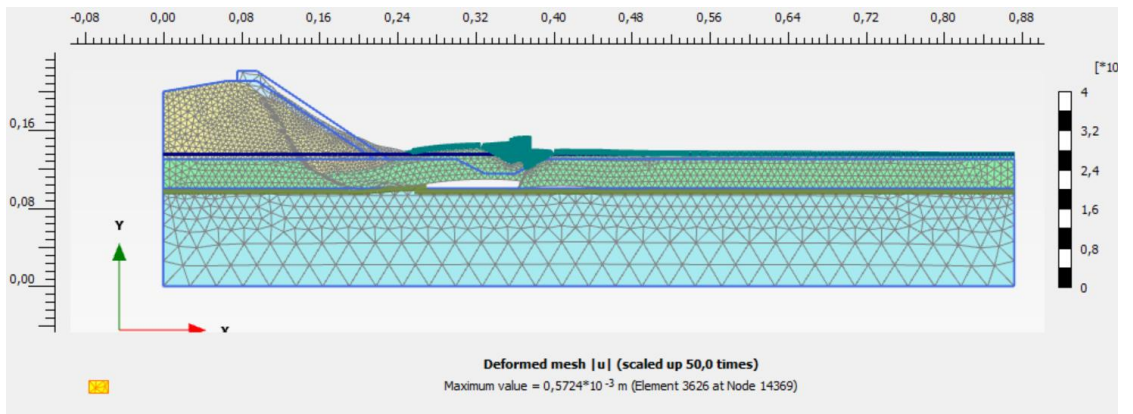


Figure A.26 Impression failure mechanism found after c' - ϕ' reduction when reaching 130g; deformed mesh.

Figure A.27 shows the vertical displacements at the locations D2, at the toe of the dike and D4 at the polder side of the dike. The vertical displacement up to 140 minutes show a settlement due to settlement induced by the increased g-level. When the hydraulic head is raised, D2, at the toe of the dike shows a clear increase, indicating the rise of the cover layer due to uplift. D4, which is positioned at the polder side of the ditch does not show a rise due to uplift.

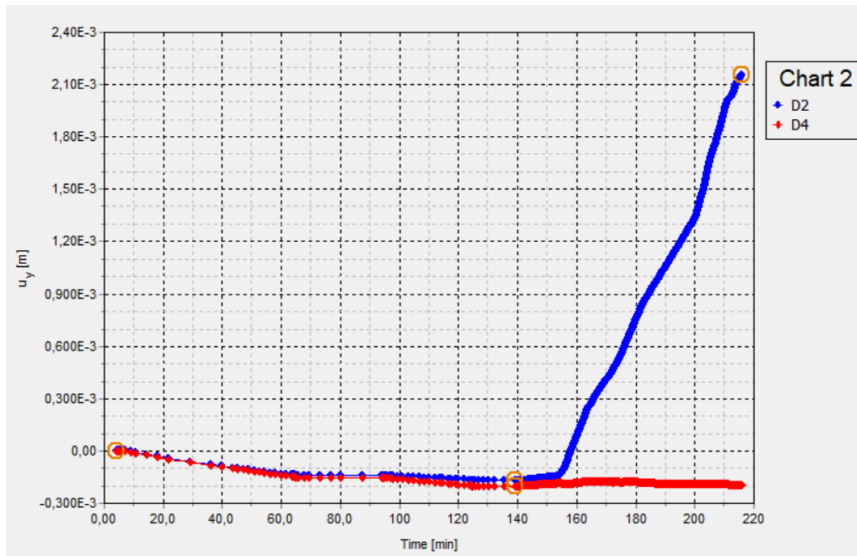


Figure A.27 The vertical displacement at sensor locations D2, at the toe of the dike and D4, polder side of the ditch.

Table A.4 shows an overview of the calculation results.

Table A.4 represents the safety factor of each modelled geometry with the name of models saved in N:\Projects\11210000\11210298\B. Measurements and calculations\003 - Centrifuge tests\FEM prediction\Elham\Virtuals.

Table A.4 Results of safety factor for all the models.

file Name	Location	Width	Depth	SF (Uplift)	90g	110g	130g
Proef 11-Ditch25CloseWide-deep-Nsteep_Preload_Time.p2dx	Very Close	Wide	Deep	1,15	1,078	1,044	*
Proef 11-DitchClose25-VSmall-deep-Nsteep_Preload_Time.p2dx	Very Close	VSmall		1,127	1,09	1,005	1,024 *
Proef 11-DitchCloseSmall-deep-Nsteep_Preload_Time-Basis-WaitingafterL	Close	Small	Deep	1,173	1,1	1,072	1,050*
Proef 11-DitchCloseSmall-deep-Nsteep_Preload_Time-Basis.p2dx	Close	Small	Deep	1,173	1,094	1,08	1,050 *
Proef 11-DitchCloseSmall-shallow-Nsteep_Preload_Time.p2dx			Shallow	1,155	1,125	1,115	1,077 *
Proef 11-DitchCloseWide-deep-Nsteep_Preload_Time.p2dx		Wide	Deep	1,189	1,133	1,079	*
Proef 11-DitchClose-Wide-shallow-Nsteep_Preload.p2dx			Shallow	1,171	1,136*	1,123*	1,081
Proef 11-DitchClose-VSmall-deep-Nsteep_Preload_Time.p2dx		VSmall		1,101	1,074	1,059	*
Proef 11-DitchMidSmall-deep-Nsteep_Preload_Time.p2dx	Mid	Small	Deep	1,199	1,00*	1,108	1,039
Proef 11-DitchMidSmall-shallow-Nsteep_Preload_Time.p2dx			Shallow	1,176	1,146	1,112*	1,058
Proef 11-DitchMid-Wide-deep-Nsteep_Preload_Time.p2dx		Wide	Deep	1,261	1,111	1,1	1,074
Proef 11-DitchMid-Wide-Shallow-Nsteep_Preload_Time			Shallow	1,182	1,133	1,092	1,07
Proef 11-DitchMid-VSmall-deep-Nsteep_Preload_Time.p2dx		VSmall		1,135	1,081*	1,062	1,072
Proef 11-DitchFarSmall-deep-Nsteep_Preload_Time.p2dx	Far	Small	Deep	1,213	1,145	1,121	1,122 *
Proef 11-DitchFarSmall-shallow-Nsteep_Preload_Time.p2dx			Shallow	1,185	1,143	1,076	1,06
Proef 11-DitchFar-Wide-deep-Nsteep_Preload_Time.p2dx		Wide	Deep	1,223	1,111	1,101	*
Proef 11-DitchFar-Wide-shallow-Nsteep_Preload_Time.p2dx			Shallow	1,19	1,129	1,110	1,084
Proef 11-DitchFarVSmall-deep-Nsteep_Preload_Time.p2dx		VSmall		1,171	1,099	1,071*	1,024
Proef 11-DitchVFarSmall-deep-Nsteep_Preload_Time.p2dx	VeryFar	Small	Deep	1,2	1,063	1,113	1,114
Proef 11-DitchCloseSmall-deep-Nsteep_Preload_Time-BM-Mesh.p2dx	Benchmark			1,19	1,141	0,98	1,11

¹* Did not converged (completely)

The configurations in red are chosen to be conducted in centrifuge test

¹ Saved in N:\Projects\11210000\11210298\B. Measurements and calculations\003 - Centrifuge tests\FEM prediction\Elham\Virtuals.

Mesh analysis

In order to study the impact of mesh discretisation, several mesh arrangements are performed. The obtained results are shown in Table A.4. The safety indicator of safety factor, ΣMsf along the time of analysis in Table A 5. The safety indicator in different phases are not changing with finer mesh than the basis model, though finer meshes significantly increase the time of calculations.

Table A 5 Mesh study.

file Name	Close Small Deep	No. Element	Min Mesh Quality	SF (uplift)	SF (90g)
Proef 11-DitchCloseSmall-deep-Nsteep_Preload_Time_VVfine.p2dx	Mod. VVFine	8715	0,51	1,17	1,08
Proef 11-DitchCloseSmall-deep-Nsteep_Preload_Time_VVfine.p2dx	Mod. VFine	4379	0,54	1,163	1,099
Proef 11-DitchCloseSmall-deep-Nsteep_Preload_Time-Basis.p2dx	Basis	3700	0,53	1,173	1,109
Proef 11-DitchCloseSmall-deep-Nsteep_Preload_Time_fine.p2dx	Fine	2053	0,42	1,168	1,108
Proef 11-DitchCloseSmall-deep-Nsteep_Preload_Time_Medium.p2dx	Medium	948	0,46	1,205	1,108
Proef 11-DitchCloseSmall-deep-Nsteep_Preload_Time_Coarse.p2dx	Coarse	542	0,52	1,215	1,108

A.8 Case of the weaker dike

The impact of the strength parameters of the dike body is tested for the model with the close, small ditch. The reduced friction and dilatancy angle is given in Table A 6.

Table A 6 Reduced friction and dilatancy angle, original values between brackets

Friction angle	φ'	°	35.0 (45.0)
Dilatancy angle	Ψ	°	5.0 (8.0)

And the model shows less safety against uplift and higher g-levels.

File Name	Geometry	SF (Uplift)	90g	110g
Proef 11-DitchCloseSmall-deep-Nsteep_Preload_Time-BM-Mesh.p2dx	Basis	1.042 (1.19)	0.99 (1.14)	0.98 (0.98)

Although the displacements in the uplift safety phase are almost the same as the basis dike, the weaker dike material forms a smaller slip surface, as shown in Figure A.28.

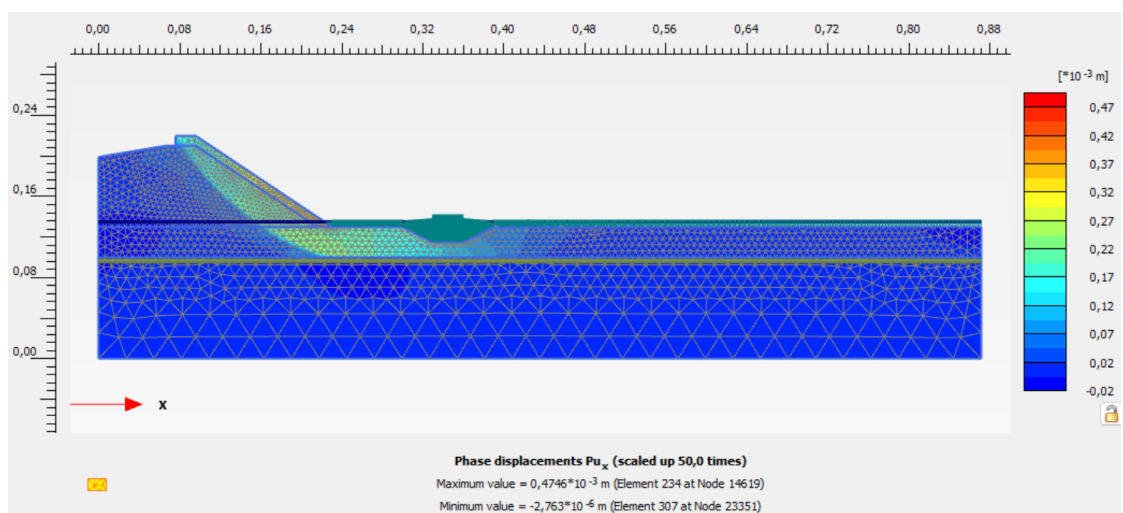


Figure A.28 Weaker model after uplift safety phase (horizontal phase displacement).

A.9 New permeability properties

Looking into the results of the performed test in 2023, the centrifuge models reached instability at lower g-level than found in the simulations above. To find better agreement between analysis and test results additional calculation have been performed. In the additional calculations the following changes were made:

- Not resetting the displacements to zero; In the previous models, after activating the dike material and also after 60g loading, the displacements were set to zero. This was not in accordance with the procedure in the centrifuge experimental tests.
- A careful study of the PWP results also showed fast dissipation of the water pressure in the cover layer, as shown in Figure A.13. It has raised some questions regarding the assigned material parameters regarding the permeability, which are considered to be equal to a set of calibrated data mentioned in a calibration memo². These are different from the main data set which has been obtained from the initial experimental studies; see Table A.7.

Table A.7 Permeability parameters.

Parameter	Symbol	Unit	11207357-028-GEO-0001	Calibration memo
permeability	k_x, k_y	[m/day]	$4,92 \times 10^{-5}$	$0,492 \times 10^{-3}$
Change in permeability	c_k	[-]	2,5	1,9

The simulation is performed with the new set of resetting displacements, while the permeability parameters are changed based on 11207357-028-GEO-0001 document. The results of the benchmark model (without ditch) are shown below.

Table A.8 The safety factors, SF, of the model with updated parameters.

file Name	SF (Uplift)	90g	110g	115g
CloseSmall-deep-Nsteep_Preload_Time-BM-Mesh-NoReset-K4.92e5-ck2.5-PermlntClay.p2dx	1.05	1.01	1.00	0.99

The centrifuge tests 1, 2, 3 and 4 found failure in the range of 110 to 115 g. This corresponds to the results given in Table A.8. Comparison of Figure A.29, which shows the observed failure mechanism and Figure A.30, which shows the calculated failure mechanism indicates a good agreement between the two.

² : N:\Projects\11207000\11207357\C. Report - advise\055 - Analyse centrifugeproeven\11207357-055-GEO-0005_v0.1-Plaxis sommen van de Geo-Centrifuge proeven.docx.



Figure A.29 Failure of test 01.

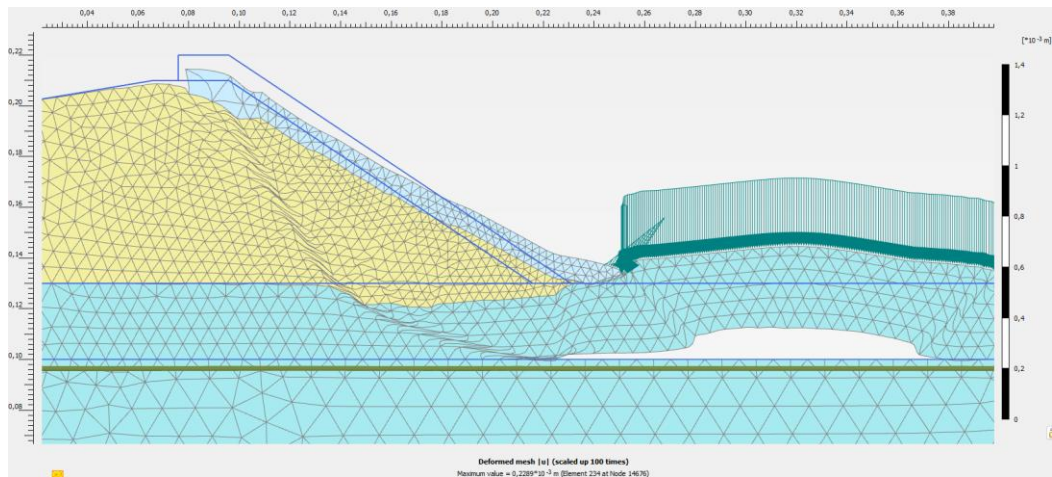


Figure A.30 Deformation after phase safety 110g.

The obtained results for the pore pressures under the dike body (in sensor P2) are depicted in Figure A.31, while Figure A.32 shows the calculated pore pressure at the location P2. The results are in close agreement, both for the trend and the range of changes.

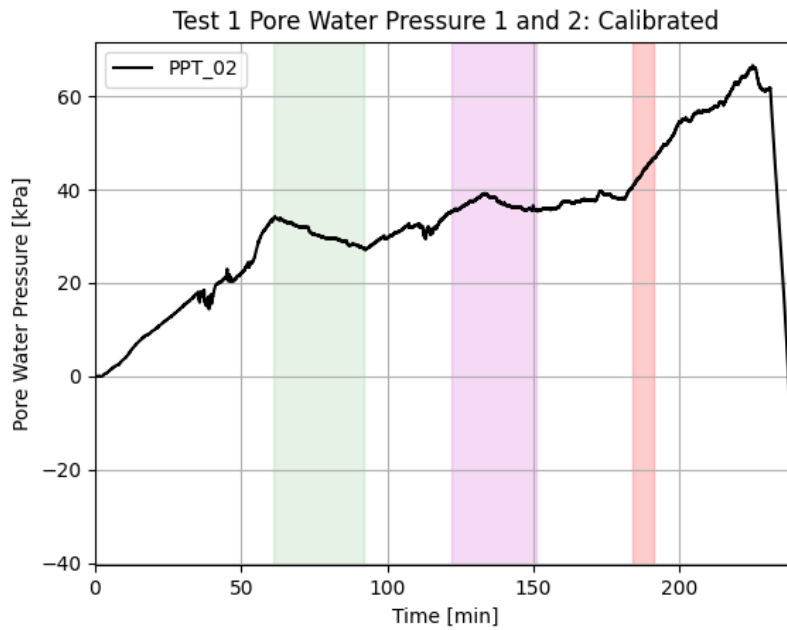


Figure A.31 Pore water pressure in P2 of test 01.

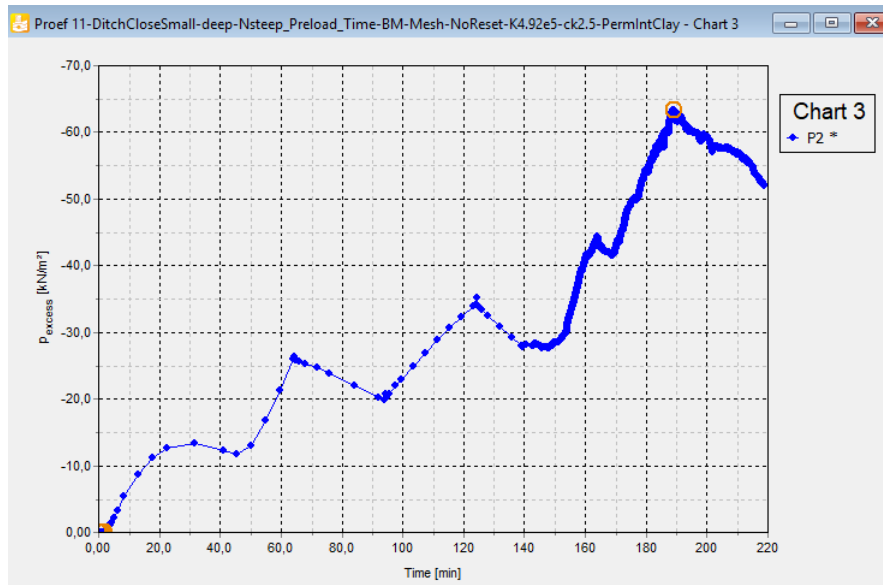


Figure A.32 Calculated pore water pressure at location of P2.

The same model configurations are applied to the model with a very small ditch at very close distance. Figure A.33 and Figure A.34 show the calculated failure mechanism for $c' - \phi'$ reduction after uplift.

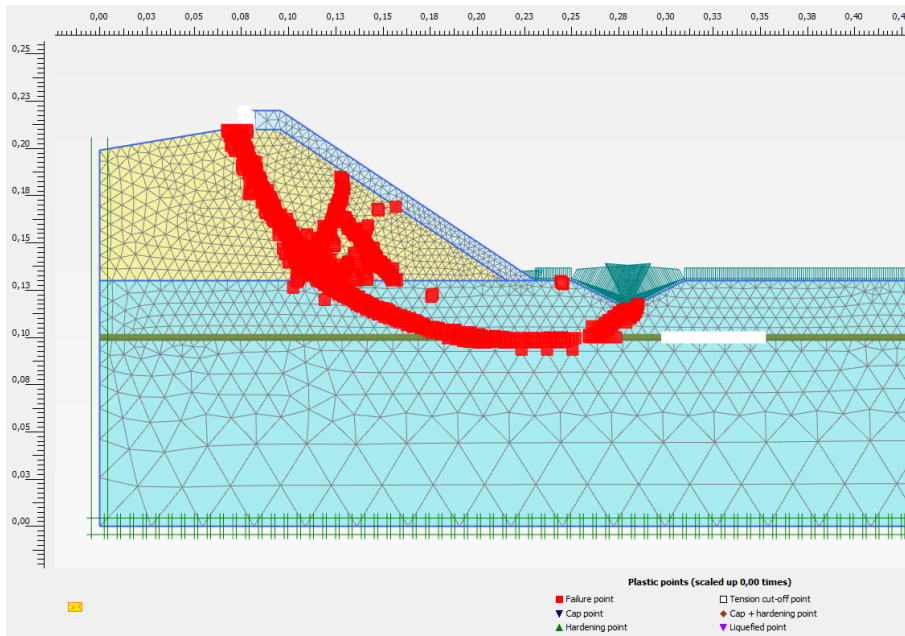


Figure A.33 Plastic points after uplift safety phase, $SF = 0.99$.

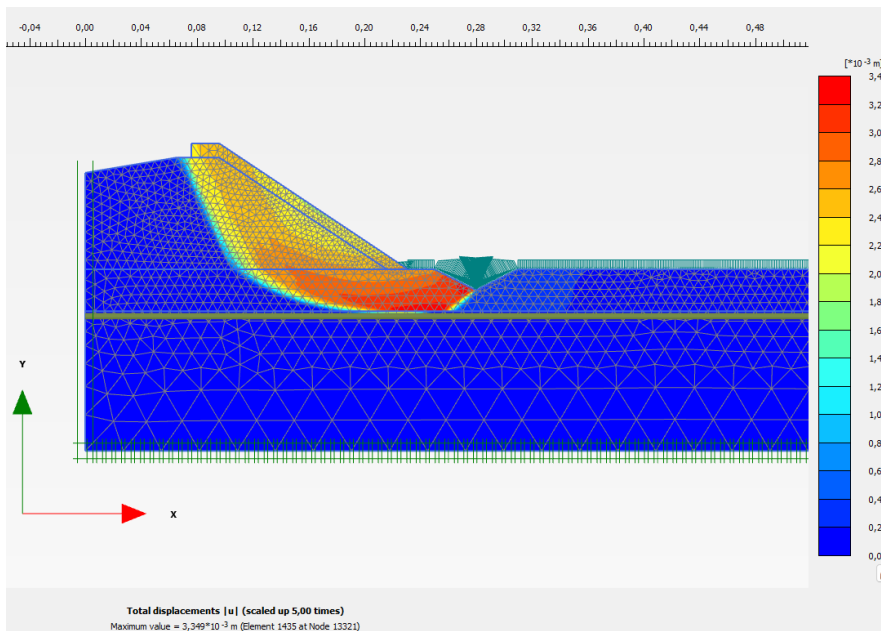


Figure A.34 Deformation after uplift safety phase (scaled), $SF = 0.99$.

Figure A.35 shows the observed failure mechanism. Comparison to the calculated failure mechanisms, Figure A.33 and Figure A.34 show a good agreement between the measured and calculated mechanism.



Figure A.35 Observed failure of test 04.

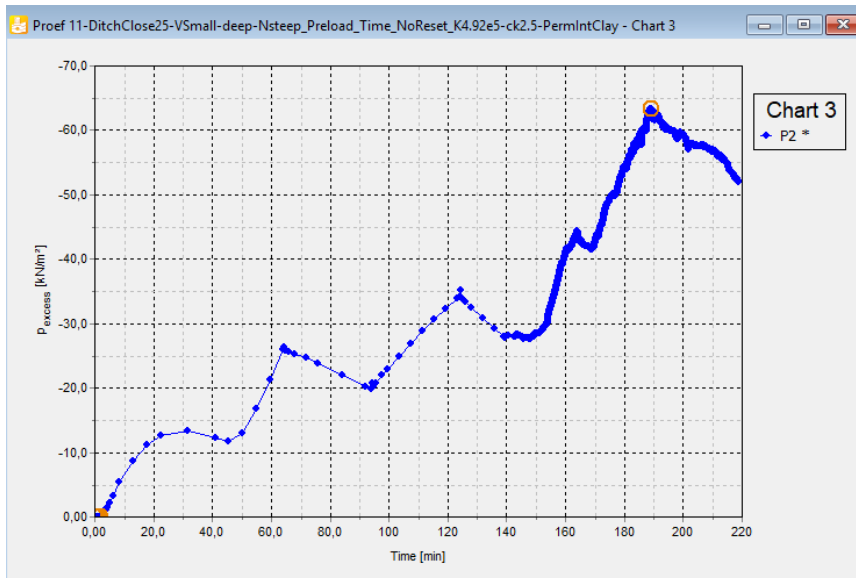


Figure A.36 Pore water pressure at location of P2.

After the uplift safety phase, the g-level increased to 90 and 110, in 10 and 20 minutes, respectively. Each phase followed by 5-minute consolidation phases. In the final phase, the g-level increased to 112g in 3 minutes, followed by a 5-minute consolidation phase. The reached safety factor (Σ Msf) of each phase is represented in Table A.9.

Table A.9 The safety indices of the model with updated parameters.

File Name	SF (Uplift)	90g	110g	112g
Proef 11-DitchClose25-VSmall-deep-Nsteep_Preload_Time_NoReset_K4.92e5-ck2.5-PermlntClay.p2dx	0.99	1.01	0.98	0.98

B Additional laboratory testing

B.1 Introduction

As explained in Chapter **Error! Reference source not found.**, the centrifuge series used remoulded Oostvaardersplassen, OVP, clay for modelling the cover layer. Since the amount available clay was limited, the clay was used multiple times, each time being remoulded before re-use. The multiple re-use of the clay posed questions on the material parameters. To check if the material behaviour, particularly the strength, remained unaltered during testing additional laboratory testing was conducted. The results were compared to test results of the same clay obtained at the start of the earlier conducted POD centrifuge series.

B.2 Comparison

The additional testing contained 1 constant rate of strain, CRS test and 2 Direct Simple Shear tests. Appendix C shows the additional test results for each of the individual tests. Former laboratory testing falls into two categories, a test series prior to the centrifuge series, conducted in October 2022, a test series conducted midway through the centrifuge programme, conducted at August 2023. The former results are documented in the design report of the POD centrifuge test series as explained in Chapter 1. Table B.1 shows a summary of the test results.

Table B.1 Summary of test results, γ = density, w = water content, e = void ratio, CR = compression ratio, b = compression ratio for natural strain.

Test nr	γ [kN/m ³]	w [%]	e [-]	CR [-]	b [-]
4A	13.6	108.0	2.56	0.27	0.16
17	13.3	111.6	2.48	0.34	0.18
20	13.2	115.3	2.59	0.35	0.17
18	13.3	110.0	2.48	0.35	0.18
23	12.4	128.7	2.48	0.32	0.17
10	12.5	124.4	2.41	0.30	0.16
11	12.9	120.4	2.57	0.31	0.17
Average	13.0	116.9	2.51	0.32	0.17
CoV*	0.03	0.07	0.03	0.09	0.04

* = coefficient of variance.

It should be noted that although the same procedure was followed in the remoulding the clay, the samples above originate from different batches, resulting in some variability.

Figure B.1 shows the stress – void ratio curves of the different tests.

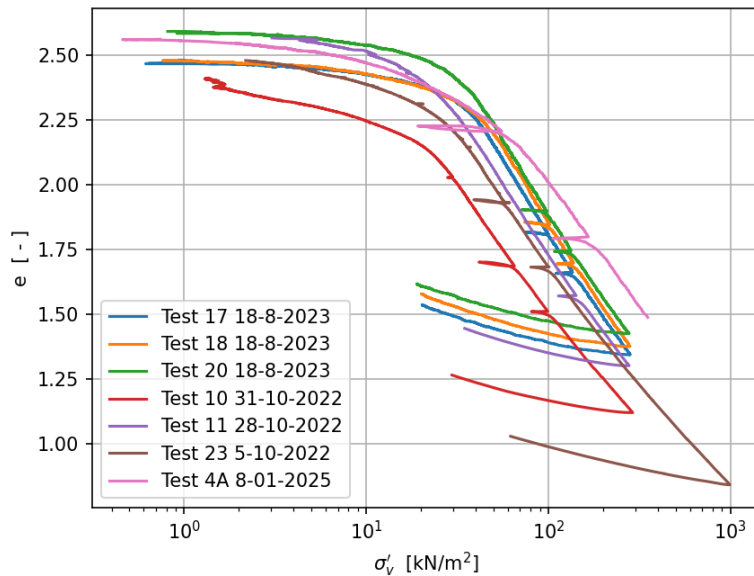


Figure B.1 Comparison stress – void ratio curves CRS tests.

Test 4A is conducted at a larger applied strain rate than the previous tests, see Figure B.2. Consequently, the stress void ratio curve falls on another isotach than the previously conducted tests. This explains the difference found in the stress – void ratio curves.

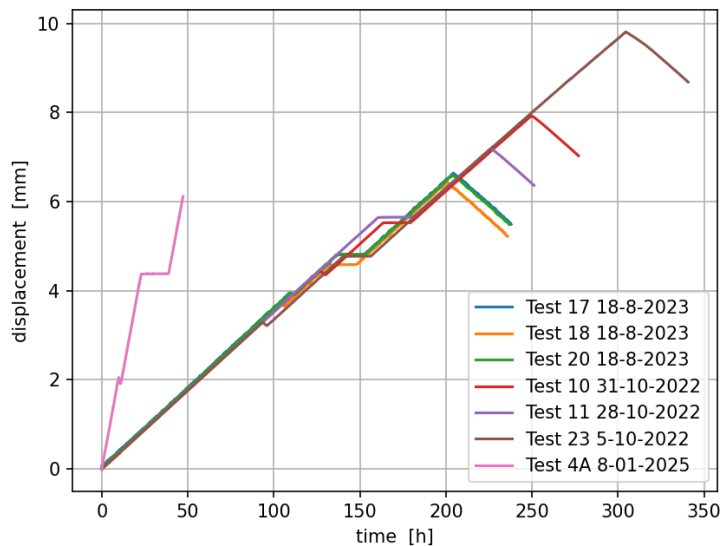


Figure B.2 CRS test results, applied displacement vs time in hours.

To improve comparison, Figure B.3a shows the different stress – void ratio curves by different colours, while in Figure B.3b the stress – void ratio curves are aligned at $\sigma'_v = 100$ kPa. The graphs show that the slopes have equivalent angles and stiffnesses obtained in the different tests are in agreement.

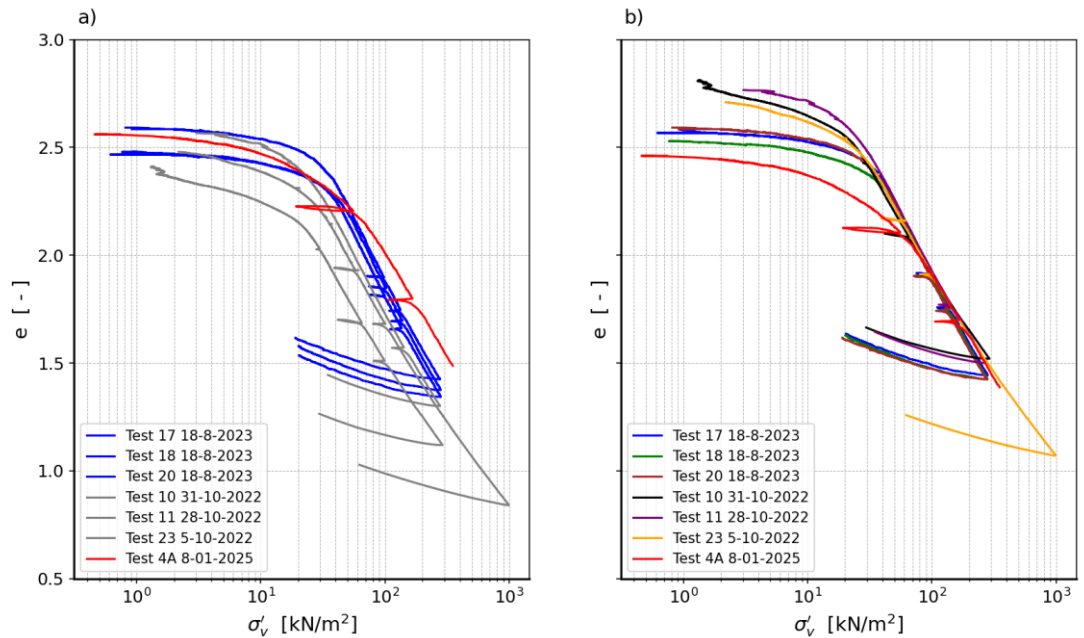


Figure B.3 Comparison stress – void ratio curve CRS tests a) presented in different colours, October 2022 in grey, tests August 2023 in blue and Test 4A, January 2025 in red and b) curves aligned at $\sigma'_v = 100$ kPa

Besides the CRS tests, two additional direct simple shear, DSS, tests have been conducted. The additional test results are compared to the results of two DSS tests conducted on OVP clay prior to the centrifuge test series. These two tests have been conducted in October and November 2022. Figure B.4 compares the stress paths of the different tests.

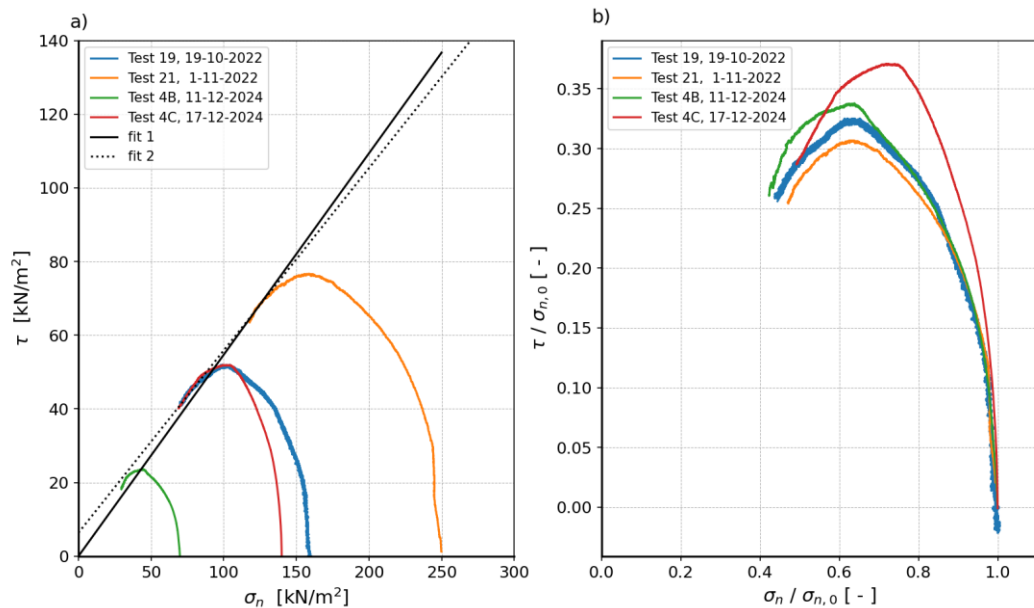


Figure B.4 DSS test results a) stress paths; fit 1 fits result Test 21 without cohesion, fit 2 fits test 19 and 21 b) stress paths normalised for initial normal stress, $\sigma_{n,0}$.

Figure B.4a shows two fits of the failure line. The first fit, shown by the solid line, disregards cohesion and fits to test 21. This fit results in $\phi' = 29^\circ$. The second fit, shown by the dotted line, includes cohesion and fits to test 19 and 21. This fit provides $c' = 6.4$ kN/m² and $\phi' = 26^\circ$.

The figure shows that the additional data comply well to the fitted failure line which includes cohesion. Figure B.4b compares the normalised stress paths. It is shown that the stress path of additional test 4C deviates from previous results, while additional test 4B resembles well to the previous data. Figure B.5 shows the comparison of the stress – strain curves.

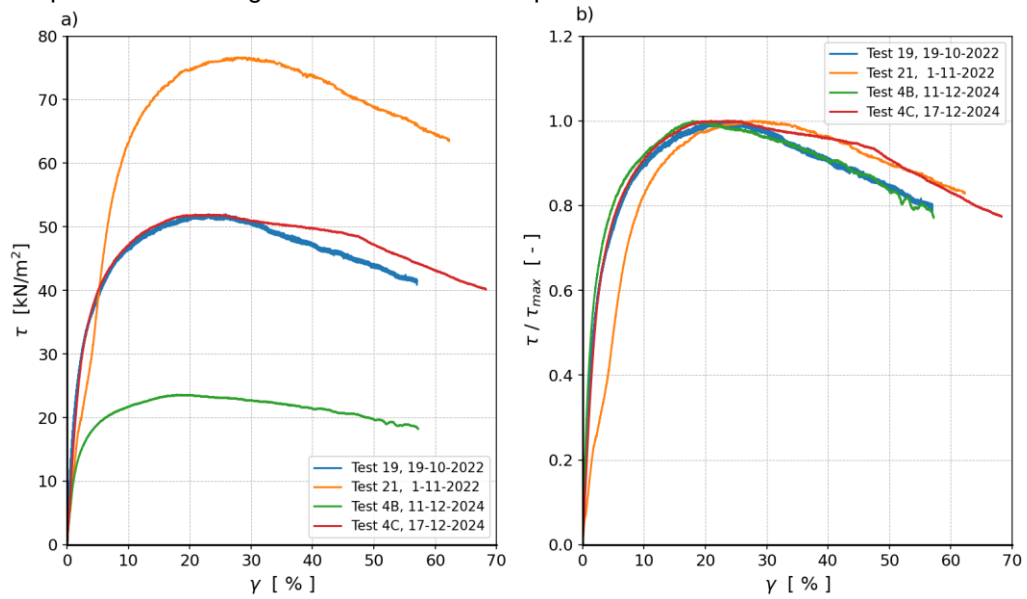


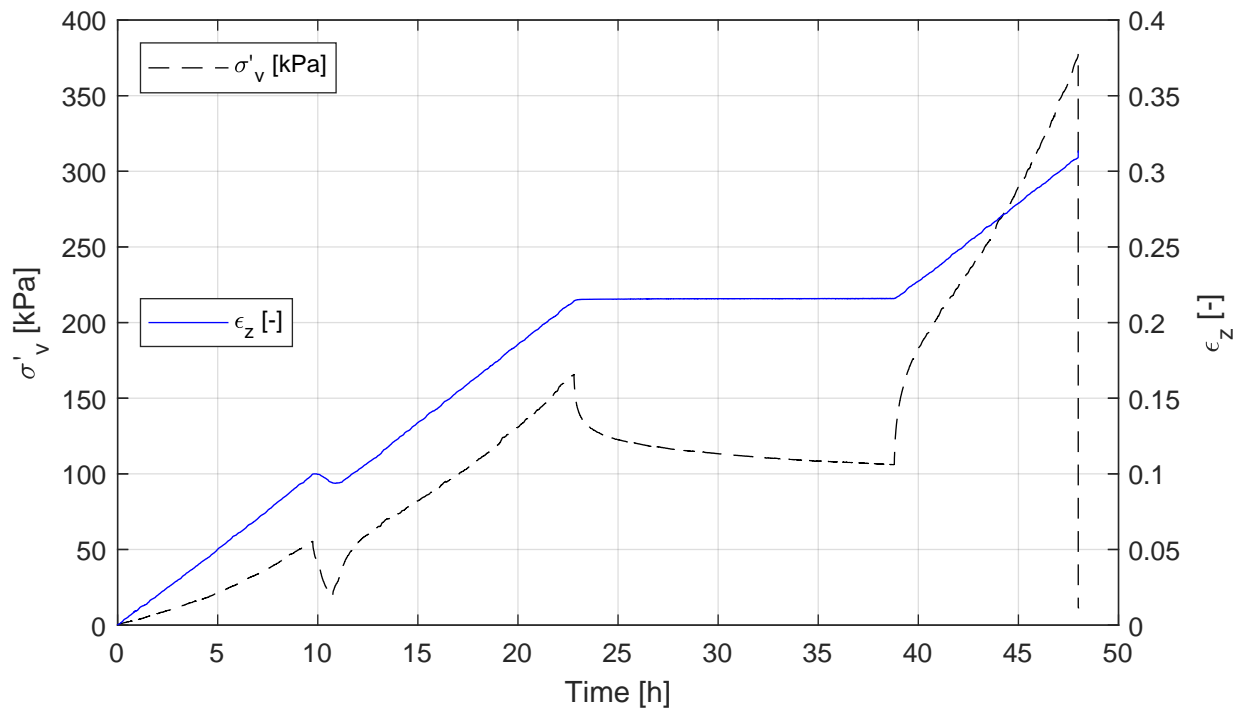
Figure B.5 DSS test results, stress – strain curves a) without normalisation, b) normalised for maximum shear stress, τ_{max} .

Minor differences in the stress – strain curves become visible after normalisation. Additional test 4B resembles test 19, while additional test 4C resembles test 21.

The comparison shows that there are difference between the results of the different tests, however, these differences seem to fall into the uncertainty due to heterogeneity and no significant change in material properties seem to be developed by re-using the clay.

B.3 Test results

B.3.1 K0-CRS 4A



Description of soil sample:

Soil description (ISO 14688)	clay, nonOrganic
Unit weight saturated soil [kN/m ³]	13.6
Unit weight dry soil [kN/m ³]	6.5
Water content [%]	108.0
Water content final [%]	71.0
Initial saturation [%]	100 (s)
Void ratio - initial [-]	2.56 (e)
Loss On Ignition [%]	16.0
Sample disturbance index [%]	-
s and e calculated with measured γ_s [kN/m ³] of	23.3

Test overview (test plan):

In-situ stress [kPa]	0
Stress loading phase [kPa]	60
Stress unloading phase [kPa]	15
Stress reloading phase [kPa]	180
Stress relaxation phase [kPa]	180
Maximum stress [kPa]	400

Deltares

PO Box 177, NL 2600 MH Delft
Boussinesqweg 1, 2629 HV Delft

Telephone +31 (0)88 335 8273
Homepage www.deltares.nl

date
2025-01-15

signed
venema

Praktijkproef Reevediep: 3c uitvoeren centrifugeproeven: Geotechnische proeven
Sample 4A, depth: 0.00 m to -0.20 m GL

project
11207357.30

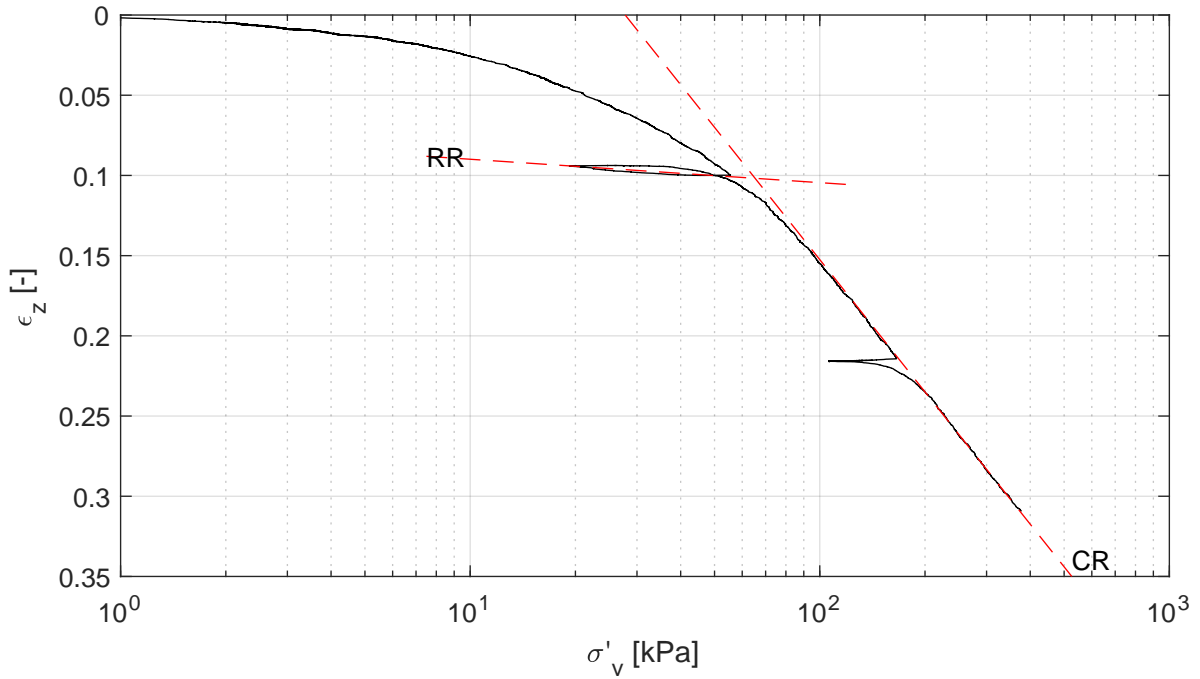
version
1.1

K0-CRS measurement

appendix
CRS 4A

page
1

Isotach method linear strain

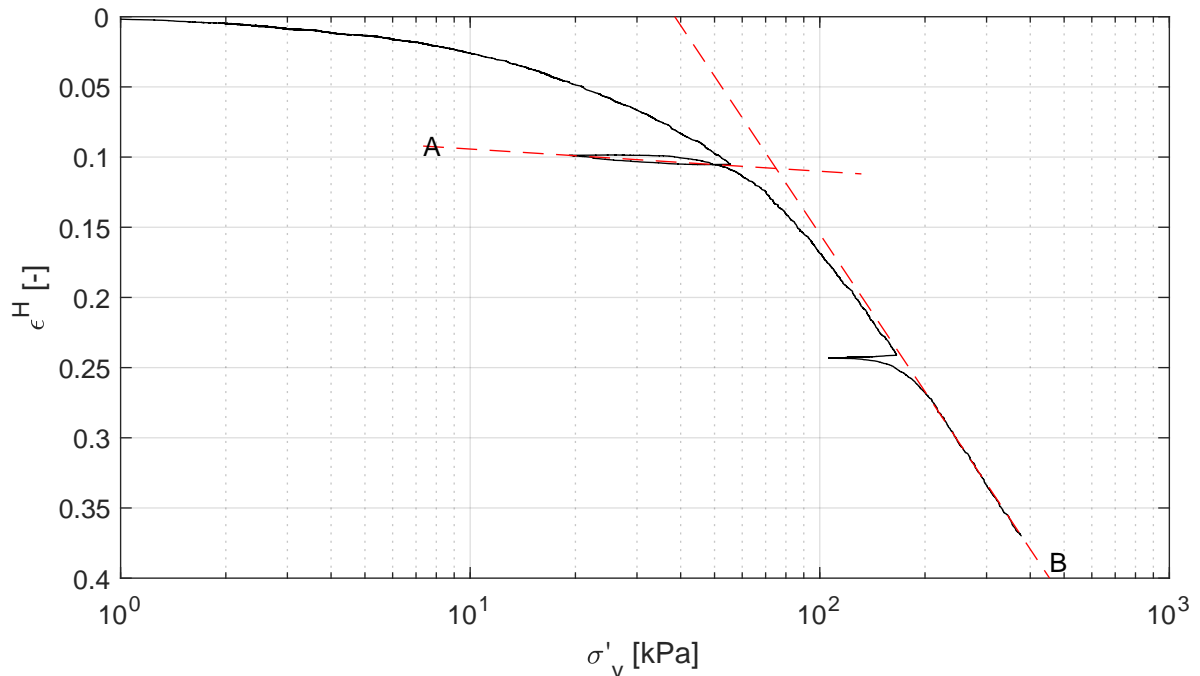


RR = 1.5e-02
CR = 2.7e-01

$C_\alpha = 1.9e-02$

Pg = NaN kPa
Pg_B = 123.0 kPa

Isotach method natural strain



A = 6.9e-03
B = 1.6e-01

C = 1.1e-02

Pg = NaN kPa
Pg_B = 203.7 kPa

Deltares

PO Box 177, NL 2600 MH Delft
Boussinesqweg 1, 2629 HV Delft

Telephone +31 (0)88 335 8273
Homepage www.deltares.nl

date
2025-01-15

signed
venema

Praktijkproef Reevediep: 3c uitvoeren centrifugeproeven: Geotechnische proeven
Sample 4A, depth: 0.00 m to -0.20 m GL

project
11207357.30

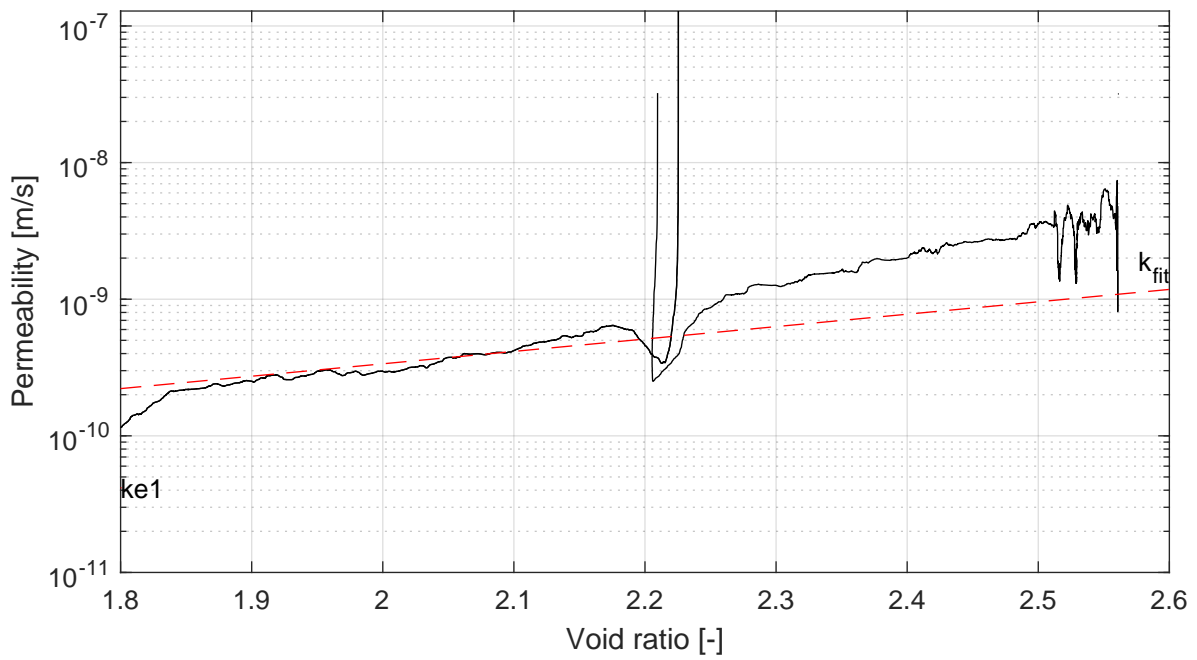
version
1.1

K0-CRS measurement

appendix
CRS 4A

page
2

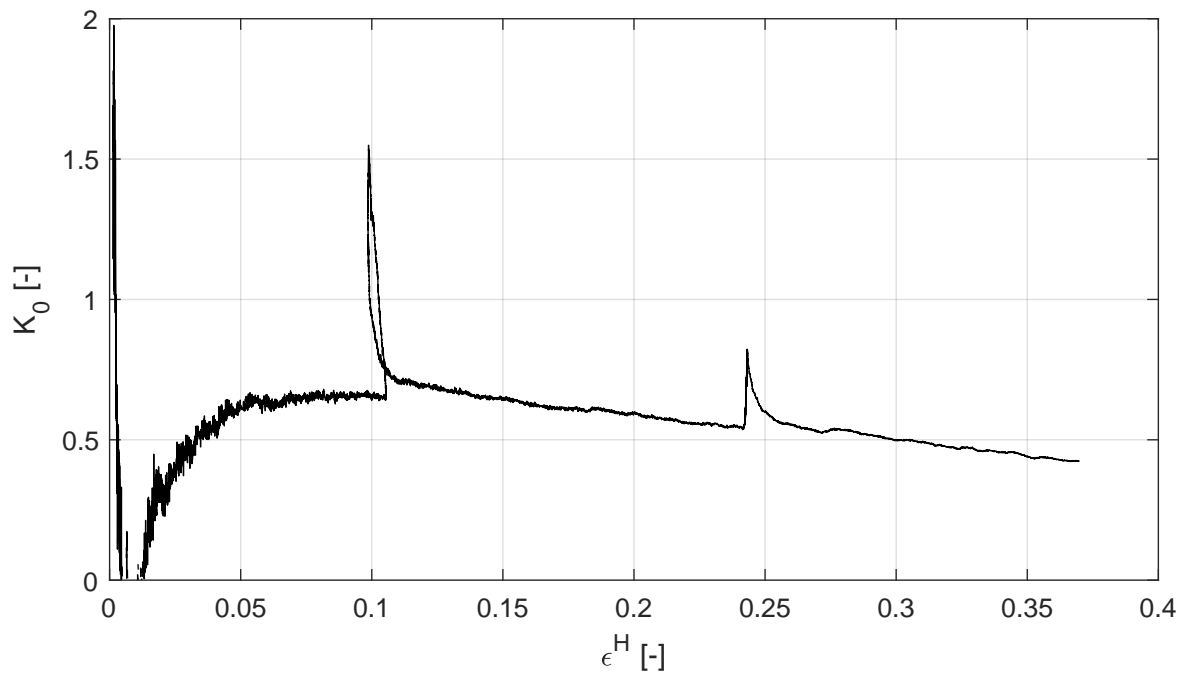
*) Gecontroleerd en vrijgegeven door ess op 2025-01-15



$k_{e1} = 4.2e-11$ m/s

$k_{e0} = 1.1e-09$ m/s

slope = $9.08e-01$



$\nu = 0.15$

$K_{0c} = 0.65$

$K_{0e} = 0.42$

Deltares

PO Box 177, NL 2600 MH Delft
Boussinesqweg 1, 2629 HV Delft

Telephone +31 (0)88 335 8273
Homepage www.deltares.nl

date
2025-01-15

signed
venema

Praktijkproef Reevdiep: 3c uitvoeren centrifugeproeven: Geotechnische proeven
Sample 4A, depth: 0.00 m to -0.20 m GL

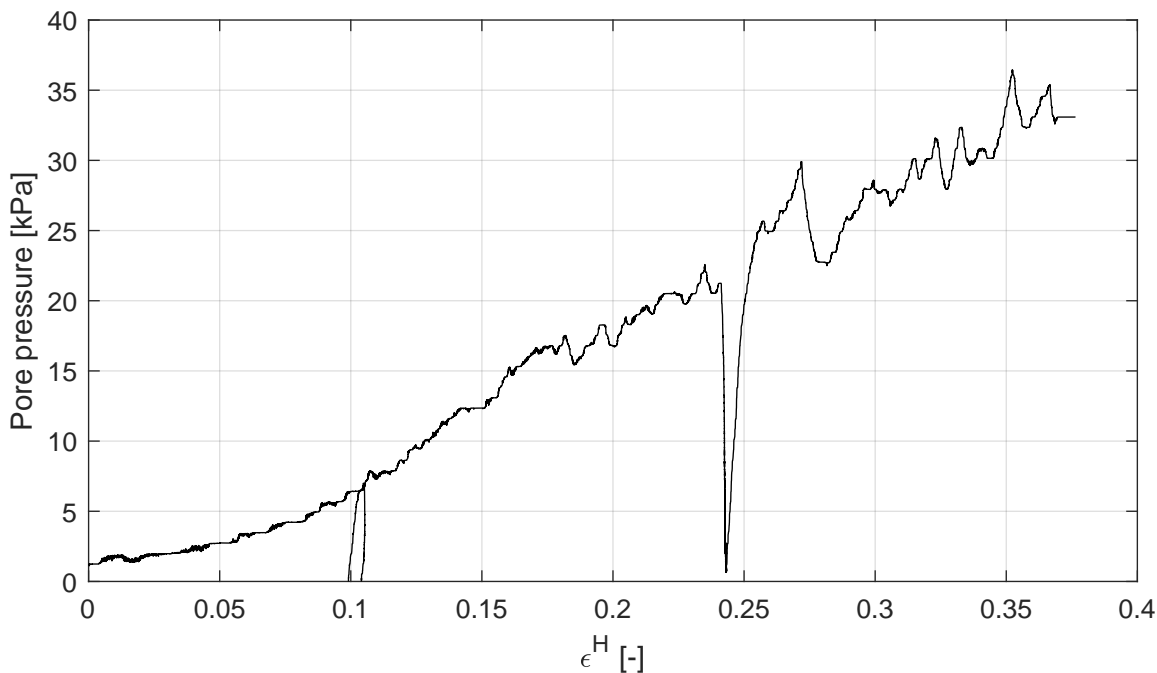
project
11207357.30

version
1.1

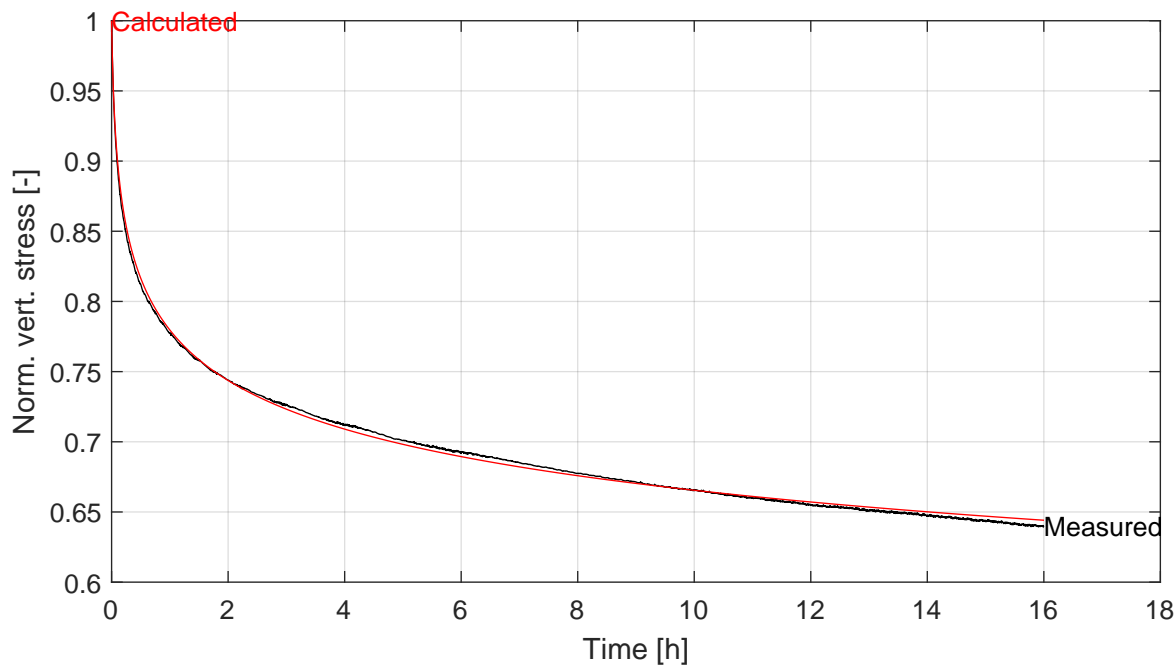
K0-CRS measurement

appendix
CRS 4A

page
3



Relaxation



Deltares

PO Box 177, NL 2600 MH Delft
Boussinesqweg 1, 2629 HV Delft

Telephone +31 (0)88 335 8273
Homepage www.deltares.nl

date
2025-01-15

signed
venema

Praktijkproef Reevediep: 3c uitvoeren centrifugeproeven: Geotechnische proeven
Sample 4A, depth: 0.00 m to -0.20 m GL

project
11207357.30

version
1.1

K0-CRS measurement

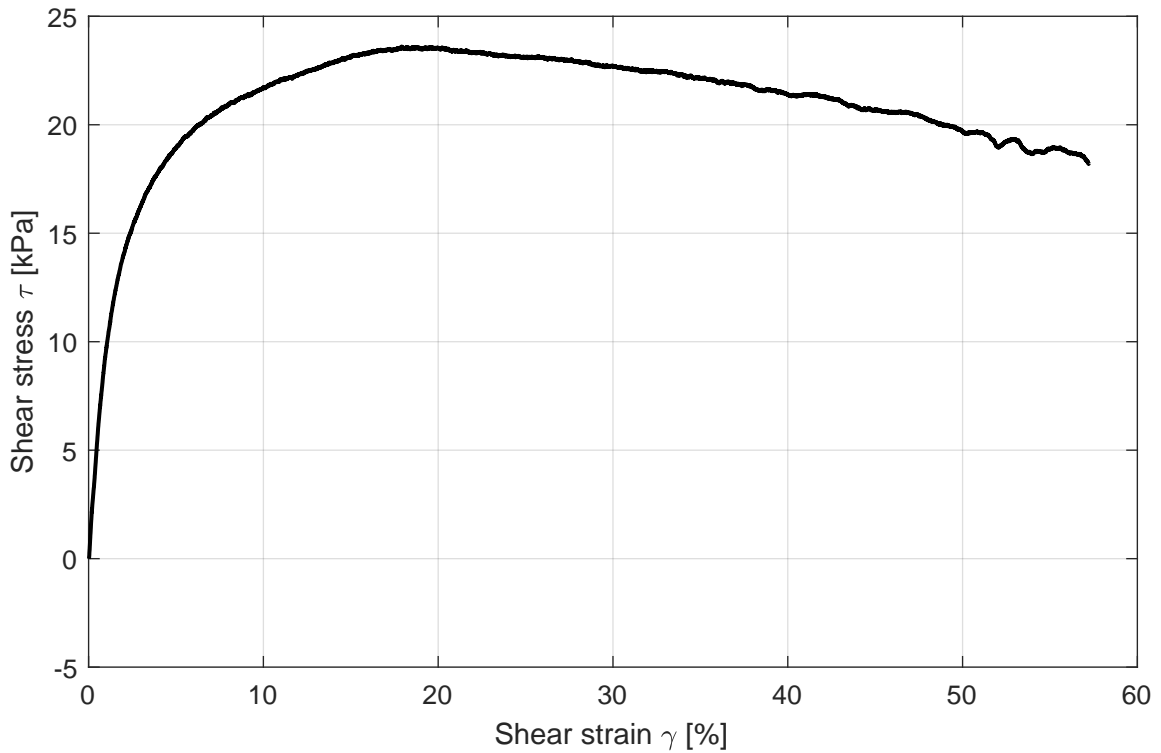
appendix
CRS 4A

page
4



Deltares PO Box 177, NL 2600 MH Delft Boussinesqweg 1, 2629 HV Delft Telephone +31 (0)88 335 8273 Homepage www.deltares.nl	date	signed
	2025-01-15	venema
	project	version
Praktijkproef Reevediep: 3c uitvoeren centrifugeproeven: Geotechnische proeven	11207357.30	1.1
Sample 4A, depth: 0.00 m to -0.20 m GL	appendix	page
K0-CRS measurement	CRS 4A	5

*) Gecontroleerd en vrijgegeven door ess op 2025-01-15



Description of soil sample:

Soil classification	clay, nonOrganic
Pressure area [cm ²]	31.17
Mean temperature during shear [°C]	21.4
Test type	Height constant
Apparatus code	DSS-D
Sample name	4B
Bore code	-
Depth from GL [m]	0.00
Depth to GL [m]	-0.20
Specimen condition	Intact
Trimming procedure	With knives and wire saw
ρ_s [g/cm ³]	1.37
S_0 [%]	95
Void ratio start shear [-]	2
w_0 [%]	97.0
w_{final} [%]	92.1
Consolidation stress [kPa]	69.9
Consolidation strain [%]	14.25
Strain rate [%/h]	5.0
Max shear stress [kPa]	23.6
Vert. stress at max shear stress [kPa]	44.6
Shear strain at max shear stress [%]	17.9
σ_v at $\gamma = 40\%$ [kPa]	33.5
τ at $\gamma = 40\%$ [kPa]	21.4
Sample Disturbance Index [%]	-
SDI qualification	-

Deltares

PO Box 177, NL 2600 MH Delft
Boussinesqweg 1, 2629 HV Delft

Telephone +31 (0)88 335 8273
Homepage www.deltares.nl

date
2024-12-19

signed
venema

Praktijkproef Reevediep: 3c uitvoeren centrifugeproeven

Direct Simple Shear test on sample 4B

Direct Simple Shear Test

project
11207357.30

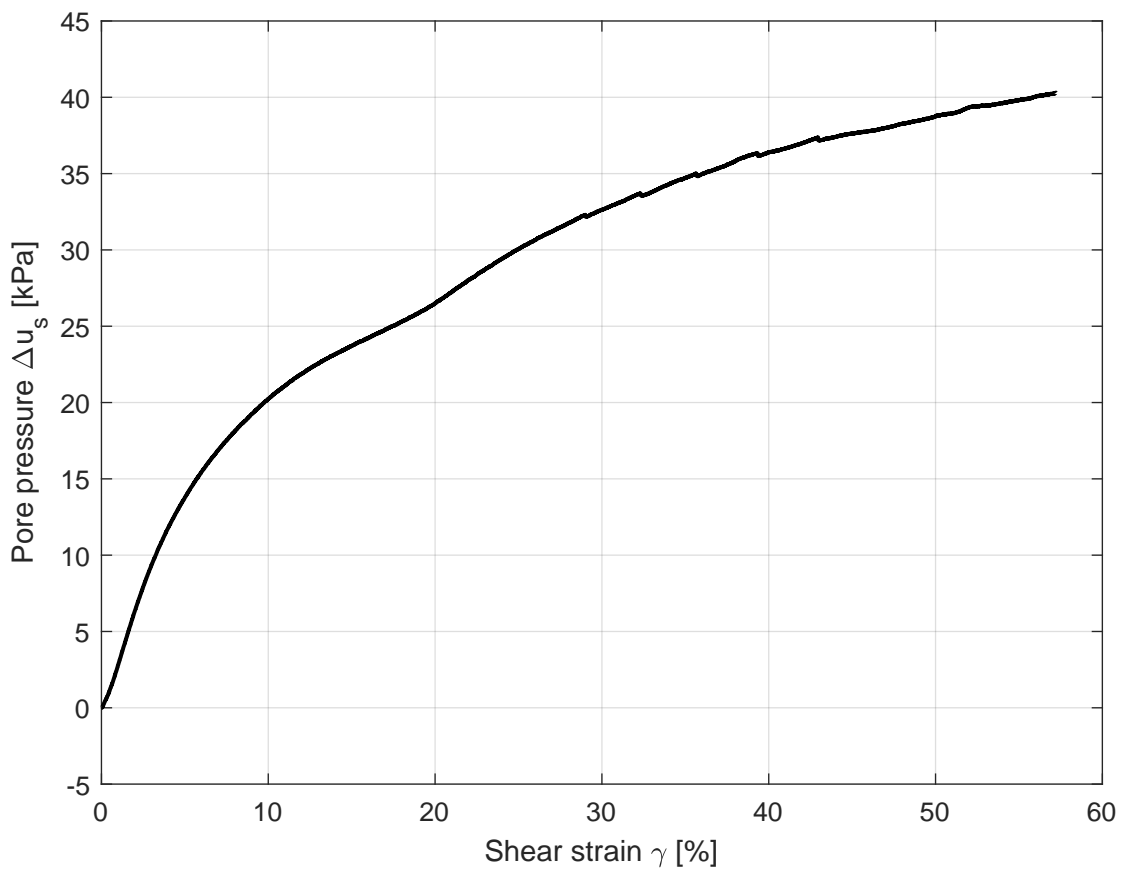
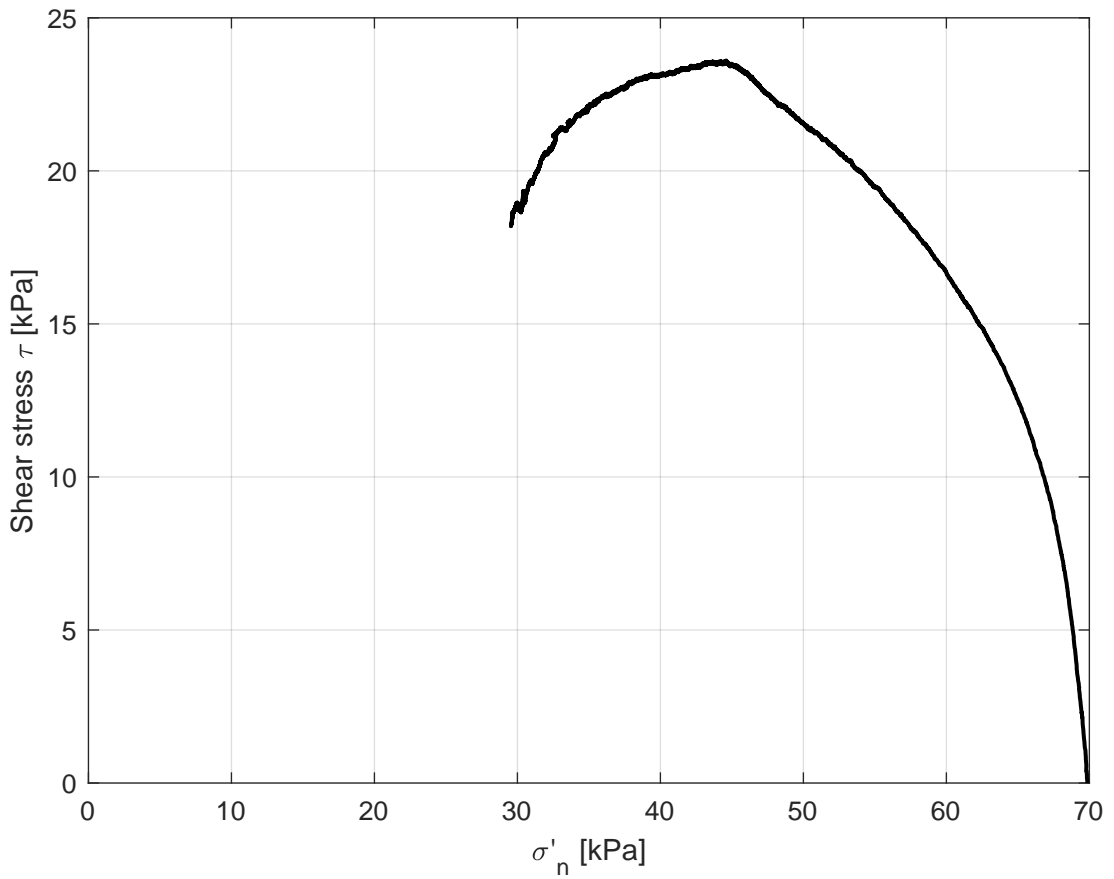
version

1.3

appendix
DSS4B

page

1



Deltares

PO Box 177, NL 2600 MH Delft
Boussinesqweg 1, 2629 HV Delft

Telephone +31 (0)88 335 8273
Homepage www.deltares.nl

date
2024-12-19

signed
venema

Praktijkproef Reevediep: 3c uitvoeren centrifugeproeven

Direct Simple Shear test on sample 4B

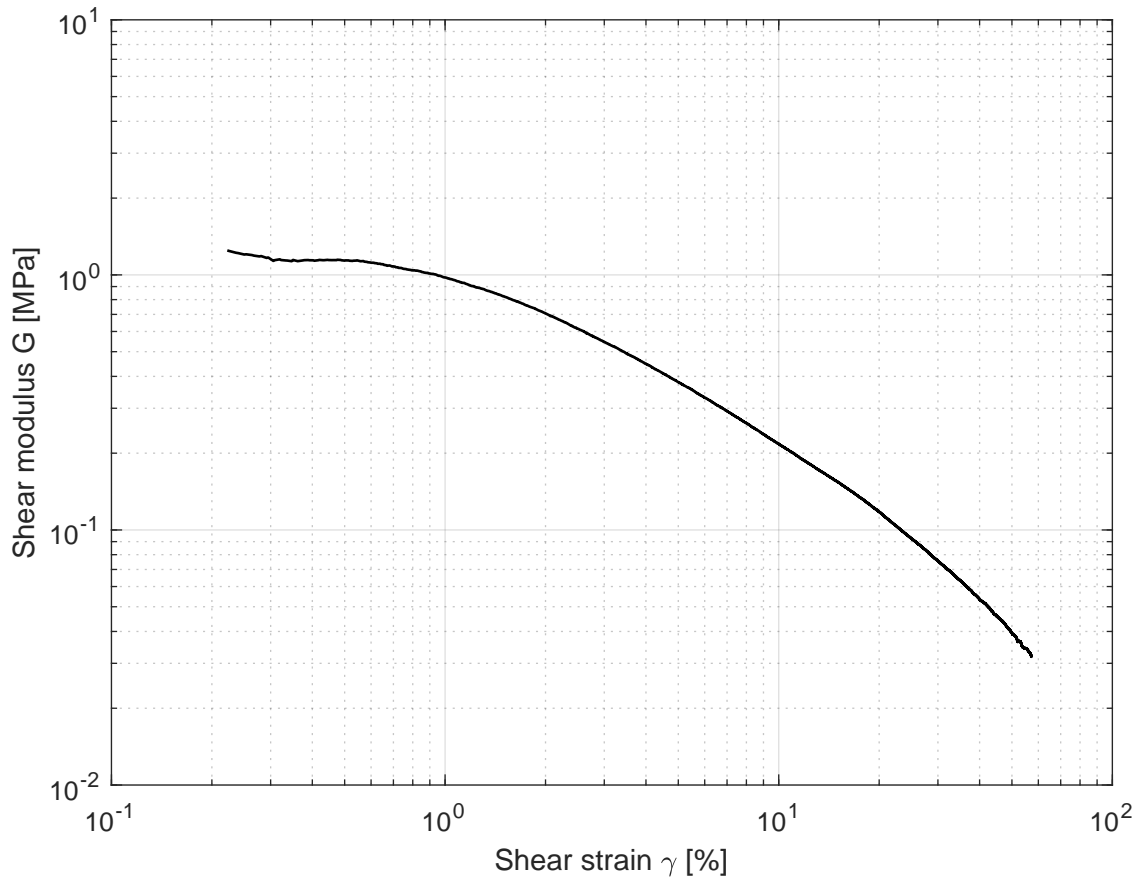
Direct Simple Shear Test

project
11207357.30

version
1.3

appendix
DSS4B

page
2



γ [%]	τ [kPa]	σ'_n [kPa]	Δu_s [kPa]	G [MPa]
5% deformation	18.9	56.1	13.8	0.38
15% deformation	23.2	46.2	23.7	0.15
30% deformation	22.7	37.2	32.6	0.08
Maximum strain	18.2	29.6	40.3	0.03
Maximum τ	23.6	44.6	25.3	0.13

Deltares

PO Box 177, NL 2600 MH Delft
Boussinesqweg 1, 2629 HV Delft

Telephone +31 (0)88 335 8273
Homepage www.deltares.nl

date
2024-12-19

signed
venema

Praktijkproef Reevediep: 3c uitvoeren centrifugeproeven

Direct Simple Shear test on sample 4B

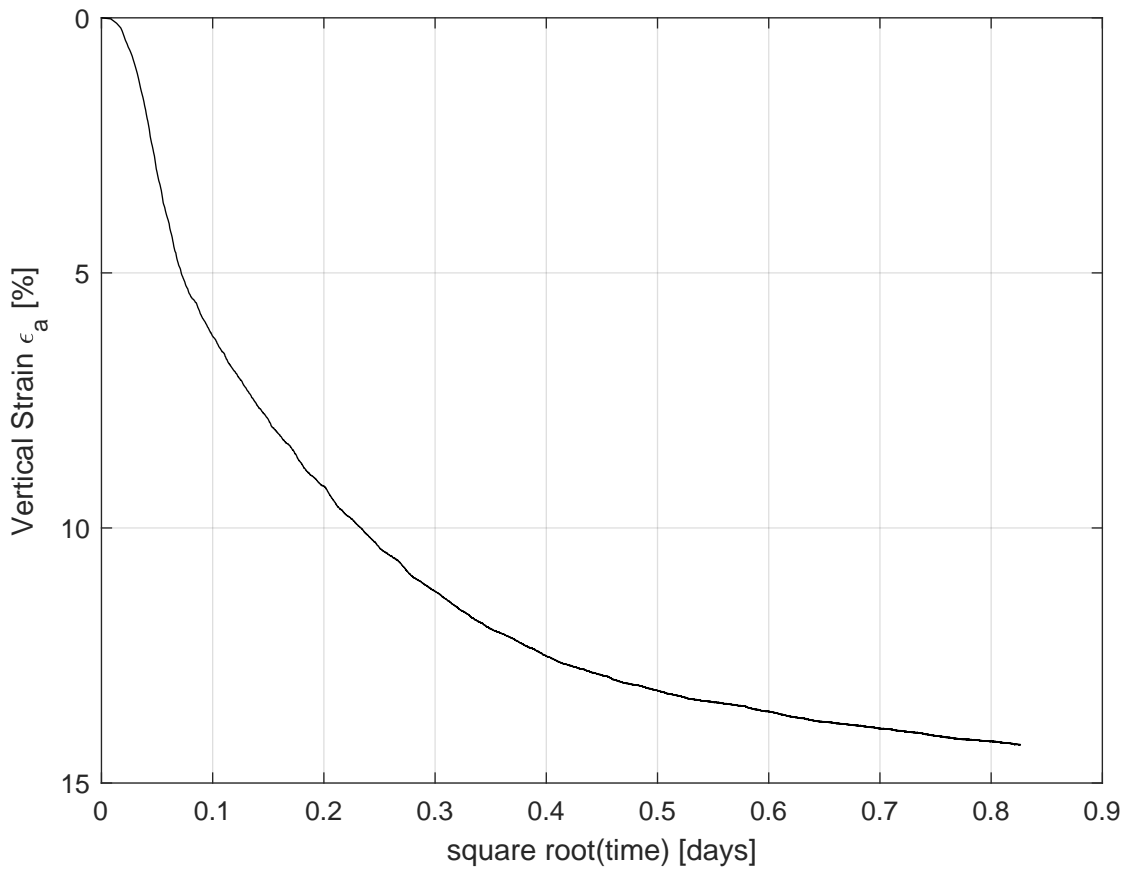
Direct Simple Shear Test

project
11207357.30

version
1.3

appendix
DSS4B

page
3



Deltares

PO Box 177, NL 2600 MH Delft
Boussinesqweg 1, 2629 HV Delft

Telephone +31 (0)88 335 8273
Homepage www.deltares.nl

date
2024-12-19

signed
venema

Praktijkproef Reevediep: 3c uitvoeren centrifugeproeven
Direct Simple Shear test on sample 4B

project
11207357.30

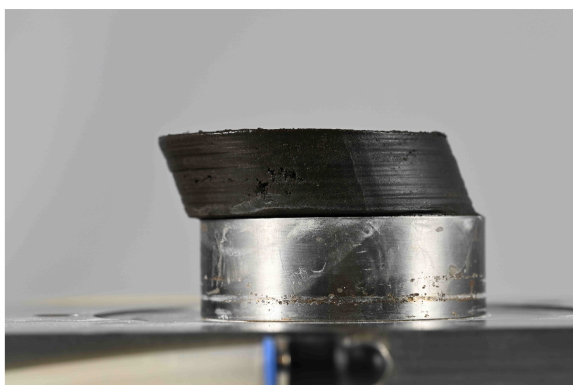
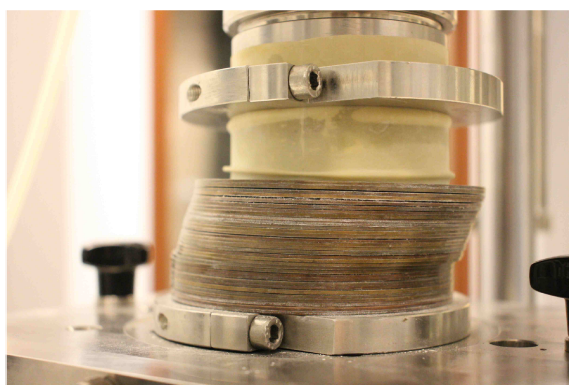
version
1.3

Direct Simple Shear Test

appendix
DSS4B

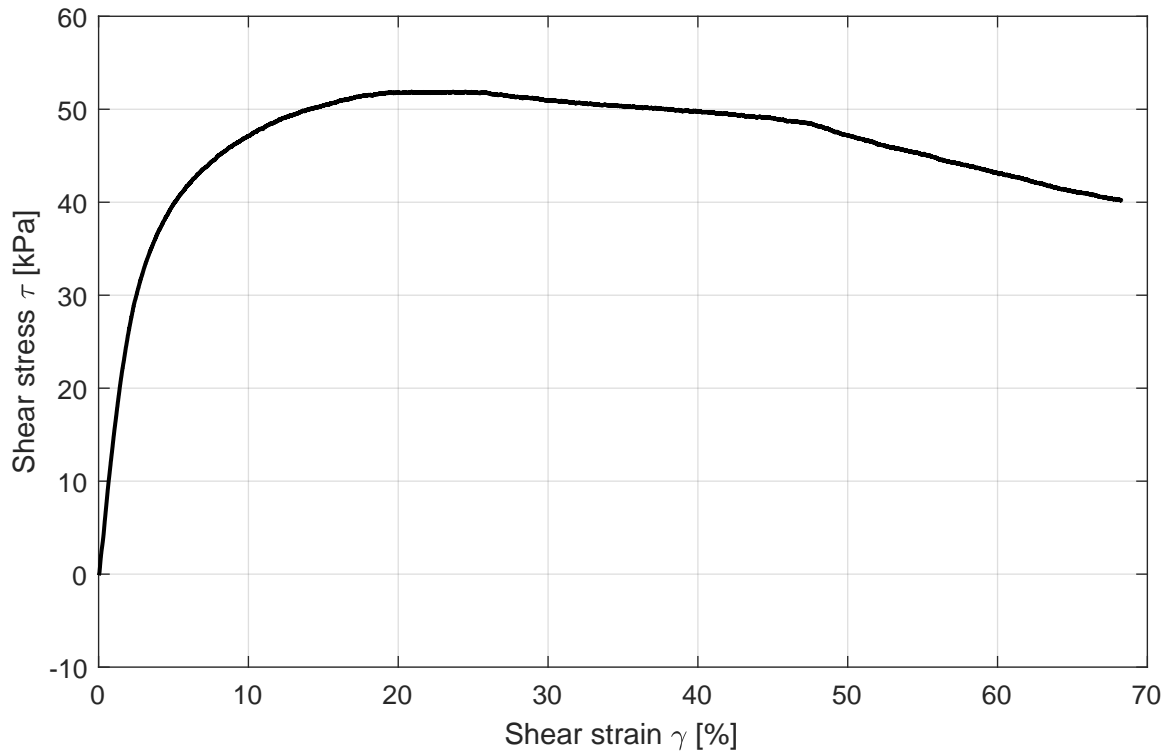
page
4

*) Gecontroleerd en vrijgegeven door ess op 2024-12-19



Deltares PO Box 177, NL 2600 MH Delft Boussinesqweg 1, 2629 HV Delft	Telephone +31 (0)88 335 8273 Homepage www.deltares.nl	date	signed
		2024-12-19	venema
Praktijkproef Reevediep: 3c uitvoeren centrifugeproeven Direct Simple Shear test on sample 4B		project	version
		11207357.30	1.3
Direct Simple Shear Test		appendix	page
		DSS4B	5

*) Gecontroleerd en vrijgegeven door ess op 2024-12-19



Description of soil sample:

Soil classification	clay, nonOrganic
Pressure area [cm ²]	31.17
Mean temperature during shear [°C]	21.7
Test type	Height constant
Apparatus code	DSS-D
Sample name	4C
Bore code	-
Depth from GL [m]	0.00
Depth to GL [m]	-0.20
Specimen condition	Intact
Trimming procedure	With cutting ring
ρ_s [g/cm ³]	1.33
S_0 [%]	94
Void ratio start shear [-]	2
w_0 [%]	107.1
w_{final} [%]	84.0
Consolidation stress [kPa]	140.0
Consolidation strain [%]	27.77
Strain rate [%/h]	5.0
Max shear stress [kPa]	51.9
Vert. stress at max shear stress [kPa]	103.6
Shear strain at max shear stress [%]	20.9
σ_v at $\gamma = 40\%$ [kPa]	87.2
τ at $\gamma = 40\%$ [kPa]	49.7
Sample Disturbance Index [%]	-
SDI qualification	-

Deltares

PO Box 177, NL 2600 MH Delft
Boussinesqweg 1, 2629 HV Delft

Telephone +31 (0)88 335 8273
Homepage www.deltares.nl

date
2024-12-19

signed
venema

Praktijkproef Reevediep: 3c uitvoeren centrifugeproeven

Direct Simple Shear test on sample 4C

Direct Simple Shear Test

project
11207357.30

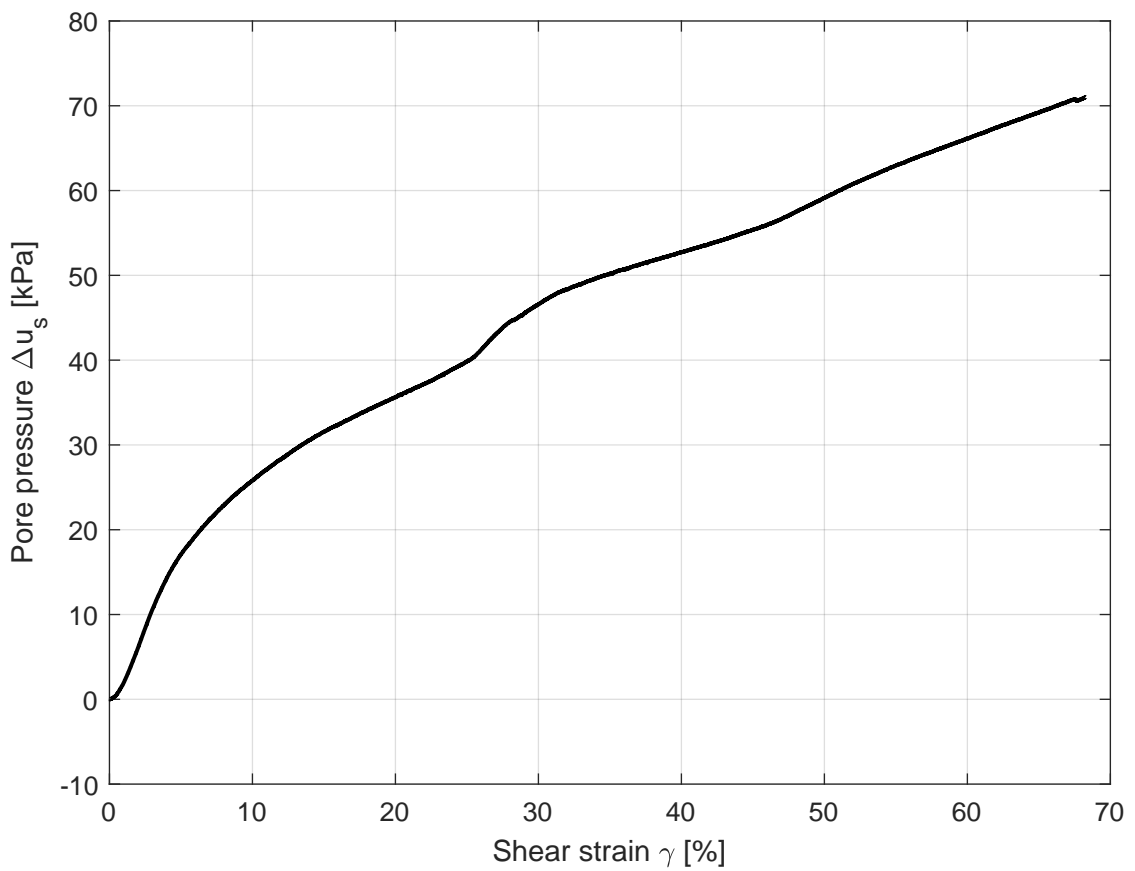
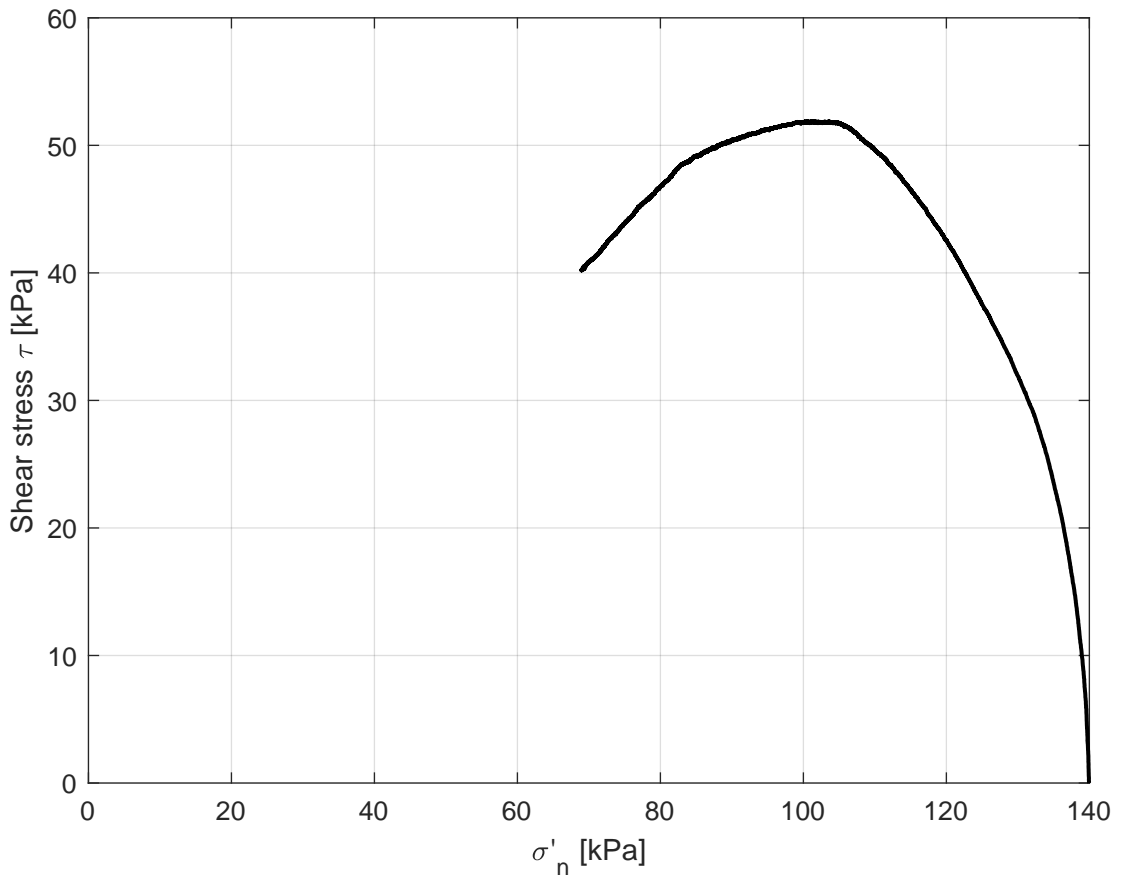
version

1.3

appendix
DSS 4C

page

1



Deltares

PO Box 177, NL 2600 MH Delft
Boussinesqweg 1, 2629 HV Delft

Telephone +31 (0)88 335 8273
Homepage www.deltares.nl

date
2024-12-19

signed
venema

Praktijkproef Reevediep: 3c uitvoeren centrifugeproeven

Direct Simple Shear test on sample 4C

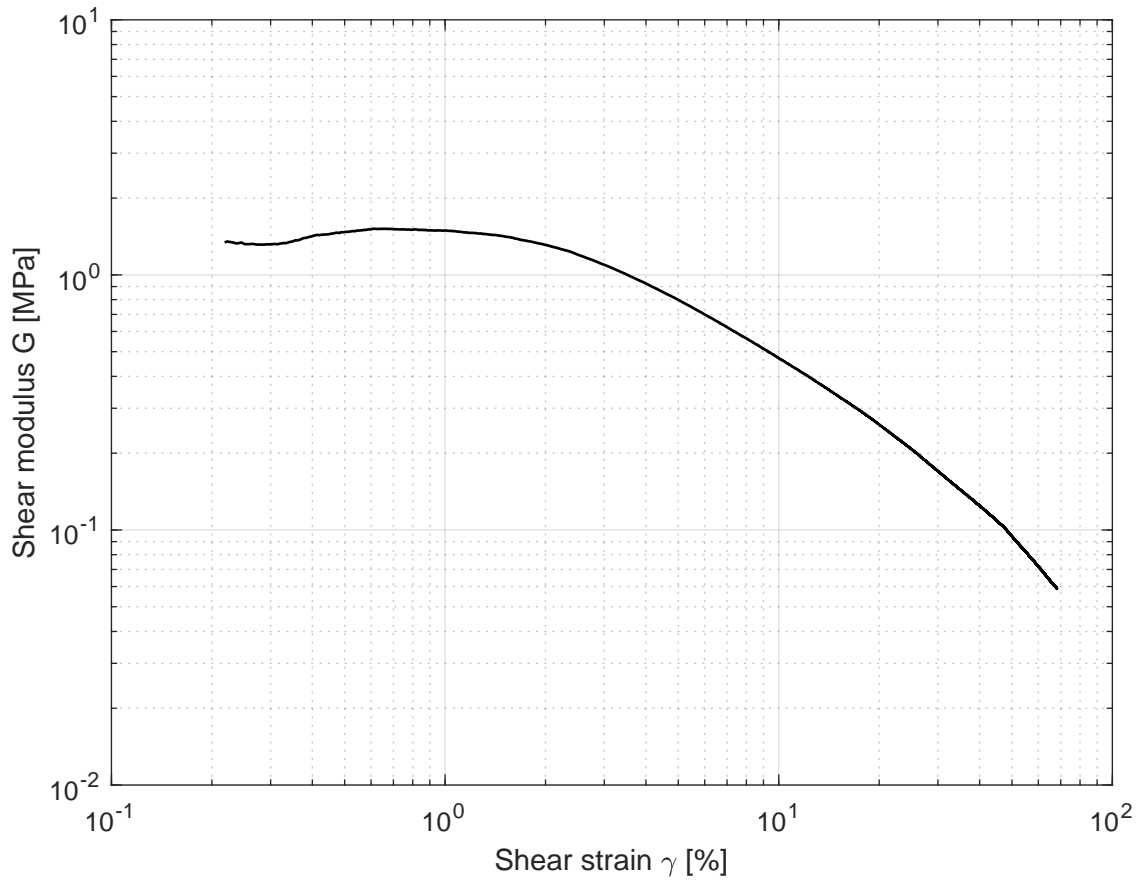
Direct Simple Shear Test

project
11207357.30

version
1.3

appendix
DSS 4C

page
2



γ [%]	τ [kPa]	σ'_n [kPa]	Δu_s [kPa]	G [MPa]
5% deformation	39.8	122.8	17.1	0.80
15% deformation	50.4	108.4	31.6	0.34
30% deformation	51.0	93.4	46.6	0.17
Maximum strain	40.2	68.9	71.0	0.06
Maximum τ	51.9	103.6	36.4	0.25

Deltares

PO Box 177, NL 2600 MH Delft
Boussinesqweg 1, 2629 HV Delft

Telephone +31 (0)88 335 8273
Homepage www.deltares.nl

date
2024-12-19

signed
venema

Praktijkproef Reevediep: 3c uitvoeren centrifugeproeven

Direct Simple Shear test on sample 4C

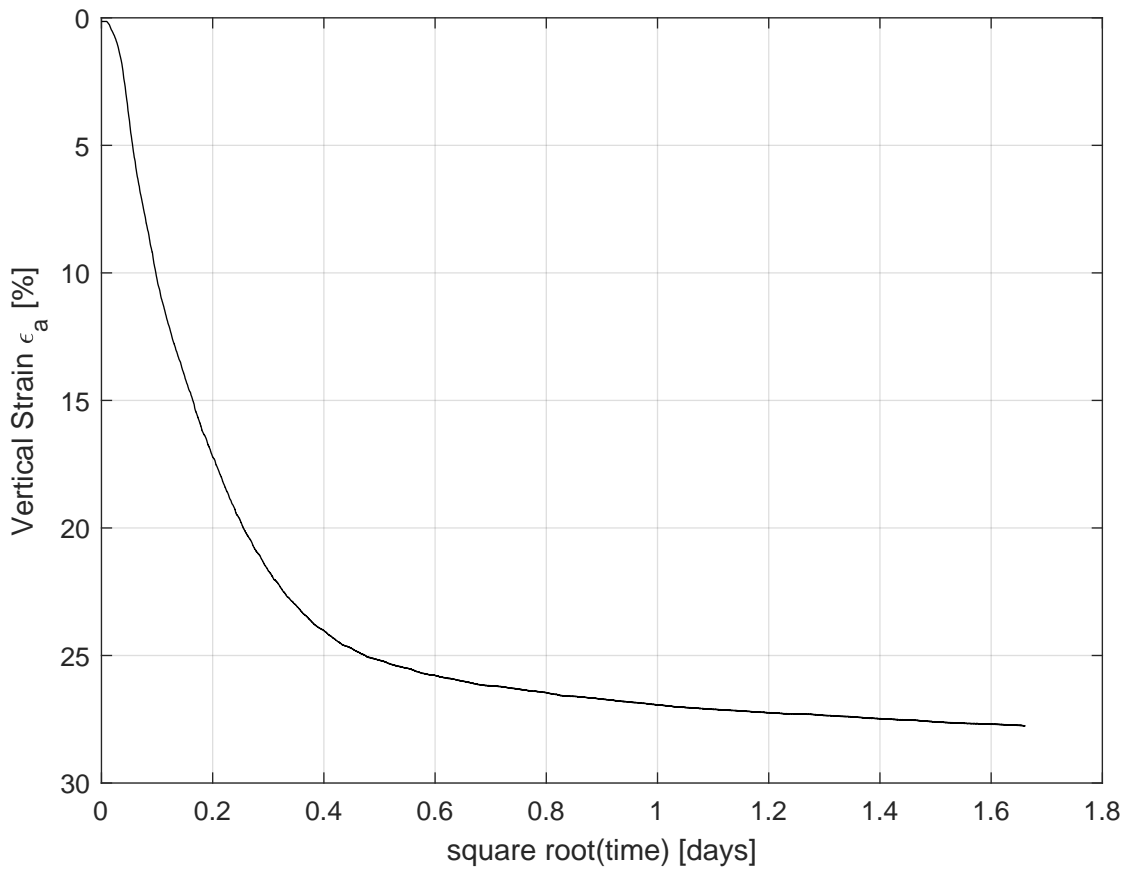
Direct Simple Shear Test

project
11207357.30

version
1.3

appendix
DSS 4C

page
3



Deltares

PO Box 177, NL 2600 MH Delft
Boussinesqweg 1, 2629 HV Delft

Telephone +31 (0)88 335 8273
Homepage www.deltares.nl

date
2024-12-19

signed
venema

Praktijkproef Reevediep: 3c uitvoeren centrifugeproeven

Direct Simple Shear test on sample 4C

Direct Simple Shear Test

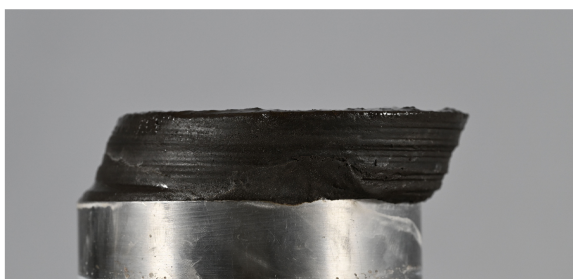
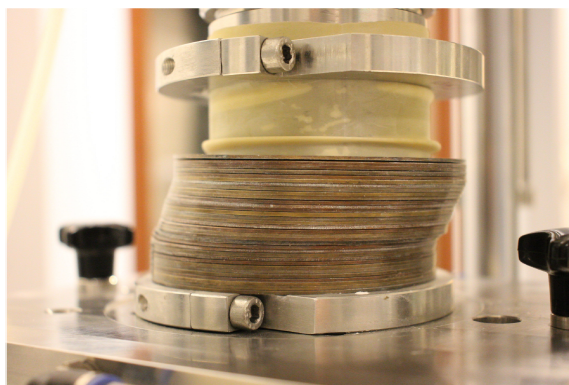
project
11207357.30

version
1.3

appendix
DSS 4C

page
4

*) Gecontroleerd en vrijgegeven door ess op 2024-12-19



Deltares

PO Box 177, NL 2600 MH Delft
Boussinesqweg 1, 2629 HV Delft

Telephone +31 (0)88 335 8273
Homepage www.deltares.nl

date
2024-12-19

signed
venema

Praktijkproef Reevediep: 3c uitvoeren centrifugeproeven

project
11207357.30

version
1.3

Direct Simple Shear test on sample 4C

appendix
DSS 4C

page
5

Direct Simple Shear Test

*) Gecontroleerd en vrijgegeven door ess op 2024-12-19

Deltares is an independent institute for applied research in the field of water and subsurface. Throughout the world, we work on smart solutions for people, environment and society.

Deltares

www.deltares.nl